Technical Memorandum 104815

Final Report for the Ultralight Fabric Reflux Tube (UFRT) Thermal/Vacuum Test

K. M. Hurlbert
M. K. Ewert
J. P. Graf
J. R. Keller
K. A. Pauley
R. J. Guenther
Z. I. Antoniak

March 1996

Technical Memorandum 104815

Final Report for the Ultralight Fabric Reflux Tube (UFRT) Thermal/Vacuum Test

K. M. Hurlbert and M. K. Ewert
Lyndon B. Johnson Space Center
Houston, Texas 77058

J. P. Graf and J. R. Keller
Lockheed-Martin Engineering & Sciences
Houston, Texas 77058

K. A. Pauley, R. J. Guenther, and Z. I. Antoniak
Battelle, Pacific Northwest Laboratories
Richland, Washington 99352

March 1996

ACKNOWLEDGMENTS

The authors would like to express their gratitude to Cindy Cross of the NASA Johnson Space Center (JSC), Crew and Thermal Systems Division (CTSD), for acting as Project Manager during the summer of 1994. Her contributions in leading the team and preparing for the thermal/vacuum testing directly supported the success of the fiscal year 1994 program.

The NASA test director, Eric Chan, and the entire test team of the CTSD Systems Test Branch are recognized for their excellence in supporting the buildup and implementation of the testing.

Cindy Dew and Leslie Haag of the GHG Corporation, supporting the CTSD, are recognized for their support of the editing of this final report.

The authors would also like to thank D.V. Archer of Battelle, Pacific Northwest Laboratories for perfecting the fabrication of the test articles. Also from Battelle, James M. Bates is recognized for his support to the testing at JSC.

Funding for the fiscal year 1994 program was provided by NASA Headquarters Office of Life and Microgravity Sciences and Applications, Code U.

This publication is available from the NASA Center for AeroSpace Information, 800 Elkridge Landing Road, Linthicum Heights, MD 21090-2934, (301) 621-0390.

CONTENTS

CONTENTS
(Continued)

FIGURES

FIGURES
(continued)

FIGURES
(concluded)

TABLES

TABLES
(concluded)

1.0 ABSTRACT

Spacecraft thermal control systems (TCSs) are essential to provide the necessary thermal environment for the crew and to ensure that the equipment functions adequately on space missions. The Ultralight Fabric Reflux Tube (UFRT) was developed by Battelle, Pacific Northwest Laboratories (PNL), with partial funding from the NASA Lewis Research Center, as a lightweight radiator concept to be used on planetary surface-type missions (e.g., Moon, Mars). The UFRT consists of a thin-walled tube (acting as the fluid boundary), overwrapped with a low-mass ceramic fabric (acting as the primary pressure boundary). The tubes are placed in an array in the vertical position with the evaporators at the lower end. Heat is added to the evaporators, which vaporizes the working fluid. The vapor travels to the condenser end above and cools as heat is radiated to the environment. The fluid condensed on the tube wall is then returned to the evaporator by gravity. The primary objectives for the fiscal year (FY) 1994 program included the design and fabrication of prototype UFRTs, and thermal/vacuum chamber testing of these test articles.

Six UFRTs with titanium liners were successfully manufactured and delivered to the Johnson Space Center (JSC) in July 1994. Five tubes were tested in a thermal/vacuum chamber in September 1994. Data were obtained to characterize the performance of the UFRTs under simulated lunar conditions and prove the design concept. In addition, an in-house trade study showed that an optimized/improved UFRT could achieve as much as a 25% mass savings in the heat rejection subsystem of future planetary-type TCSs.

2.0 ACRONYMS/NOMENCLATURE

A_s	surface area
CTSD	Crew and Thermal Systems Division
D	diameter
F	view factor
H	Henry's Constant
IR	infrared
JSC	Johnson Space Center
L	length
k	thermal conductivity
n	number of moles of gas
NASA	National Aeronautics and Space Administration
NCG	non-condensable gas
NW	no wick
P	pressure
PA	projected area
PNL	Pacific Northwest Laboratory
Q	total heat transfer
q	heat flux
R	universal gas constant
SINDA	Systems Improved Numerical Differencing Analyzer
T	temperature
TA	true anomaly
T/C	thermocouple
TSS	Thermal Synthesizer System
TCS	Thermal Control System
UFRT	Ultralight Fabric Reflux Tube
V	volume
W	wick
x	concentration

Greek

α	absorptivity
ε	emissivity
σ	Stefan-Boltzman Constant

Subscripts

evap	evaporator
env	environment
heater	heater
loss	loss to surroundings
sink	ambient sink
surf	surface
tube	tube surface

3.0 INTRODUCTION

The heat rejection radiator section of a human spacecraft TCS comprises typically 30% to 45% of its overall system mass. As the power levels of these spacecraft increase over time, this heat rejection section will grow proportionally. Therefore, the need for lightweight radiators to reduce the overall system mass for these missions is significant. Lightweight radiators for future planetary-type missions (e.g., Moon, Mars), which can also take advantage of partial gravity environments, are also needed and may provide mass savings for the entire TCS.

The UFRT was developed by PNL, operated by Battelle Memorial Institute for the Department of Energy. The UFRT design utilizes a thin-walled tube which acts as the fluid boundary. A low-mass ceramic fabric is braided and placed over the liner to act as the primary pressure boundary to minimize the overall mass of the tubes. Concentric rings are compressed over the fabric at the ends of the UFRT to hold the fabric in place. End caps, which are electron beam welded to the thickened end lengths of the tube, comprise the remainder of the pressure boundary.

The UFRT radiator concept uses gravity as the main fluid transport mechanism. The tubes are oriented vertically with an evaporator at the lower end. Heat added to the evaporator vaporizes the working fluid. The vapor travels to the cooler condenser end where the heat is conducted through the tube wall and radiated to the environment. The fluid then returns to the evaporator by means of gravity and the process is repeated.

The major objectives of the UFRT development program in FY94 included fabricating prototype UFRTs with an improved titanium liner and evaluating the tubes under simulated lunar environmental conditions using a thermal/vacuum chamber. The project activities described in this report were funded through NASA Headquarters Office of Life and Microgravity Sciences and Applications, Code U.

4.0 BACKGROUND

The National Aeronautics and Space Administration (NASA) JSC Crew and Thermal Systems Division (CTSD) initiated work on the UFRT concept with Battelle during FY92 under an existing contract. Eight prototype UFRTs were designed and manufactured under the program during that year, and were sent to JSC to be tested under thermal/vacuum conditions.

These first-generation UFRTs were constructed using a thin copper liner with a Nextel overwrap, held in place with compression rings. The tubes were 1.1 m (43.3 in.) in length and had a nominal diameter of 0.025 m (1 in.). Charge fittings were soldered to the condenser end caps to allow the tubes to be filled with the working fluid (water). Inside the evaporator section of the UFRTs was a wick (also Nextel) to ensure that liquid was distributed over the entire heat transfer (evaporator) surface.

The 1992 thermal/vacuum chamber testing was conducted at JSC in August of that year. The test matrix included nominal startup and shutdown, frozen startup, transient loading, operation for simulated lunar day and night, and maximum heat transfer. The results from the testing were limited. All but three of the UFRTs failed during installation into the chamber, due to their fragility. In addition, instrumentation failures prevented the tubes from being tested above 90 watts (W). However, the testing did indicate that the UFRTs operated isothermally along the condenser sections and performed as expected in nominal operations. The tubes also performed startup from a full frozen state without incident, and performed as expected during transient loading. Results of this testing are documented in Guenther et al., 1992.

Several areas of improvement were identified from the 1992 testing, with the foremost being improvement of the liner material to withstand handling operations. Optimization studies conducted at Battelle showed that the UFRT mass could potentially be lowered to <2 kg/m^2 without compromising performance by a number of design changes, including potentially smaller tube diameters (i.e., greater length-to-diameter ratios), thinner or smaller attachment components, materials with lower densities, and the use of fins.

Work on the program continued during FY93 to further optimize the design and fabricate an improved UFRT. A primary goal was to use a titanium liner. Titanium was selected due to its strength and low mass, which are attractive features for the UFRT design. Battelle began operations using a new cluster mill, and successfully fabricated liners using copper. A titanium preform was also constructed to support the development of the improved UFRTs during FY94.

This report documents the major UFRT development activities for FY94, including the fabrication of improved UFRTs and thermal/vacuum chamber testing conducted at JSC, as well as related analyses. Six UFRTs were successfully fabricated during this year, however, limited funding and schedule constraints permitted the incorporation of only a few improvements identified during previous years. The major design changes for the new UFRTs included 1) substituting titanium liners for the copper liners; 2) redesigning the end caps to minimize uncertainties in collecting temperature data and evaluating the test results; and 3) reducing the length of the evaporator, and its end cap length, to reduce overall weight and increase the heat flux. Also, wicks were included in only half of the UFRTs to allow evaluation of their performance. Five of these UFRTs were tested under thermal/vacuum conditions in September 1994. The following sections provide additional detail on the UFRT design, fabrication, testing, and results from this work.

5.0 UFRT DESCRIPTION

Six UFRTs were built by Battelle and sent to JSC, including one pretest UFRT used for thermal testing at PNL. Only five of the UFRTs were scheduled for thermal/vacuum testing at JSC. Details are provided in the following sections on the design (Section 5.1), fabrication and assembly (Section 5.2), and qualification testing (Section 5.3) conducted prior to shipment.

5.1 UFRT DESIGN

The UFRTs built and tested in FY94 consisted of a titanium liner with a ceramic fabric overwrap, stretched over the condenser region and held in place with copper compression rings. The overall design is summarized in Table 5.1 and compared with the UFRTs built previously for testing in 1992. Schematics of the overall design, the preform used to make the liner, the titanium liner, the end caps, and the crimping (or compression) rings for the UFRTs built in 1994 are shown in Figures 5.1 through 5.5, respectively. The UFRTs built for testing in 1994 were similar to those built and tested in 1992 (Pauley et al., 1993), although some dimensions and materials were changed. A titanium preform (Figure 5.2) was used to produce the titanium liner (Figure 5.3) that consisted of a 2.5-cm (1-in.)-diameter tube with a length of 111.8 cm (44 in.), thick ends, and a thin central region. The 305-μm (0.012-in.)-thick ends facilitate welded end caps, while the thin central region (66 μm, 0.0026 in.) reduces the UFRT overall weight, while still acting as a permeation barrier for the water working fluid.

Table 5.1. Comparison of 1994 and 1992 UFRT Designs

Design Aspect	1994 Design	1992 Design
General Dimensions	nominal 2.5-cm (1-in.) diameter, 1.13 m (44.4 in.) long from end cap to end cap	nominal 2.5-cm (1-in.) diameter, 1.00 m (39.6 in.) long from end cap to end cap
Materials		
Liner	Ti ASTM B338, Grade 2, unannealed after forming	Copper, annealed after forming
End caps	Ti ASTM B338, Grade 2	Copper, annealed after forming
Crimping Rings	Copper	Copper
Fabric	Nextel 312	Nextel 312
Spring	Spring steel	none
Wick	SiO_2	Nextel 312
Working fluid	Water	Water

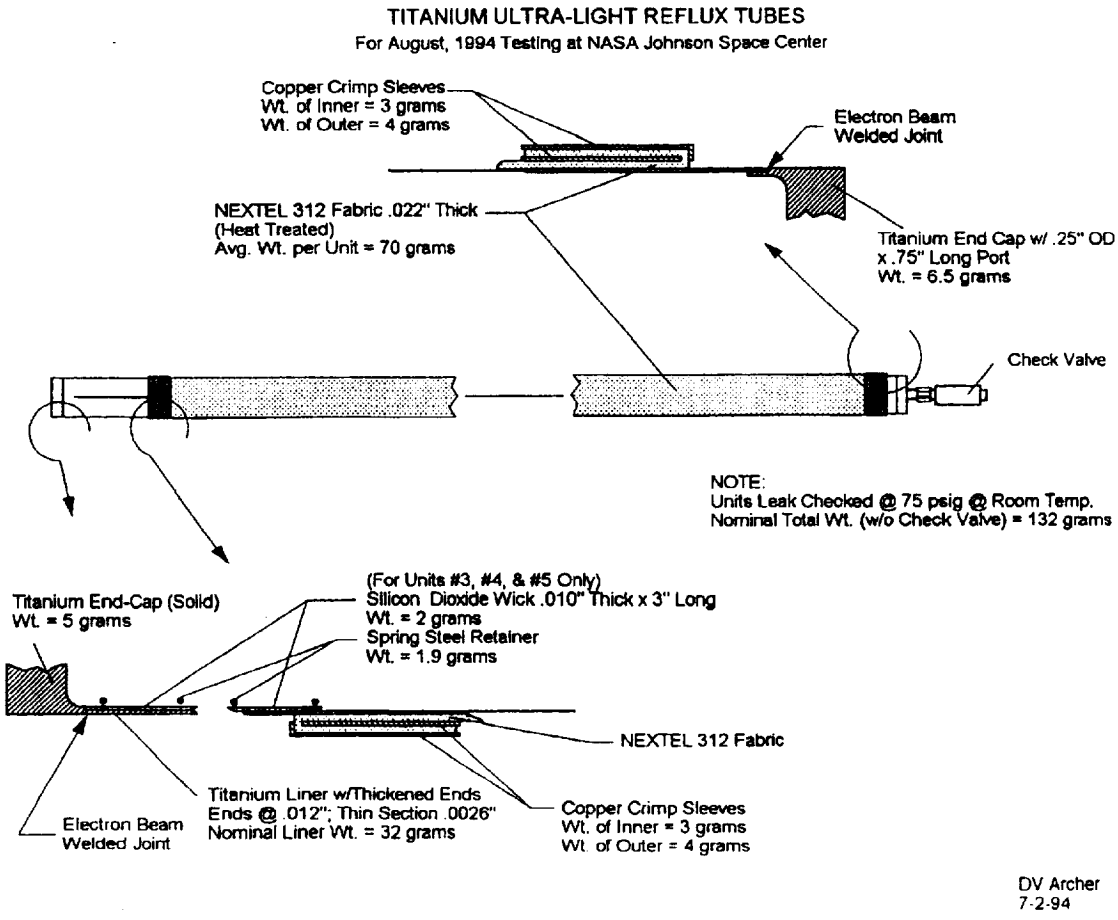

Figure 5.1. Overall Design of UFRT With Titanium Liners for 1994 Tests.

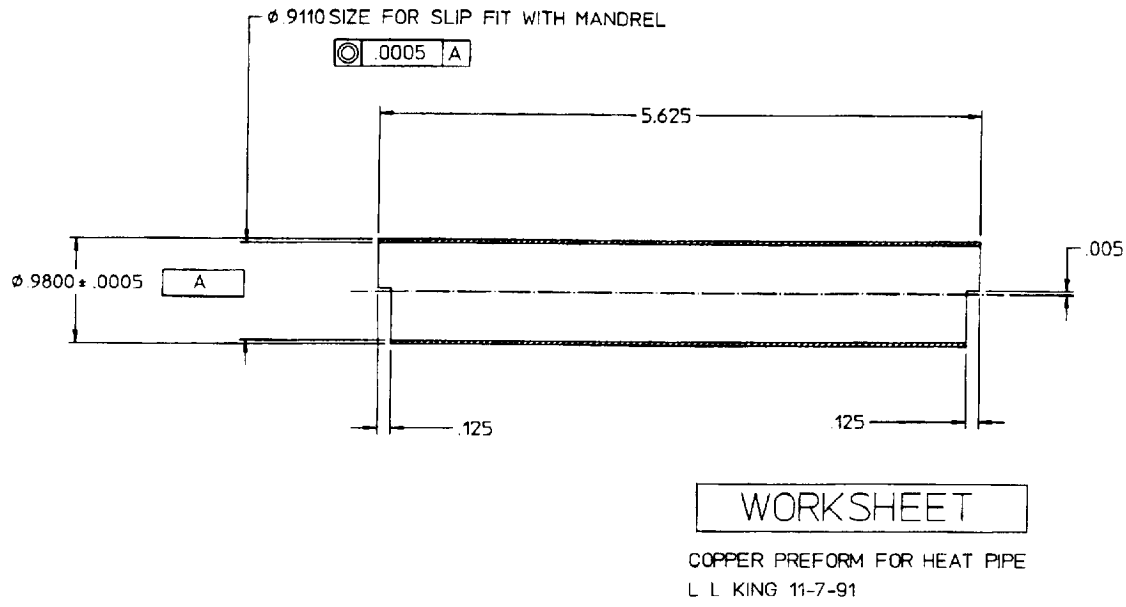

Figure 5.2. Preform Design Used for Making Titanium Liners.

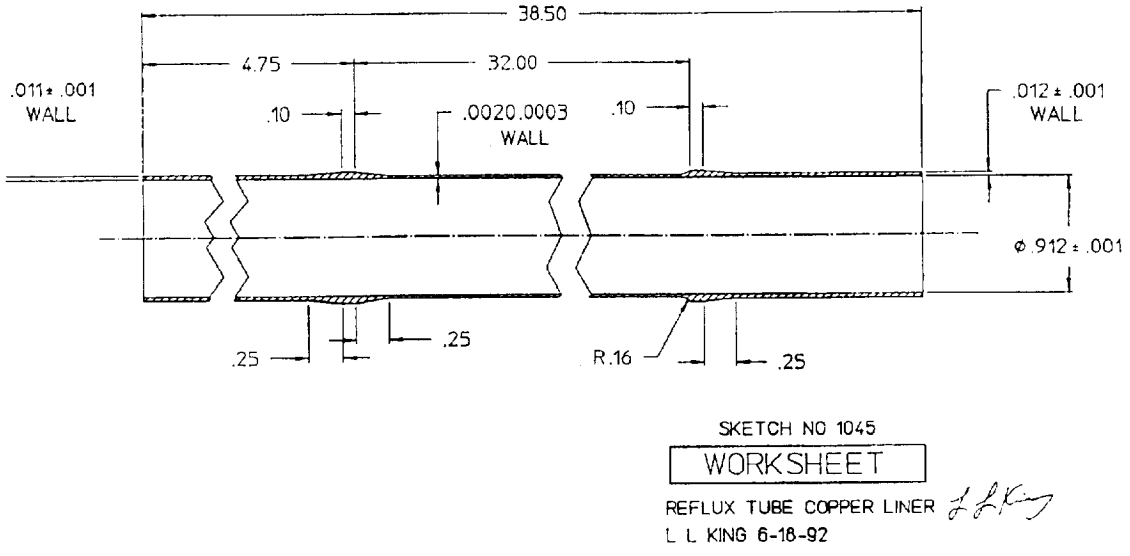

Figure 5.3. Liner Design for UFRT With Titanium Liners.

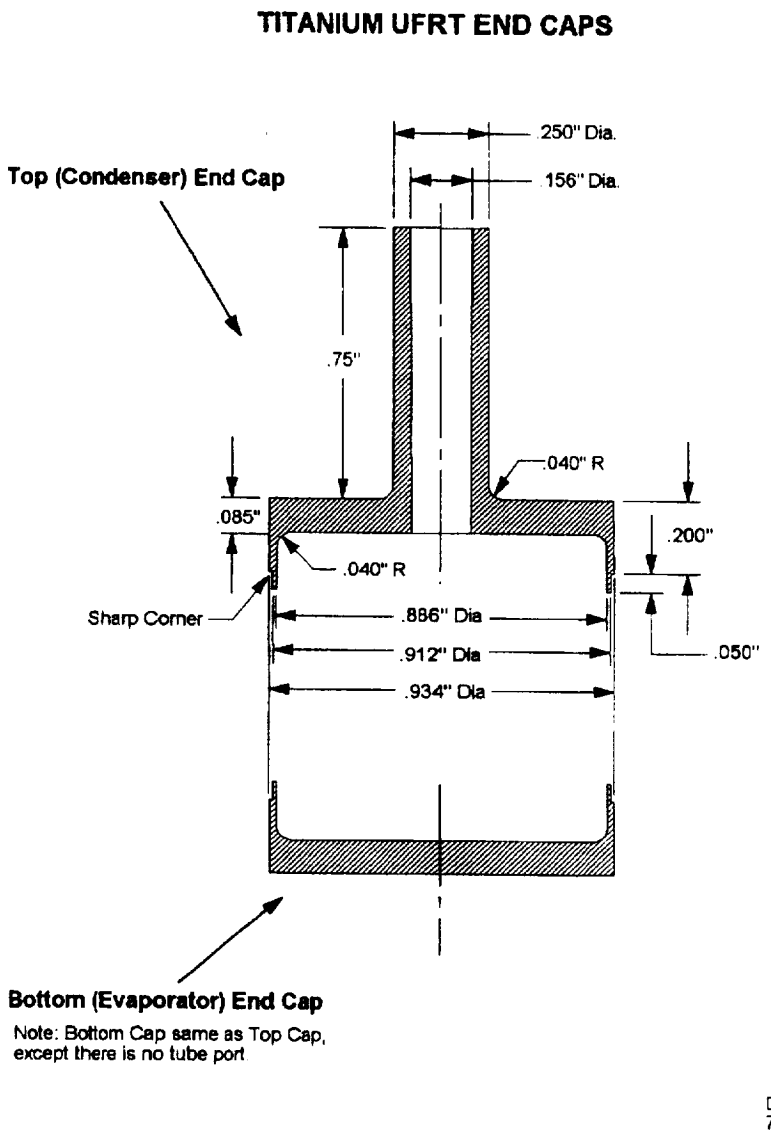

Figure 5.4. Titanium End Caps Used for UFRTs With Titanium Liners.

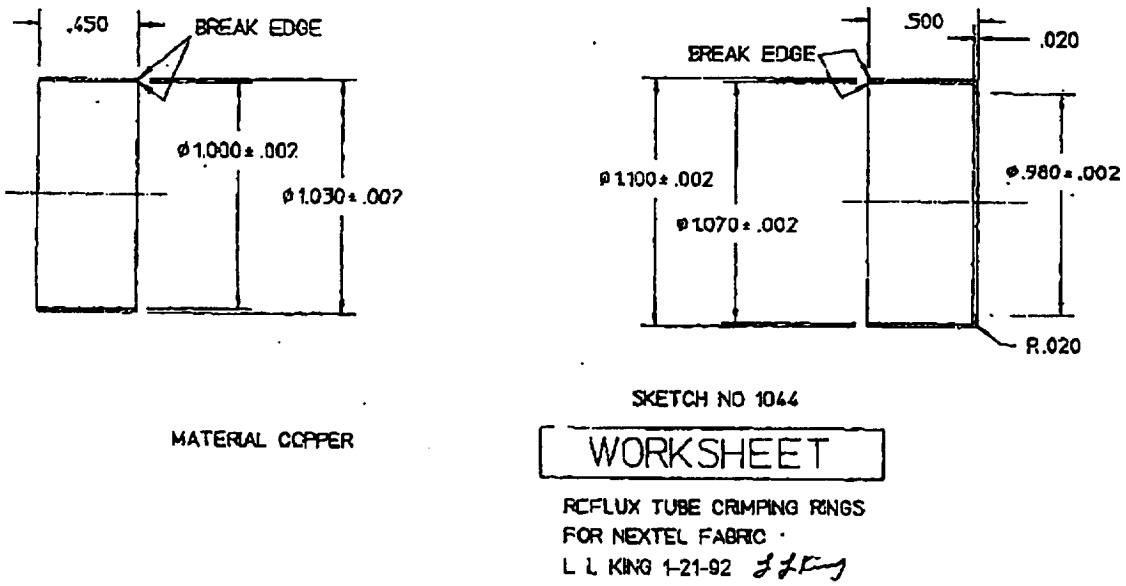

Figure 5.5. Crimping Ring Design Used for UFRTs With Titanium Liner.

Nextel 312 with a biaxial weave has been used as the overwrap for all of the UFRTs built for JSC. Selection of this material was based primarily on its absorptance and emittance characteristics in the solar spectrum: Battelle tests indicate an emittance measured at approximately 0.93 at 425 K (306°F) and an absorptance of 0.1 in solar wavelengths. The as-woven fabric was heat-treated before assembling the UFRTs, which consisted of baking the fabric at 1173 K (1652°F) for 16 hours to remove the sizing on the woven material (here, sizing refers to the starch, wax, or other organic ingredient applied to the fiber strands to protect them and aid in handling; the sizing of a fabric is normally removed before the final product is used).

The flat end cap design shown in Figure 5.4 was chosen to minimize machining costs and reduce uncertainties from water in the evaporator region below the heated zone during testing. Stress analyses conducted at Battelle using the ALGOR finite element program indicated that the end cap design would withstand 1.86 MPa (270 psia) at 450K (350°F) without yielding.

Additional components used in the UFRTs included crimping (or compression) rings, fabric wicks, and retaining springs. The crimping rings (Figure 5.5) were used to attached the fabric to the titanium liner. The rings were made of copper because they could be compressed easily onto the fabric, and this eliminated concerns of

corrosion from contact of the copper with the titanium liner. Titanium would have been a preferred material because of its lower mass, but tests indicated that development work would be required to determine the proper way to crimp the tough titanium. A section of silicon dioxide (SiO_2) fabric was heat-treated and placed in the evaporator end before closure. The fabric was held in place against the inner liner by using music wire that was rolled into a helical spring. All of the required components and related design drawings for the current UFRT design are summarized in Appendix A.

5.2 FABRICATION

The various stages in the fabrication and assembly of the UFRTs are shown in Figure 5.6. Four of the UFRTs contained wicks made of SiO_2. Three of the UFRTs had no wicks. The as-fabricated weights of the various components in each UFRT are provided in Table 5.2. Also provide in Table 5.2 are the Battelle and NASA designation numbers (similar to a serial number) for each UFRT fabricated. The NASA numbers are used throughout the remainder of this report.

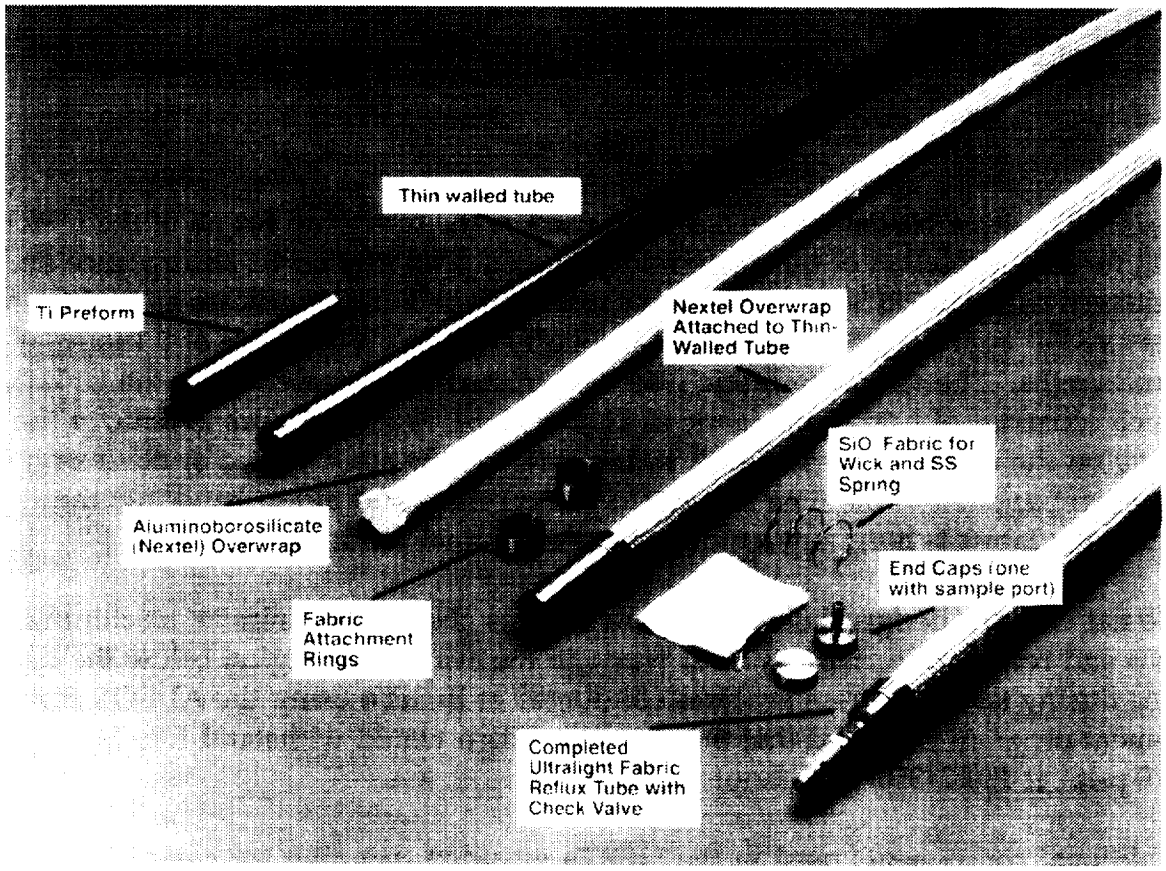

Figure 5.6. Stages of Fabrication of a UFRT With Titanium Liner and Nextel Overwrap.

Table 5.2. Weights of Components in As-Fabricated Titanium UFRTs, (g)

NASA UFRT No.	Battelle No.[1]	Ti Liner Weight	Ti End Caps (Top)	Ti End Caps (Bottom)	Copper Sleeves	Nextel Fabric[2]	Overall	Comments
0	1	30.7	6.3	5.0	14.8	71.8	133.5	w/wick[3] (2.8 g) & retainer[4] (2.1 g); collapsed & ruined during end cap welding
1	2	33.2	6.4	5.0	15.0	71.5	131.1	
6	3	31.5	6.5	5.0	14.0	76.1	136.8	w/wick[3] (1.9 g) & retainer[6] (1.8 g); ugly outer fabric, has 4" section of loose weave
2	4	33.3	6.6	5.0	14.0	69.0	131.7	w/wick[5] (2.0 g) & retainer[6] (1.8 g)
3	5	31.1	6.5	5.0	14.3	69.4	130.2	w/wick[5] (2.0 g) & retainer[6] (1.9 g)
4	6	32.5	6.5	5.0	14.3	69.9	128.2	
5	7	31.9	6.5	5.0	13.6	69.5	126.5	

[1] All of the UFRTs were marked at Battelle with an identifying number (1 through 7) on the end caps.

[2] Nextel 312 (P.O. 167687); Heat-treated at 1173K (1652°F) for 16 hrs.

[3] Silicon Dioxide fabric 7.62 cm wide x 11.4 cm long (3 in. x 4.5 in.); Heat cleaned at 823K (1022°F) for 4 hrs.

[4] Spring fabricated from 0.104-cm (0.041-in.)-dia. music wire 25.4 cm (10 in.) long.

[5] Silicon Dioxide fabric 7.62-cm wide x 8.9-cm long (3 in. x 3.5 in.); Heat Cleaned at 823K (1022°F) for 6 hrs.

[6] Spring fabricated from 0.104-cm (0.041-in.) dia. music wire 22.9-cm (9-in.) long.

Notes: Original units measured in grams, inches, °C, and psig. Units leak checked with argon at 0.62 MPa (89.7 psia) for 1 hr. Units fitted with a check valve on condenser end and backfilled with argon at 0.31 MPa (44.7 psia) for shipment.

A key element in the fabrication of the UFRT is the forming of a titanium tube, or liner, with thick ends and an intermediate region with very thin walls in one continuous piece. The proprietary process used to make the liners with thin central regions and thick ends is conducted at room temperature without any lubricants. A preform (see Figure 5.2) is placed over a long mandrel that is centered in a cluster of rollers. The specially designed rollers are compressed onto the preform at a controlled rate while the mandrel rotates. This spinning process extrudes out the formed material. The initial wall thickness of the preform is reduced by about 98% in a single pass to form the thin wall region, and by a smaller percentage to form the thick ends. No special heat treatment was used to condition the initial or final

titanium material. After cutting off the ends of the titanium liner to the proper length, a pressure test was conducted with air at 0.45 MPa (65 psia) for 1 hour or longer to ensure the integrity of the finished liner.

A woven tube of Nextel 312 ceramic fabric with a biaxial weave was attached using concentric pairs of copper rings that were crimped over the fabric at both ends of the liner. The UFRT fabrication was completed by the electron beam welding of the end caps.

5.3 QUALIFICATION TESTING

Two types of qualification tests were conducted at Battelle: a thermal test for UFRT 1 and integrity tests on all of the liners and completed UFRTs. UFRTs 2 through 6 were fabricated, filled with argon, and shipped to JSC without system level thermal or pressure testing.

The detail of the qualification testing is included in two appendices. Appendix B describes the qualification test plan and procedures. Appendix C outlines the test results and conclusions.

All test criteria for thermal testing of UFRT 1 were accomplished during the qualification test. Specifically, Table 5.3 describes the manner in which each test objective was met. No deviations from the test plan were observed.

In summary, UFRT 1 was tested to 175 W without failure or loss of heat rejection capability. No problems were encountered with the Nextel/titanium heat pipe operating in the vertical (reflux) mode other than some evaporator liquid dryout. Test data indicated that this heat pipe operating in a space (non-convective) environment would not be performance limited, but would reach radiative limits well before reaching other thermodynamic limits. Therefore, based on the criteria presented above, the prototype UFRT (UFRT 1) met all requirements, and general production of the test article UFRTs was initiated.

Table 5.3. Accomplishment of Test Objectives for UFRT 0

Test Objective	Test Result
Successful charging and startup	Startup was accomplished with less than 1 g of working fluid loss.
Operation up to the minimum ambient atmospheric operating temperature (377 K)	The UFRT was tested to a condenser temperature of 410 K.
General isothermicity over the condenser length during steady state operation	Condenser isothermicity was verified using an infrared (IR) camera during steady state operation.
Pressure containment throughout the test	No breach of the pressure containment was observed during the test.
Successful shutdown without pressure anomalies at the conclusion of the test	Since pressure was not directly measured during the test, no pressure information can be reported to verify this result. However, pressure was indirectly calculated using the vapor temperature of the working fluid. This calculation did not indicate anomalies during the shutdown procedure.

The remaining qualification tests conducted on the UFRTs to be shipped to JSC (UFRTs 1 through 6) consisted of checking the integrity of the liners after they were formed and after final assembly. The liners were leak-tested for 1 hour after pressurizing with argon to 0.45 MPa (65 psia). In addition, the assembled UFRTs were leak checked with argon gas at 0.62 MPa (90 psia) for 1 hr, fitted with a check valve on the condenser end, and backfilled with argon at 0.3 MPa (45 psia) for shipment.

In addition to the qualification tests conducted on the test articles, several pressure tests were conducted on both thin-walled titanium tubes and fabricated UFRTs. The results of the tests on short thin-walled tubes indicated that the 51-μm (0.002-in.)-thick wall would not survive stresses caused by atmospheric pressure if the tubes were evacuated. For this reason, the UFRTs were filled with the water working fluid at JSC before thermal/vacuum testing. Furthermore, a titanium liner was pressure tested to 3.5 MPa (515 psia) at room temperature without failure, well above the expected limit of 1.9 MPa (280 psia) for this temperature.

6.0 TEST PROGRAM DESCRIPTION

The UFRT thermal/vacuum test was run to simulate the lunar environment. Environmental conditions were chosen to represent a combination of solar and infrared (IR) intensities. Of the two possible space-related uses of the UFRT, Moon and Mars bases, the lunar environment provided a wider and more severe range, hot to cold, of temperature environments. The test simulated these environments at various times in the lunar day, as well as various lunar latitudes. A transient step down test was also run to determine whether ice crystals would form in the condenser section of the UFRTs, thus decreasing their efficiency. These environments were simulated in Chamber E, Building 33, at JSC using the combination of a solar lamp (simulated sun) and IR lamps (simulated lunar IR). The following sections provide additional detail on the test procedures (Section 6.1), test setup (Section 6.2), and test conditions (Section 6.3) for the thermal/vacuum testing conducted in September 1994.

6.1 TEST PROCEDURES

The UFRTs were subjected to extreme warm and cold lunar environments, as well as nominal, full sun, warm, and frozen startup tests. To achieve these environments, one solar lamp and several IR lamps were used. IR lamps simulated the lunar surface while the solar lamp simulated the sun. The solar lamp was adjusted according to equation 6.1:

$$\text{Incident Solar Flux} = \text{Sun} * \sin(\text{latitude}) \qquad (6.1)$$

to account for the UFRTs' locations at various lunar latitudes. The amount of solar flux equal to one sun is 1370 W/m^2, at nominal conditions.

The test setup in Chamber E simulated the UFRTs mounted perpendicular to the lunar surface as shown in Figure 6.1. The test also simulated the UFRT array's orientation to the sun at lunar noon as shown in the figure.

The UFRT was tested at the extreme temperature environments found during the lunar day. The hot case environment simulated a UFRT array located on the lunar equator at lunar noon (Test Series 1). Also, the cold case environment simulated a UFRT array operating during lunar night (Test Series 6a). This case simulated the UFRT operation at any latitude or time during the lunar night, since the IR is negligible during the lunar night. During the cold case test, the maximum heat transfer and frozen startup characteristics of the UFRT were evaluated. A summary of the IR lamp power and solar lamp inputs for the hot and cold cases is shown in Table 6.1.

Two warm cases simulated the UFRT operations at the 30° and 45° latitudes (Test Series 3 and 4, respectively) and lunar noon as shown in Figure 6.1. One test series investigated the UFRT operation at 1/8 of the lunar day or True Anomaly (TA) = 45° past lunar noon on the equator (Test Series 2) as shown in Figure 6.1. A test series (Test Series 5) was run to determine the UFRT response to a full solar environment as if the UFRT array were located on the lunar poles (latitude = 90°), also shown in Figure 6.1. Again, a summary of the IR lamp power input and solar lamp input for these cases is shown in Table 6.1.

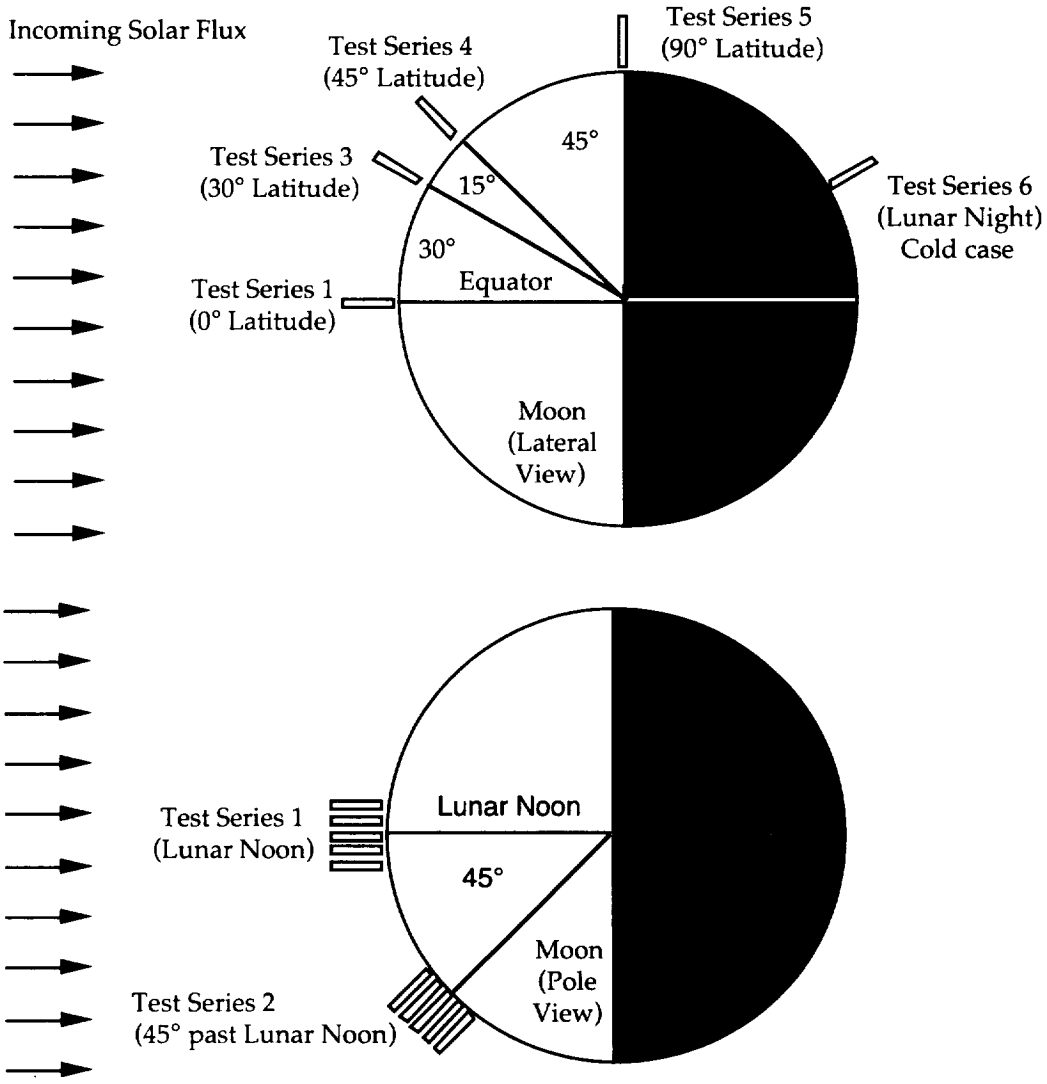

Figure 6.1. UFRT Lunar Simulation Locations.

Table 6.1. UFRT Test Procedures Matrix

Test Series	Solar (suns)	Main IR Lamps (W)	Side IR Lamps N/S (W)	Lunar Environment Description
1	0	200	75	Lunar noon
2	0	160	150/250	1/8 Lunar day
3	0.5	300	150	30° Latitude
4	0.71	142	75	45° Latitude
5	1	0	0	Full Solar
6a	0	0	0	Maximum Heat Transfer
6b	0	0	0	and Frozen Startup

6.1.1 UFRT Venting Procedure

Since the UFRTs were filled in atmospheric conditions, air was introduced inside the tubes and dissolved in the water. If this non-condensable gas (NCG) had not been removed before testing, the heat rejection performance of the UFRTs could have been severely degraded. Therefore, a venting procedure was developed to remove these undesirable gases. This procedure, and the equations used to develop this procedure, are described in Appendix D.

6.1.2 UFRT Test Procedure

For the lunar noon, 1/8 lunar day, 30° latitude, and 45° latitude tests (Test series 1, 2, 3, and 4, respectively), the Chamber E solar lamp and IR lamps were set to the parameters shown in Table 6.1. The UFRT heaters were set to 5 W. When the tubes reached steady-state conditions, the heater power was increased in 10 to 15 W increments, and again the UFRTs were allowed to reach steady-state. Steady-state conditions were defined as when the UFRT fabric or titanium liner temperature changed less than 0.3°C per hour. The process was repeated until the test article temperature (internal temperature probe) reached 155°C ± 5°C.

The full solar test (Test Series 5) began by setting Chamber E solar lamp and IR lamps to the parameters shown in Table 6.1, while the UFRT clamp heaters were set to the 20 W power setting. After the UFRTs reach steady-state conditions, the power was increased in 15 W increments. This process was repeated until the test article temperature (internal temperature probe) reached 155°C ± 5°C.

The maximum heat transfer (Test Series 6a) and frozen startup (Test Series 6b) began with the solar lamp, IR lamps, and evaporator heaters turned off. When the evaporator end cap TC reached a temperature of -18°C (225.2 K), the water is in a frozen state and the evaporator heaters were increased to the 65 W power setting. The UFRTs were again allowed to reach steady-state conditions before the power input was increased in 10 W increments. This process was repeated until the test article temperature (internal temperature probe) reached 155°C ± 5°C. For the transient step down test, the power was then decreased by 10 W increments. The power was decreased every 10 minutes until the UFRT evaporator heater power was 0 W.

6.2 TEST SETUP

Testing was conducted in Chamber E, Building 33, at JSC. The UFRTs were placed in Chamber E side by side in an array as shown in Figure 6.2.

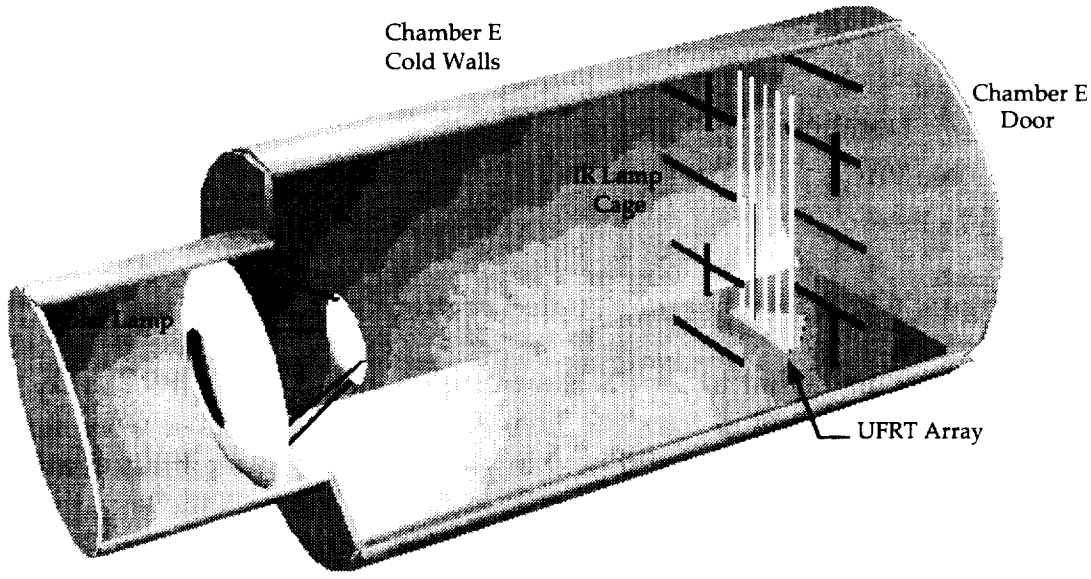

Figure 6.2. UFRT Chamber E Layout.

As seen in Figure 6.3, the SiO_2 wicked UFRTs (designated 2 and 3) were placed in positions 2 and 3, while UFRTs 1, 4, and 5 were wickless. Because of the IR lamp arrangement, the outer UFRTs experienced a colder environment than the middle UFRTs. The UFRTs were separated into groups as follows:

A. Middle UFRT - Tube 3
B. UFRTs 2 and 4
C. Outer UFRTs - Tubes 1 and 5

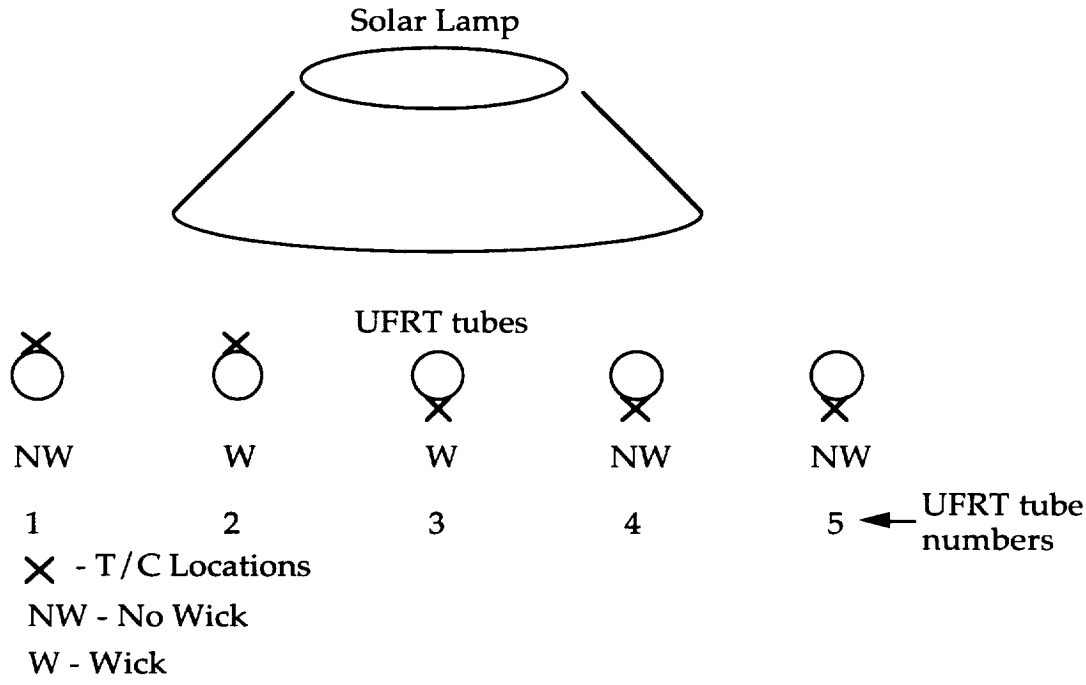

Figure 6.3. UFRT Thermocouple Locations and Tube Numbering.

Figure 6.4 shows the layout of the chamber in more detail. The UFRT array was located approximately 0.58 m from the Chamber E door. The tubes were suspended 0.05 m above the chamber floor and held in place by a mounting bracket attached to the Chamber E I-beam on top, and by a test stand supplied by Battelle at the bottom. The UFRT array tubes were placed on 0.1-m centers perpendicular to the solar beam. To provide the IR heating, twelve IR lamps surrounded the test article. Four "20-inch" lamps, were mounted 0.29 m from the UFRT array, between the tubes and the solar lamp. Four more "20-inch" IR lamps were mounted 0.29 m away from the array, between the tubes and the Chamber E door. To add heat flux to the outer UFRTs, two "10-inch" IR lamps were mounted perpendicularly to each side of the UFRT array as shown in Figure 6.4. The pneumatic valves used in the venting procedure were mounted to the chamber I-beam between the UFRT array and the chamber door. The test stand, pneumatic valves, and associated tubing were covered with aluminized Mylar to prevent heat leak to or from the UFRTs.

A rectangular heat flux coupon measuring 0.076 m x 0.076 m was instrumented with three thermocouples. The flux coupon was installed in the test stand between UFRTs 2 and 3. The front (side facing the solar lamp) of the square was covered with the Nextel fabric, while the back of the square was covered with aluminum tape. The flux coupon was oriented perpendicular to the solar rays in the chamber as shown in Figure 6.4. A close-up of the UFRT array and a photo showing its installation in the chamber are shown in Figures 6.5 and 6.6, respectively.

Eight type T thermocouples were used to monitor the performance of each UFRT as shown in Figure 6.7. Two thermocouples were attached to the UFRT evaporator section, one on the end cap and one between the UFRT clamp heaters. One thermocouple was located at the UFRT condenser end cap and a probe thermocouple was mounted inside the UFRT to monitor the internal temperature. The tips of the probe thermocouples on UFRTs 1 and 2 were located 0.3 m from the UFRT condenser end cap, while the probe thermocouple tips on UFRTs 3 through 5 were located 0.1 m from the UFRT condenser end cap. Four thermocouples were mounted on the Nextel fabric of the UFRT condenser section. Three thermocouples were epoxied to the fabric at 1/4 UFRT condenser section length intervals (approximately 25 cm) as shown in Figure 6.7. The fourth, a hypodermic thermocouple, was mounted 1/3 of the way down the length of the condenser section (approximately 0.3 m). The hypodermic probe was located just underneath the top layer of the Nextel fabric and was secured with epoxy. The thermocouples mounted to the condenser section were in the solar beam on UFRTs 1 and 2, while the UFRT condenser section thermocouples on UFRTs 3 through 5 were not mounted in the solar beam as shown in Figure 6.3.

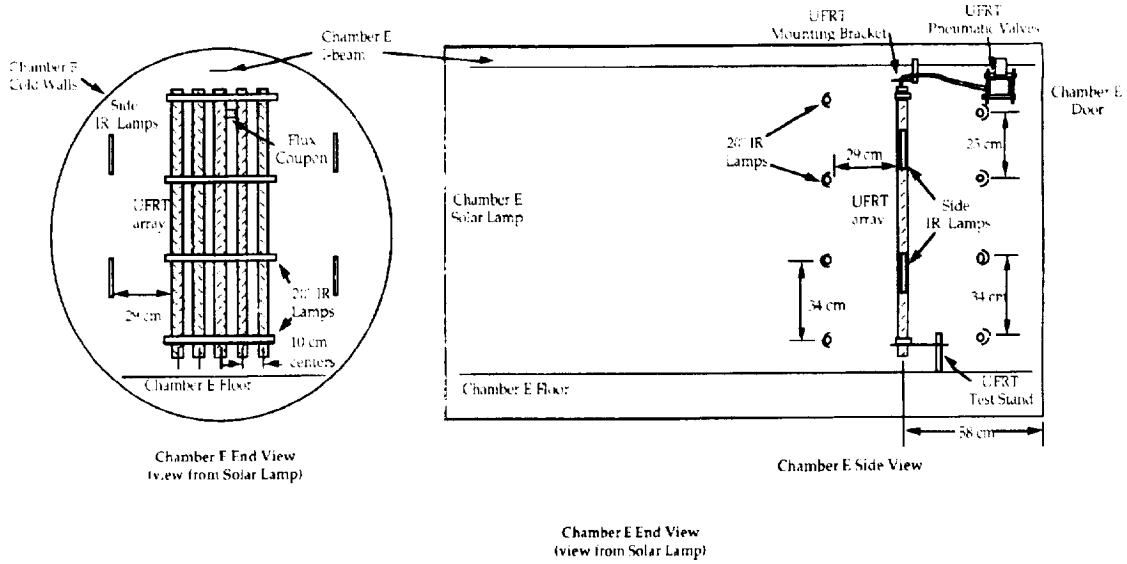

Figure 6.4. UFRT Test Configuration in Chamber E.

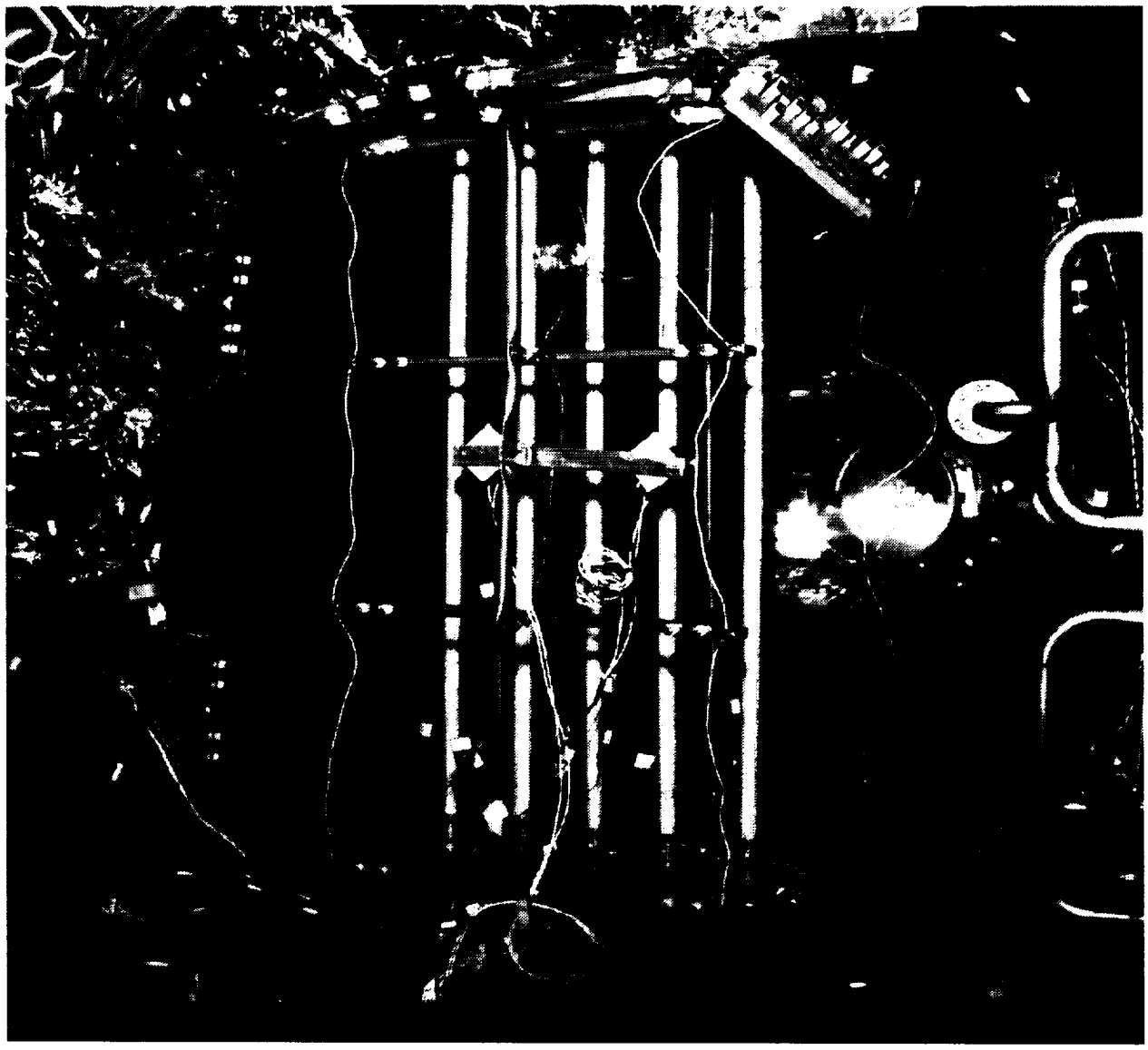

Figure 6.5. UFRT Array.

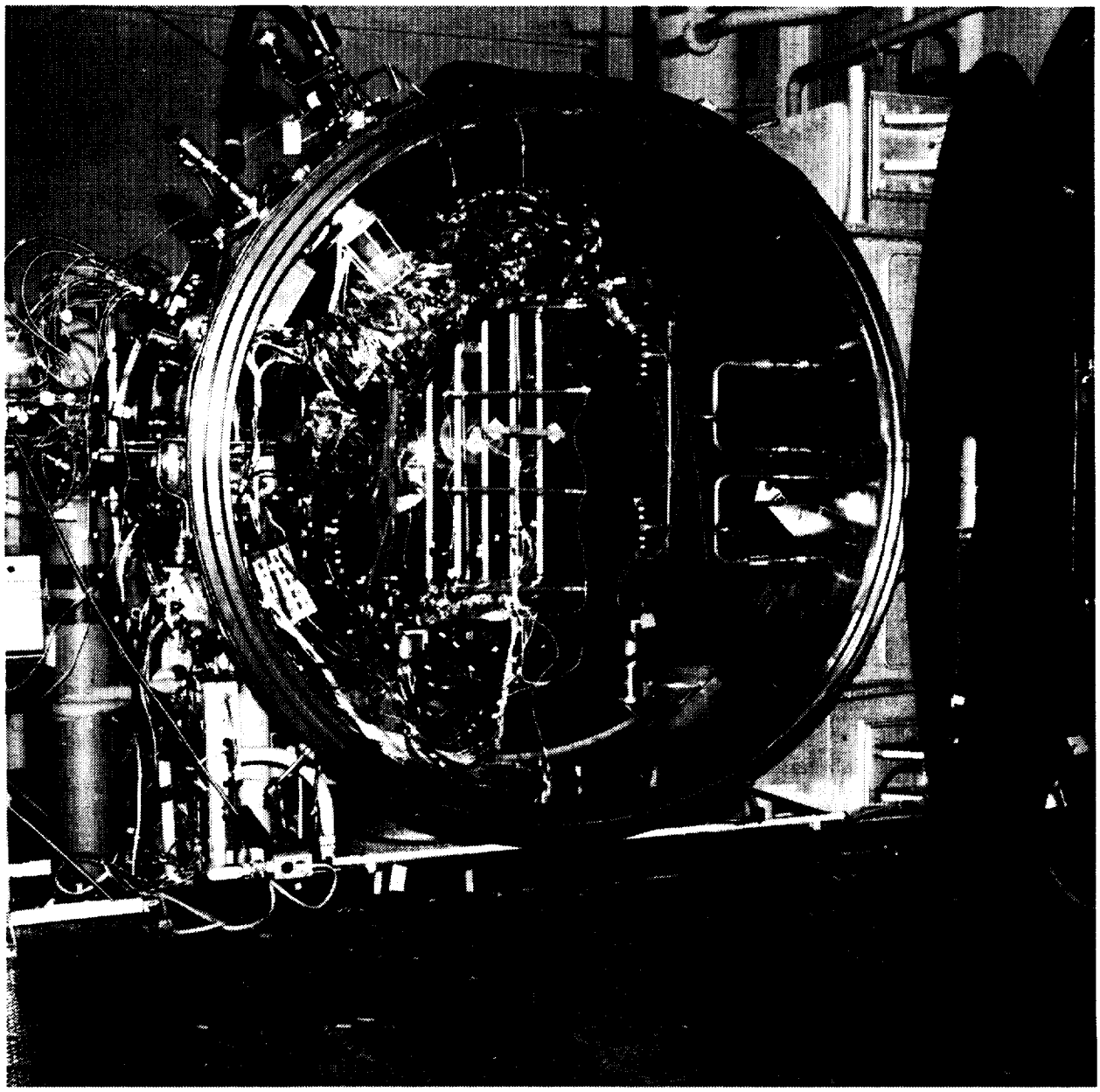

Figure 6.6. UFRT Array in Chamber E.

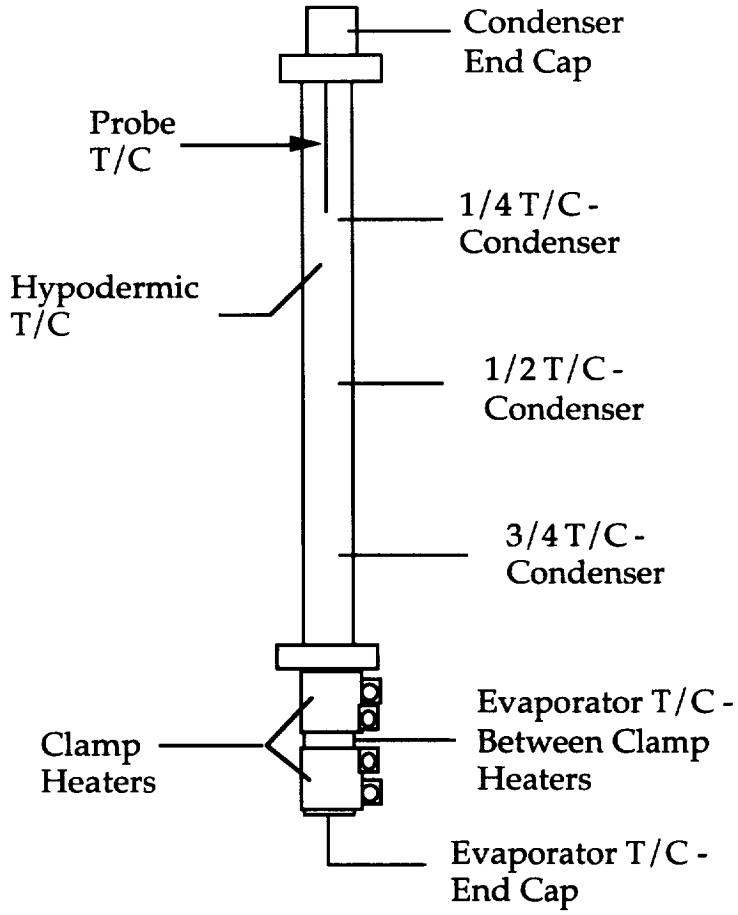

Figure 6.7. UFRT Thermocouple Locations.

As shown in Figure 6.8, heat was applied to the evaporator section by the use of screw-type clamp heaters. Metal shims were placed between the heaters and the outer surface of the evaporator section to reduce contact resistance, thereby increasing heat transfer to the evaporator section. The heaters were powered by VARIAC power supplies.

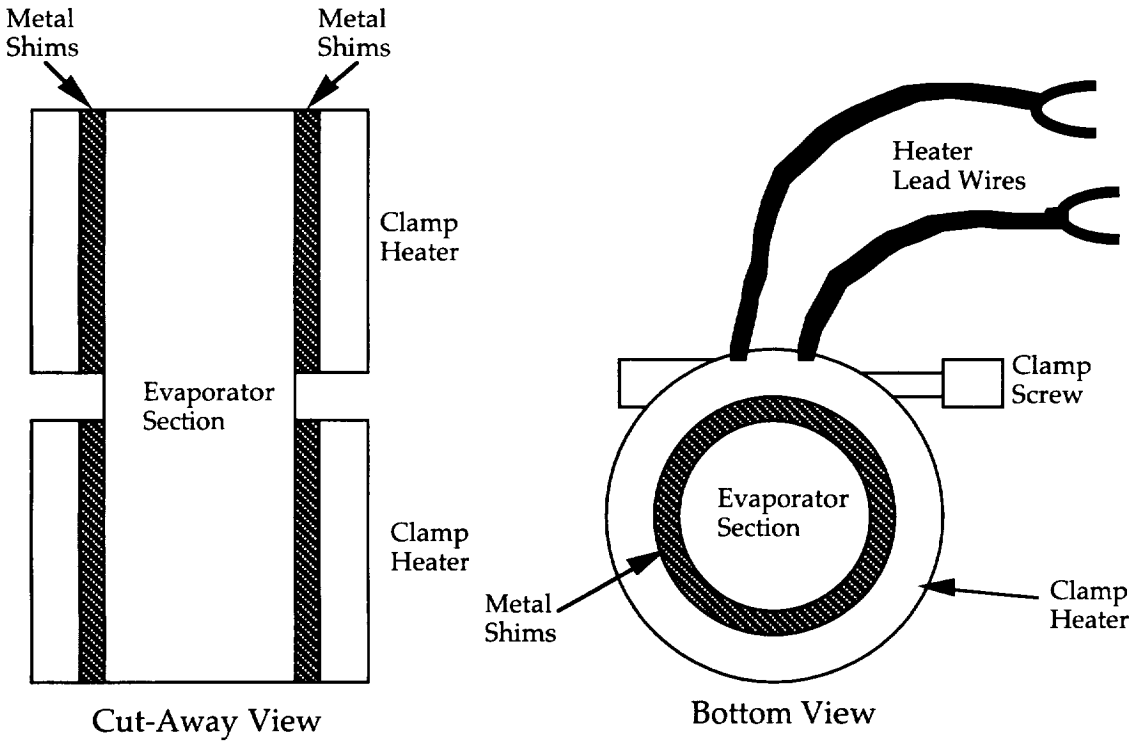

Figure 6.8. UFRT Evaporator Clamp Heaters.

6.3 TEST CONDITIONS

Table 6.2 shows the IR lamp settings, solar lamp setting, and resulting environmental estimates for the UFRT tests. These estimates are a result of a TSS/SINDA model of the test setup in Chamber E, correlated with the test results. The TSS/SINDA model is described in Appendix E. Because each tube did not operate under the same environmental conditions, the environmental settings (solar lamp and IR lamps) measured during the test were modified in the analysis to reflect the various environments across the UFRT array.

Table 6.2. UFRT Model Test Environments

Test Series	Solar (suns)	Forward and Aft IR Lamps (W)	Side IR Lamps N/S (W)	Simulated Environments 0 W on evaporator heaters (K)			Environmental Coupon Temp (K)
				Middle Tube	Tubes 2 and 4	Outer Tubes	
1	0	200	75	308	303	293	328
2	0	160	150/250	294	289	287	311
3	0.5	300	150	348	342	333	357
4	0.71	142	75	300	296	290	334
5	1	0	0	232	232	228	277
6	0	0	0	120	120	120	125

An example of the sink temperature variation across the tubes is shown in Figure 6.9. Table 6.2 shows each UFRT environment at the 0 W power setting. As can be seen from the table, the curve in Figure 6.9 represents a 7° to 15 °C drop in the environmental temperature from the middle tube to the outer tubes. The temperature drop was most pronounced when the IR lamps were in use. The environmental temperatures become greater at higher power settings due to the interaction between the UFRTs, as shown in Figures E.3 through E.8 in Appendix E. The plots of the post test analysis depicting both the UFRT sink temperatures and surface temperatures are shown in Figures E.9 through E.14. A portion of the environmental temperature drop at the outer tubes occurred because these tubes were closer to the Chamber E cold walls. This was observed during the full solar and the maximum heat transfer cases.

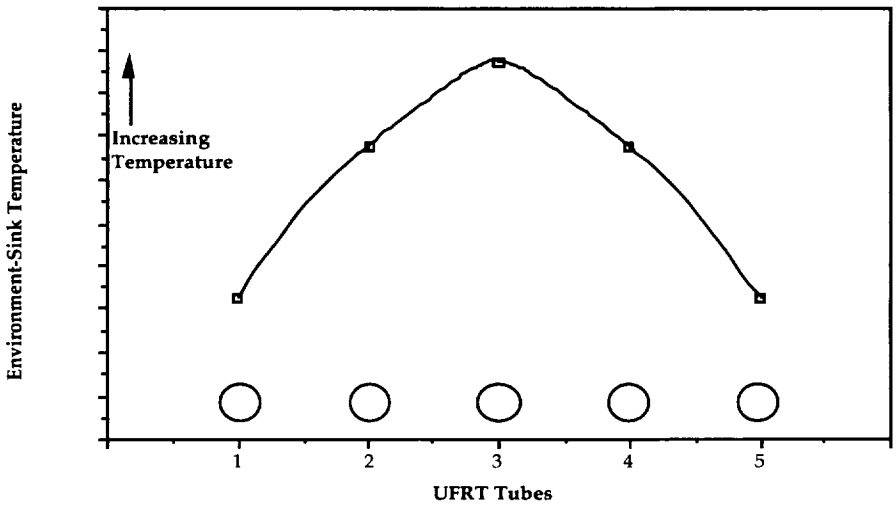

Figure 6.9. Test Environment Across UFRT Array.

In the post-test model correlation described in Appendix E, the environmental coupon showed a higher sink temperature with both IR and/or solar input, as shown in Figures E1 to E5. This occurred because the flux coupon presented less surface area to the incoming flux than the UFRT as shown in Figure 6.10. The flat surface represents the flux coupon while the curved surface represents the UFRT. Therefore, less heat per unit of surface area was applied to the UFRT than to the flux coupon. However, when no heat flux, solar or IR was imposed on the UFRT array, as shown in Figure F.6, the flux coupon temperatures remained below the estimation of the UFRT sink temperatures.

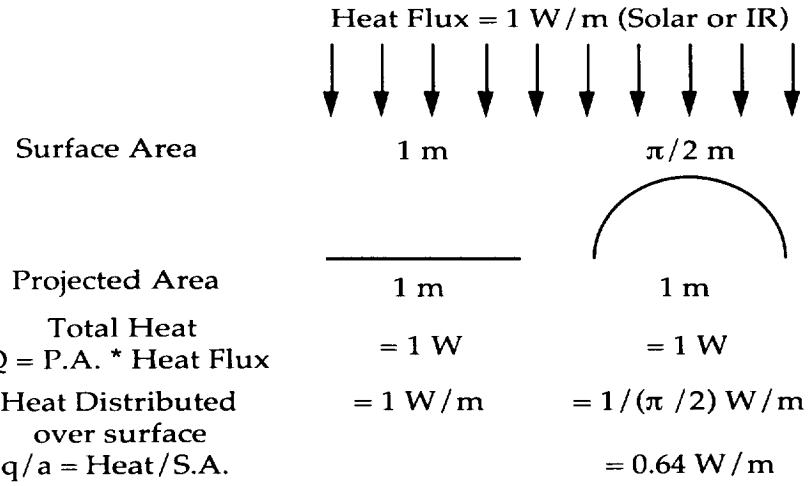

Figure 6.10. Heat Flux Distribution Over Flat and Curved Surfaces.

Each UFRT was charged with 21 grams of water, and was weighed before and after the charging procedure to ensure that the proper amount of water was placed into the tubes. After the test, the tubes were re-weighed. Three of the tubes lost less than 2 grams of water. However, tubes 2 and 5 lost approximately half of their original charge of water (> 10 grams). The amount of water that remained in each UFRT during the test is shown in Table 6.3. Some loss of the water charge was expected during the procedure to vent the NCGs from the UFRTs; however, too much water was inadvertently vented from UFRTs 2 and 5. The Battelle recommendation for the amount of water in each UFRT during operation was 20g. UFRTs 1, 3, and 4 had the required amount of water for the test within ±1g.

Table 6.3. UFRT Water Charge

UFRT	Water Charge Weight (g)		
Number	Before	Test	Loss
1	21	19.1	1.9
2	21.1	9.9	11.2
3	20.9	20.5	0.4
4	21	20.1	0.9
5	21	10.8	10.2

7.0 TEST RESULTS

Multiple analyses were conducted to determine the characteristics of the UFRTs under simulated lunar conditions. The following sections describe the analytical results, including an assessment of the UFRTs using heat pipe theory (Section 7.1), an evaluation of steady-state temperature data from the thermal/vacuum chamber testing (Section 7.2), an analysis of heat leakage from the UFRTs during testing (Section 7.3), and overall results of the test series conducted in the chamber (Section 7.4), including a theory on the potential presence of non-condensable gases (NCGs) or vapor void at the top of the tubes. The last section (Section 7.5) presents a summary of the overall characteristics of the UFRTs based on all of the analyses completed.

7.1 HEAT PIPE THEORY

It is proposed that the operation of the UFRT may be described by modeling the heat transfer and fluid flow behavior using conventional heat pipe analysis. The "radiative heat transfer from a gray-body equations" used came from Wein, Stefan, and Boltzmann (Siegel, 1981). The mathematical description of the fluid and thermal behavior of heat pipes came from Dunn and B&K Engineering. A brief summary of these equations and behaviors is presented in Appendix F.

The heat transfer limits, shown in Table 7.1, have been calculated with the HTPIPE code using the methodology described in the appendix. It is obvious that the UFRT design is limited by the surface area available for radiative heat transfer.

Table 7.1. Thermodynamic Heat Transfer Limits From HTPIPE

Evaporator Temp. (K)	Capillary Limit (W)	Entrainment Limit (W)	Sonic Limit (W)	Boiling Limit (W)	Area Limit (W)
290	21000	5600	5600		28
310	65000	9000	9000		36
330	170000	13000	13000		47
350	395000	19000	19000		59
370	820000	25000	25000		74
390	1555000	32000	32000		91
410	2730000	40000	40000		111
430	4499000	47000	47000		134
450	7032000	55000	55000	84000	161
470	10521000	62000	62000	69000	191
490	15188000	68000	68000	55000	226

7.2 STEADY STATE TEMPERATURE DATA

Observations were made from the raw data, resulting in an evaluation of thermocouple accuracy. Plots of the steady-state data are shown in Appendices G through K for Test Series 1 through 5, respectively. The accuracy of the thermocouples determined whether or not the readings were included in this analysis. The nominal uncertainty of a thermocouple is approximately ±2°C. For the purposes of this analysis, if the thermocouples were within ±3°C, they were considered to be similar. In some cases where 0 W is plotted, this refers to conditions when a UFRT evaporator heater was turned off and it was no longer monitored.

A principle indicator that the UFRTs are operating as a closed system heat pipe is the isothermicity along the condenser length. The temperature distribution, demonstrated in Figure 7.1, is relatively flat, which indicates adequate operation.

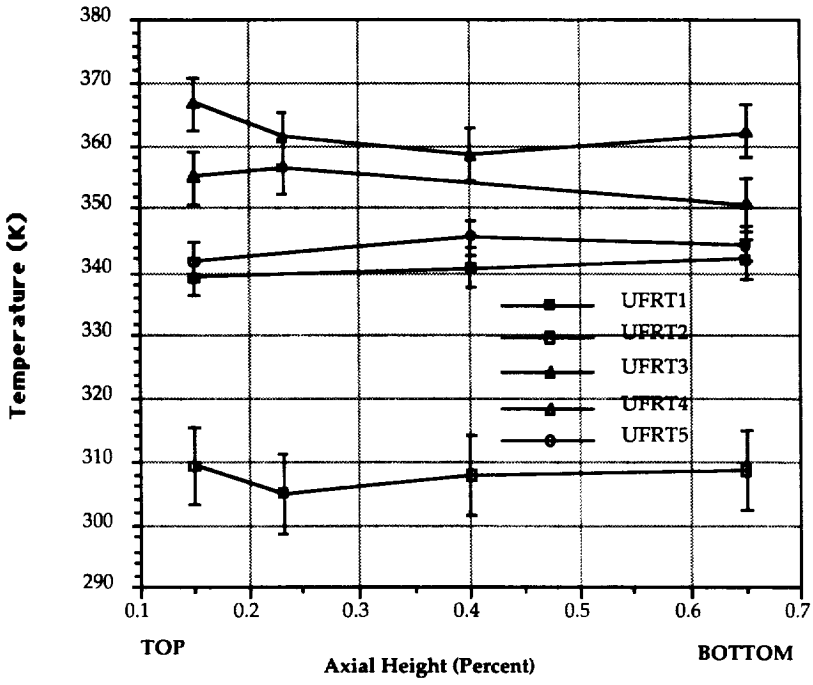

Figure 7.1. Axial Temperature Distribution in the UFRT Condenser Region for Test Point 1C.

The error bands for this figure were derived from an analysis of the thermocouple responses after a steady state frozen condition was achieved before starting Test Series 6. With no IR or solar radiation fields, and no fluid flow within the UFRTs,

the error bands were calculated from the deviation from the average condenser thermocouple responses.

7.2.1 UFRT 1

The surface temperature consisted of an average of the thermocouple readings at positions of 1/4, 1/2, and 3/4 along the condenser section. The surface thermocouple temperature readings consistently read within ±3°C of each other and followed a similar trend for the entire test. For this tube, the tip of the hypodermic thermocouple was inadvertently in contact with the titanium liner surface, and therefore followed the internal temperature. Hence, the hypodermic thermocouple was excluded from the surface temperature calculations. The internal probe was used to measure the internal temperature, while the evaporator end cap thermocouple was used to measure the evaporator temperature.

7.2.2 UFRT 2

UFRT 2 was only used during Test Series 1 and Test Series 3 because of its low water charge after the venting procedure. UFRT 2 dried out in both test series when the evaporator end cap temperature increased above the calibration range of the evaporator thermocouple at approximately 15 W of heat rejection. The average of the condenser section thermocouple readings was used to determine the surface temperature of UFRT 2. Probe temperature represents internal temperature and evaporator end cap temperature was representative of evaporator temperatures.

7.2.3 UFRT 3

In UFRT 3, the condenser section thermocouple readings and the hypodermic thermocouple reading were similar, ±3°C, for all of the test series. Therefore, the average of the condenser surface thermocouples and the hypodermic thermocouple was used as the UFRT condenser section surface temperature. Probe temperature represents internal temperature and evaporator end cap temperature was representative of evaporator temperatures.

7.2.4 UFRT 4

In UFRT 4, condenser section surface thermocouple readings at 1/4, 1/2, and 3/4 measured similar temperatures within (±3°C of each other). The hypodermic thermocouple read consistently halfway between the condenser surface temperature and the internal probe temperature and, therefore, was not used for surface temperature analysis. The average of the condenser surface thermocouples

represents the UFRT condenser surface temperature. The internal temperature probe and evaporator end cap thermocouple reading represent the internal and evaporator temperatures of UFRT 4, respectively.

7.2.5 UFRT 5

In UFRT 5, condenser section surface thermocouple readings at 1/4, 1/2, and 3/4 measured similar temperatures within ±3°C of each other. The hypodermic thermocouple read temperatures between the internal and surface temperatures. Therefore, the hypodermic thermocouple readings were not used to represent the UFRT 5 surface temperature. The average of the condenser section thermocouples was used to represent the UFRT condenser surface temperature. The probe and condenser end cap thermocouples read the same temperatures throughout the test. However, only the internal probe was used to represent the internal temperature of UFRT 5. The evaporator end cap thermocouple represents the evaporator temperature of UFRT 5.

7.3 UFRT Heat Leak Analysis

During the thermal/vacuum test, it was discovered that the amount of heat rejected by the radiating surface was not equal to the heater input. Since an earlier uncertainty analysis showed that the error in heater power measurement is small (Paul, T. H., 1994) and thermocouple error for this test was minimized by applying the lessons learned from a previous test (Graf, J. P. and Keller, J. R., 1994), the difference between heater input power and the heat rejected is assumed to be due to heat leaks. As will be shown in an upcoming section, the heat leak equations developed here are sufficient to correct the problem.

A schematic of a UFRT is shown in Figure 7.2. The main heat rejection surface is the ceramic fabric; however, it is clear that heat may also be rejected from the other components. The heaters have a relatively large surface area and also have the highest temperature in the system. Heat is also lost from the exposed metal areas of the end cap, the holding rings and the evaporator section. An attempt was made to minimize the heat losses from these surfaces by covering them with Mylar; however, due to the high temperature associated with the heaters, the Mylar insulation was degraded and physically changed during testing (possibly melting or oxidizing), thereby reducing its effectiveness. Finally, though not shown here, heat leak to the holding fixtures of the UFRT may also occur.

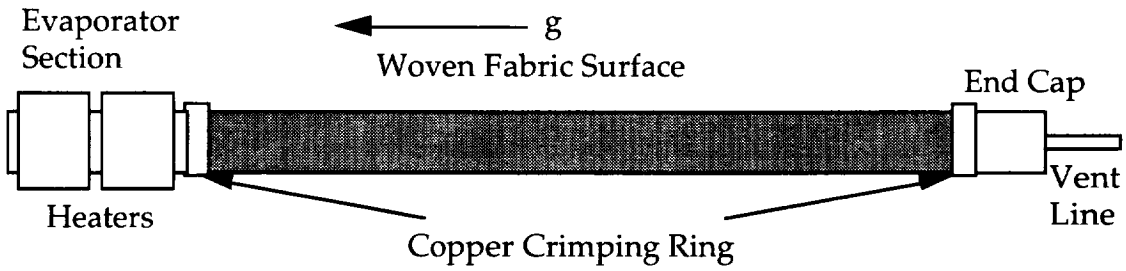

Figure 7.2. Schematic of the UFRT System.

Since the UFRT test was conducted in a vacuum, convective heat transfer did not exist and radiative heat transfer was the primary method of heat rejection. For any surface, the heat loss by radiation is given by:

$$Q = \varepsilon\sigma A_S(T_{surf}^4 - T_{env}^4) \qquad (7.1)$$

where Q, A_S, T_{surf}, T_{sink}, ε, and σ are the heat loss, surface area, surface temperature, environmental temperature, emissivity and Stefan-Boltzmann constant, respectively. The surface area, emissivity, and corresponding radiative heat loss equation for each component are listed in Table 7.2. Since the Mylar was degraded during the test, the emissivity of the heaters was assumed to be double the standard emissivity of a sheet of Mylar. The equation describing the heat loss from the holding rings may overestimate the actual heat leak, since the holding rings are insulated from the condenser by the Nextel fabric. It should be noted, however, that the contribution to the overall heat leak equation by this term is small compared to all the other components. In addition, temperatures associated with this component are the lowest measured in the test (T_{tube} is the coldest component temperature).

Table 7.2. Component Area, Emissivity, and Heat Loss Equation

Component	Emissivity	Area (m^2)	Heat Loss Equation (W)
End Cap	0.30	0.00200	$Q = 6.0*10^{-4}\sigma(T_{tube}^4 - T_{env}^4)$
Heaters	0.10	0.00760	$Q = 7.6*10^{-4}\sigma(T_{heater}^4 - T_{env}^4)$
Holding Rings	0.10	0.00106	$Q = 1.0*10^{-4}\sigma(T_{tube}^4 - T_{env}^4)$
Evaporator	0.30	0.00042	$Q = 1.2*10^{-4}\sigma(T_{evap}^4 - T_{env}^4)$

In addition to radiative heat losses, there were small conduction heat losses to the holding fixtures. The conduction heat losses can be calculated by:

$$Q = (kA/L)^*(T_{evap} - T_{env}) \tag{7.2}$$

where k is the thermal conductivity of the insulation between the UFRT and the holding fixture, A is the conduction area, and L is the thickness of the insulation. For this test set-up, the thermal conductivity was estimated at 0.10 W/m-K (Incropera, F.P. and DeWitt, D.P., 1985), the contact area was estimated at 0.0000806 m^2, and the thickness of the insulation was estimated at 0.001778 m. Substituting these values into equation 7.2 yields the conduction heat loss (in W).

$$Q = 4.6^*10^{-3}(T_{evap} - T_{env}) \tag{7.3}$$

Summing the heat leak equations listed in Table 1 and equation 7.3 produces an overall heat loss equation given by:

$$\begin{aligned} Q_{loss} = {} & 7.6^*10^{-4}\sigma(T_{heater}^4 - T_{env}^4) + 1.2^*10^{-4}\sigma(T_{evap}^4 - T_{env}^4) + \\ & 7.0^*10^{-4}\sigma(T_{tube}^4 - T_{env}^4) + 4.6^*10^{-3}(T_{evap} - T_{env}) \end{aligned} \tag{7.4}$$

As will be shown in a later section, this equation was able to correct the discrepancy between the heat rejected and the heat input.

7.4 UFRT Test Series Steady-State Analysis

The data collected during testing showed that a temperature front moved up the length of the UFRTs during startup. Possible explanations for this phenomena are described below, theorizing the presence of noncondensable gases (NCGs) or a vapor void at the top of the tubes.

UFRTs 1, 3, and 4 exhibited the presence of NCGs or vapor void in the region below the internal temperature probe at specific heat rejection values in each test series. NCG or vapor void presence in the UFRTs was determined by observing the internal temperature, when the internal temperature made a sharp increase of up to 25°C with respect to the surface and evaporator temperatures. At low powers, the temperature front moved past the highest external thermocouple, but remained below the tip of the internal probe thermocouple. As the evaporator heater power was increased, the NCGs or vapor void were believed to pass from below the internal temperature probe to above, as shown in Figure 7.3.

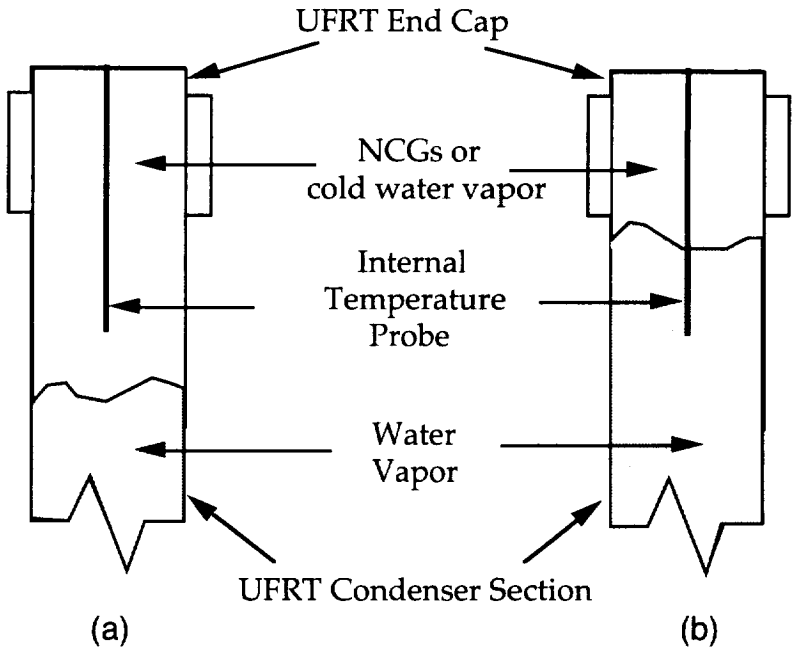

Figure 7.3. NCG or Vapor Void Location Identification.

One explanation for this sheathing of the internal probe thermocouple is that NCGs were liberated from the working fluid. NCGs are initially trapped in the water after it is added to the tubes. Although procedures were employed to attempt to release these NCGs from the water in the UFRTs before testing, as described in Section 6.1.1, there was no adequate method to determine the amount released or still remaining in the tubes. A post-test analysis based on the data in Figure J.1 of Appendix J did result in an estimated concentration of 24 ppm, using the ideal gas law to calculate the amount of air in the top quarter of the tube. This result supports the assumption that NCGs were present during the test.

Battelle personnel have also seen this phenomena in previous testing conducted in their facilities. They described the phenomena at that time using a heat balance theory. As certain heat inputs are provided to the evaporator, only discreet areas are required in the condenser region to radiate the heat from the UFRT, as described in equation F.1 of Appendix F. The remaining interior volume of the UFRT above the radiating area is believed to be filled with a low density vapor void. As the condenser becomes coupled with the evaporator to radiate the input heat load, the temperature front moves up the condenser. Finally, at a given heat load for each test series, the vapor void disappears as the entire condenser area is used.

With either theory, it is clear that there was a presence of NCGs or vapor void. This phenomena was considered in the post-test analyses described in the following sections.

There are two possible methods to evaluate the temperature differences seen in the UFRT test. For the first method, the radiative power can be calculated using equations F.4 and F.5 and thermocouple data collected during the thermal/vacuum tests. The environmental temperatures were determined from thermocouple measurements on an unheated coupon of Nextel fabric in the chamber and further refined by employing a calculated distribution for both the infrared and solar lamps. The UFRT temperatures were averages of the epoxy-mounted thermocouple measurements over the length of the condenser region. The temperature drop was calculated using equation F.6 and the appropriate thermocouple data. The evaporator end cap thermocouple was used to measure the evaporator temperature. The condenser temperature was an averaged reading of the epoxy-mounted thermocouples along the condenser region.

The second method for evaluating the temperature differences used the steady-state test points. The steady-state test points shown in Appendix L were found by taking the steady-state raw data shown in Appendices G-K and subtracting the amount of heat leak (described in Section 7.3) from the evaporator heater power settings to determine for the heat rejected by the condenser section. The condenser temperatures were calculated using the average of the condenser T/Cs as specified in Section 7.2.

The second method's results are presented here because the data correlated well with the post test model (shown in Appendix E). Detailed descriptions of the results and their associated tables and plots are located in Appendix L. These descriptions include a presentation of all of the test points. In the cases where dryout occurred, the highest power setting and internal temperature were noted for each test series. In the remaining UFRTs, the power setting and internal temperature prior to NCG or vapor void passage by the internal temperature probe are shown. The maximum power setting and internal temperatures of each UFRT were also noted. This combined to define the operating range of the UFRTs during this test.

The characteristics of UFRT dryout will be determined using UFRTs 2 and 5. Dryout is characterized by a sharp increase in the evaporator end cap temperature. UFRTs 1, 3, and 4 will be used to characterize the normal operation of the UFRT.

7.4.1 Test Series 1 (Lunar Noon)

UFRTs 1 and 3 followed the same surface and internal temperature trend as shown in Figures L.1 and L.2. However, UFRT 1 surface and internal temperatures were approximately 20°C less than UFRT 3. UFRT 4 had a shallower slope than both UFRTs 1 and 3. All of the UFRTs followed the same trend in the evaporator temperatures as shown in Figure L.3. While evaporator temperatures of UFRTs 3

and 4 were nearly the same, UFRT 1 environmental temperatures were approximately 15°C less than both UFRTs 3 and 4 at all of the power settings.

UFRTs 1 and 3 had approximately the same internal to surface temperature differences, 17°C to 30°C. In nearly the same power range, UFRT 4 had smaller internal to surface temperature differences, 12°C to 23°C, than UFRTs 1 or 2. However, the wicked UFRT (UFRT 3) had almost negligible temperature differences between the evaporator and internal temperatures with a 2°C to 7°C temperature difference range. UFRT 1 was nearly the same as UFRT 3 in evaporator to internal temperature differences with a range of 2.6°C to 9°C. UFRT 4 had much higher temperature differences between the evaporator and internal locations, 14°C to 40°C. The total temperature difference for UFRTs 1 and 3 were approximately 24°C to 40°C. UFRT 4 had a total temperature difference that ranged from 27°C to 50°C.

While remaining within the internal pressure limits, the maximum heat rejection output by UFRTs 1, 3, and 4 in Test Series 1 were 47.7 W, 38.9 W and 49.1 W, respectively. UFRT 2 dried out at the 12.1 W heat rejection with an internal temperature of approximately 320 K. UFRT 5 dried out at 36.9 W heat rejection and 367 K internal temperature.

7.4.2 Test Series 2 (45° Past Lunar Noon)

UFRTs 1 and 3 followed the same temperature trend for surface and internal temperatures as shown in Figures L.4 and L.5. However, UFRT 1 surface and internal temperatures were approximately 16°C less that UFRT 3. UFRT 4 had a shallower slope than both UFRTs 1 and 3. All of the UFRTs followed the same trend in the evaporator temperatures as shown in Figure L.6. While UFRT 3 was the warmest, UFRT 4 was approximately 4°C to 15°C less than UFRT 3 and UFRT 1 was approximately 15°C to 25°C less than UFRT 3.

UFRT 4 had the smallest internal to surface temperature differences of 8°C to 21°C. UFRT 1 had internal to surface temperature differences of approximately 17°C to 26°C. UFRT 3 had the greatest internal to surface temperature differences of 18°C to 38°C. UFRT 3 had almost negligible evaporator and internal temperature differences (1°C to 4°C). UFRT 1 was slightly higher than UFRT 3 in evaporator to internal temperature differences with a 4°C to 12°C range. UFRT 4 had the highest temperature difference between the evaporator and internal locations (18°C to 29°C). The total temperature difference for UFRTs 1 and 3 were approximately 20°C to 40°C while UFRT 4 had a total temperature difference that ranged from 27°C to 50°C.

The maximum heat rejection tested for UFRTs 1, 3, and 4 was 45.6 W, 43.5 W, and 40.5 W, respectively, and maximum heat rejections were limited by the maximum

internal pressure limit. UFRT 2 was not tested. UFRT 5 dried out above the 18.7 W heat rejection and 328K internal temperature.

7.4.3 Test Series 3 (30° Latitude)

UFRTs 1 and 3 followed similar surface temperature trends as shown in Figure L.7 in Appendix L. UFRT 4 had a shallower surface temperature slope and was approximately 10°C less than UFRT 1. UFRTs 1 and 3 followed the same temperature trend for internal temperatures as shown in Figure L.8. However, UFRT 1 internal temperatures were approximately 25°C less than UFRT 3. UFRT 4 had a slightly shallower internal temperature slope than both UFRTs 1 and 3. UFRTs 1 and 3 followed the same trend in the evaporator temperatures as shown in Figure L.9. UFRT 1 was approximately 15°C to 25°C less than UFRT 3. UFRT 4 had a shallower evaporator temperature slope and was located between the evaporator curves for UFRTs 1 and 3.

UFRT 1 had the least internal to surface temperature differences of 11°C to 21°C. UFRT 4 had internal to surface temperature differences of approximately 25°C to 35°C. UFRT 3 had the greatest internal to surface temperature differences ranging from 38°C to 49°C. UFRT 3 had almost negligible evaporator to internal temperature differences of 3°C to 5°C. UFRT 1 was slightly higher than UFRT 3 in evaporator to internal temperature differences with a 7°C to 13°C range of temperature differences. UFRT 4 had the highest temperature difference between the evaporator and internal locations of 23°C to 28°C. The total temperature difference for UFRT 1 was approximately 19°C to 35°C. UFRT 3 had a total temperature difference that ranged from 42°C to 52°C. The total temperature differences were largest for UFRT 4 and ranged from approximately 49°C to 63°C.

The maximum heat rejection for UFRTs 1, 3, and 4 was 43.3 W, 39.5 W, and 42.8 W, respectively, without exceeding the UFRT internal pressure limits. UFRTs 2 and 5 dried out prior to 14.6 W and 18.4 W, respectively, while the internal temperatures were 323K and 337K, respectively.

7.4.4 Test Series 4 (45° Latitude)

UFRTs 1, 3, and 4 followed the same temperature trend for surface and internal temperatures as shown in Figures L.10 and L.11. UFRTs 1 and 4 had approximately the same surface and internal temperatures. However, these UFRTs surface and internal temperatures were approximately 10°C and 20°C less, respectively, than UFRT 3. UFRTs 1, 3, and 4 followed the same evaporator temperature trends as shown in Figure L.12. While UFRTs 1 and 3 were the warmest, UFRT 1 was approximately 12°C to 20°C less than UFRT 3 and UFRT 1.

UFRT 1 had an internal to surface temperature differences ranging from 17°C to 23°C, respectively. UFRT 4 had internal to surface temperature differences of approximately 13°C to 28°C. UFRT 3 had the greatest internal to surface temperature differences of 24°C to 43°C. UFRT 3, had almost negligible evaporator and internal temperature differences, 1°C to 3°C. UFRT 1 was slightly higher than UFRT 3 in evaporator to internal temperature differences with a 2.4°C to 12°C range of temperature differences. UFRT 4 had the highest temperature difference between the evaporator and internal locations, 19°C to 38°C. The total temperature difference for UFRT 1 was approximately 19°C to 35°C. UFRT 3 had a total temperature difference that ranged from 25°C to 45°C. The total temperature differences were largest for UFRT 4 and ranged from approximately 33°C to 65°C.

The maximum heat rejection for UFRTs 1, 3, and 4 was 38.2 W, 44.9 W, and 41.7 W, respectively, without exceeding the internal pressure limits. UFRT 5 dried out at the 22.4 W heat rejection with an internal temperature of 357K.

7.4.5 Test Series 5 (Full Solar)

UFRTs 1 and 3 had nearly the same surface temperature trends as shown in Figure L.13. UFRT 4 had a similar surface temperature trend that was approximately 12°C to 20°C less than UFRT 1. UFRTs 1, 3, and 4 followed the same temperature trend for internal temperatures as shown in Figure L.14. However, UFRT 1 internal temperatures were approximately 8°C to 30°C less than UFRT 3. UFRT 4 internal temperatures were approximately 20°C to 30°C less than UFRT 3. UFRTs 1, 3, and 4 followed the same trend in the evaporator temperatures as shown in Figure L.12. UFRT 4 evaporator temperature was approximately 4°C less than UFRT 3 while UFRT 1 was approximately 12°C to 20°C less than UFRT 3.

UFRT 1 had internal to surface temperature differences of 17°C to 25°C. UFRT 4 had an internal to surface temperature differences of approximately 25°C to 33°C. UFRT 3 had the greatest internal to surface temperature differences of 32°C to 57°C. UFRT 3 had almost negligible evaporator and internal temperature differences, -5°C to 10°C. UFRT 1 was slightly higher than UFRT 3 in evaporator to internal temperature differences with a 5°C to 14°C range of temperature differences. UFRT 4 had the highest temperature difference between the evaporator and internal locations, 21°C to 35°C . The total temperature difference for UFRT 1 was approximately 22°C to 40°C. UFRT 3 had a total temperature difference that ranged from 41°C to 53°C. The total temperature differences were largest for UFRT 4 and ranged from approximately 46°C to 69°C.

The maximum amount of heat rejection for UFRTs 1, 3, and 4 was 43.6 W, 58.0 W, and 32.3 W, respectively, without exceeding the internal pressure limits of the UFRT. UFRT 5 dried out when the heat rejection of 29.5 W was exceeded. The internal temperature of UFRT 5 was 328K at dryout.

7.4.6 Test Series 6 (Maximum Heat Transfer, Frozen Startup, and Transient Step Down)

All of the UFRTs reached a frozen state at an evaporator temperature of less than -20 °C. The heaters were turned on and set to a power setting near the expected maximum heater input power of 65 W. UFRTs 2 and 5 dried out at the high power setting. UFRTs 1, 3, and 4 performance was not affected by the frozen condition, indicating that no damage occurred to the UFRTs during the frozen startup. UFRTs 1 and 4 reached the maximum internal pressure at the 65 W input power setting. UFRT 3 approached the internal pressure limit at the 70 W power setting during the maximum heat transfer case.

UFRTs 1 and 4 started at the 50 W input power, while UFRT 3 began at the 70 W power setting. The input power was then decreased by 10 W every 10 minutes until the input power was 0 W. The purpose of this test was to determine whether ice crystals would form on the UFRT condenser section wall and result in evaporator dryout. This was not shown to occur because the internal temperatures remained above the freezing point of water as shown in Figures 7.4 through 7.6. In addition, the evaporator temperature did not rise sharply as seen in the other dryout situations in this test.

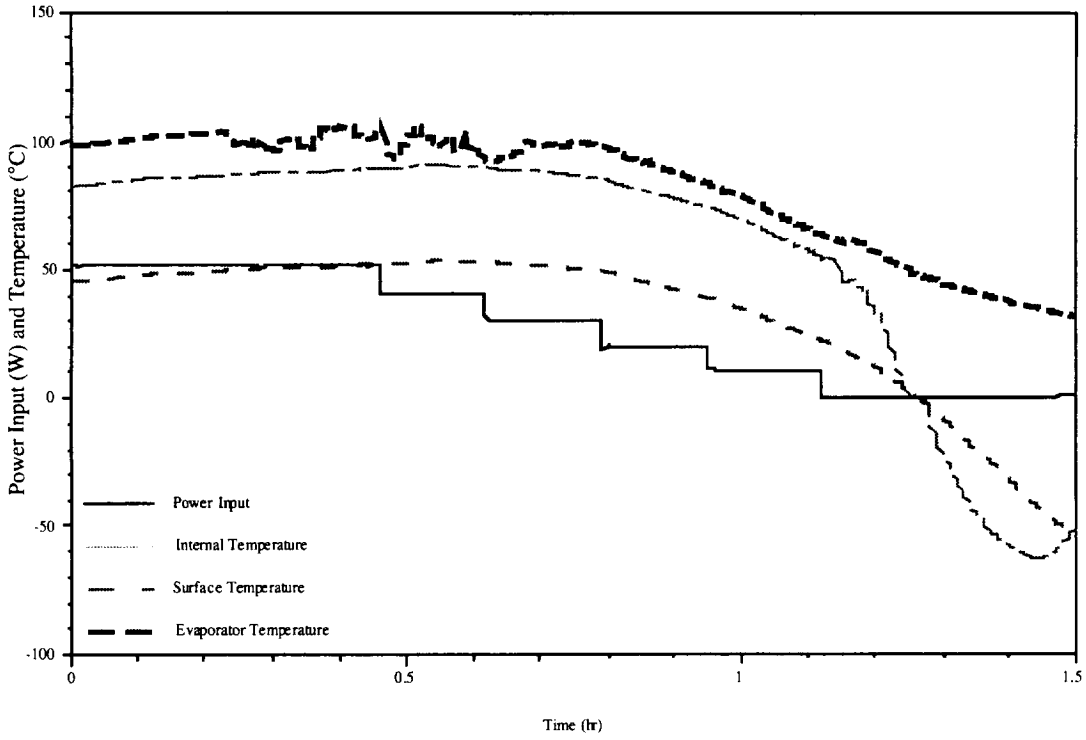

Fig. 7.4. UFRT 1 Transient Step Down Test.

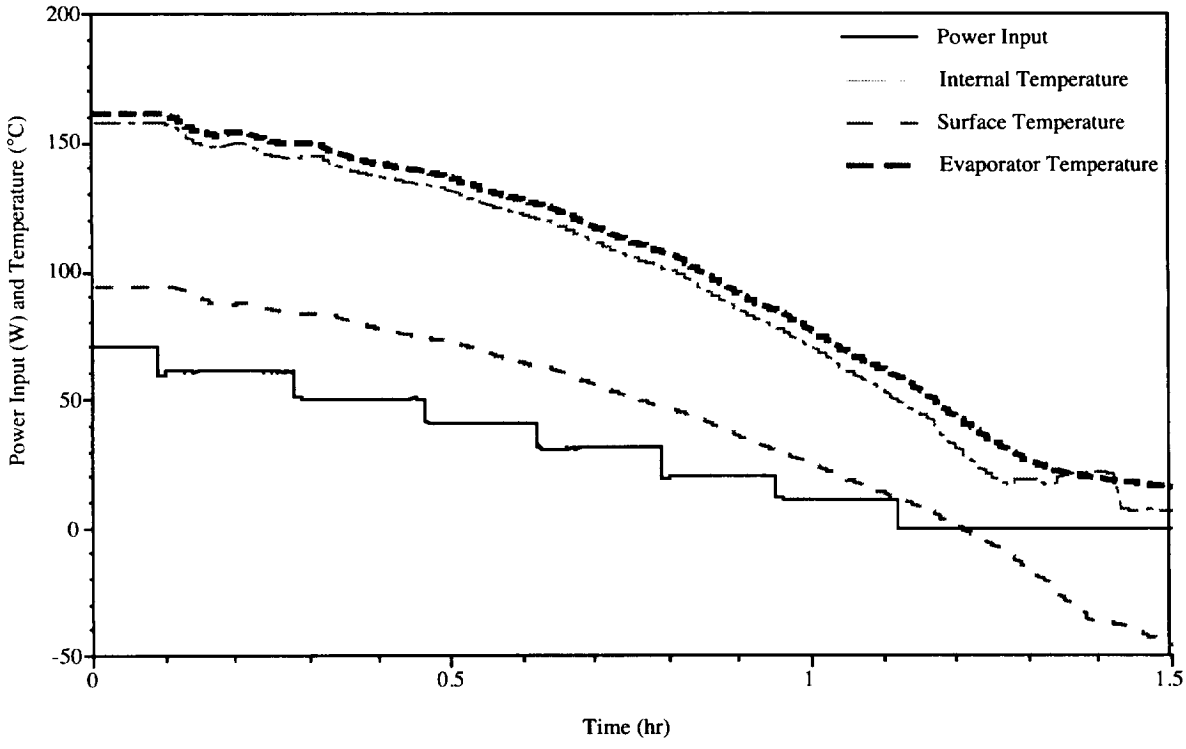

Fig 7.5. UFRT 3 Transient Step Down Test.

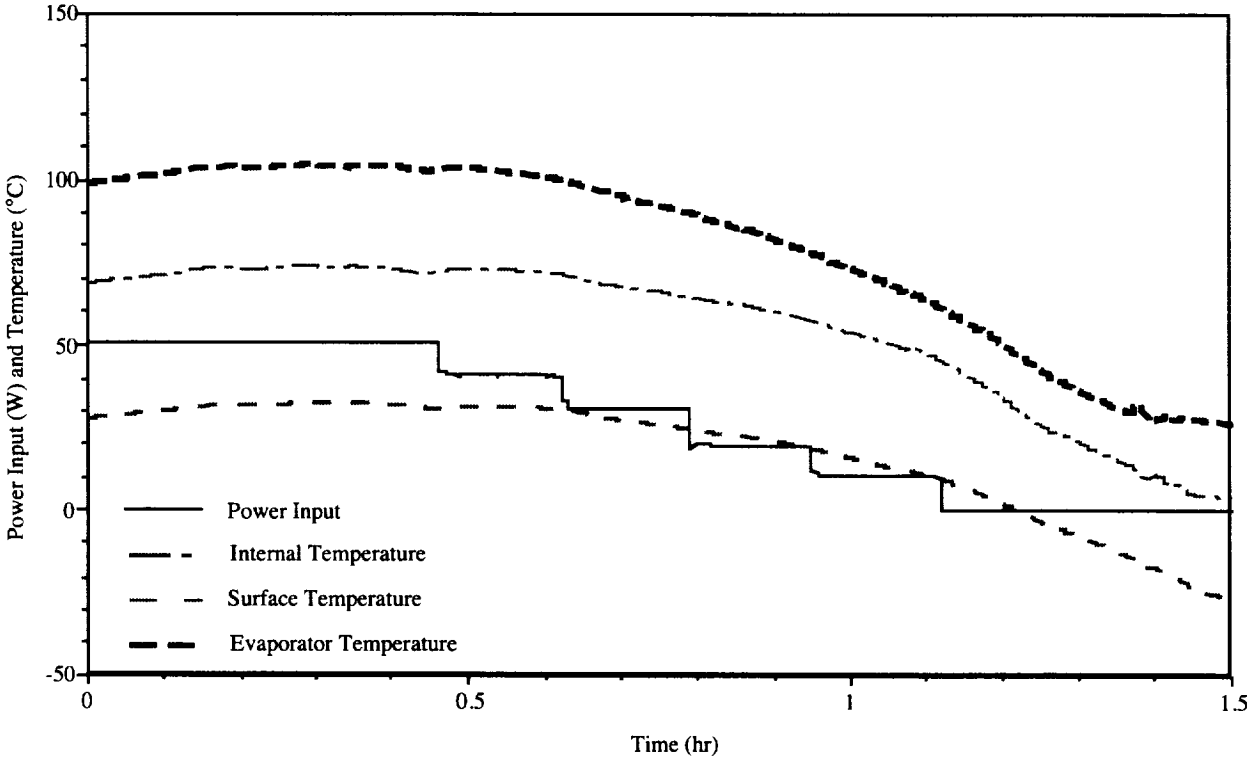

Fig. 7.6. UFRT 4 Transient Step Down Test.

7.5 Steady State Results Summary

7.5.1 UFRT Dryout Characteristics

Examining dryout characteristics of the UFRT was not originally a test objective. However, because UFRTs 2 and 5 were found to have approximately half of the required water charge, as shown in Table 6.3, the UFRT dryout conditions were observable at heat rejection values and internal temperatures that were below the maximum internal pressure of 100 psi.

Near dryout, both UFRTs 2 and 5 exhibited the tendency for surface and internal temperatures to remain nearly constant while evaporator temperatures rose more than 90°C as the power setting was increased. This showed that there was a lack of water in the evaporator to transport the heat to the UFRT condenser section. The two remaining methods of heat transfer that remained, conduction along the titanium walls and internal convection, did not make up for the lack of liquid water in the evaporator. Therefore, the UFRT dryout condition can be defined as a condition where the UFRT evaporator temperature rises at a high rate while internal and condenser surface temperatures remain constant.

For the UFRTs used in this test, it is uncertain exactly at which power setting and internal temperature that each UFRT experienced dryout. This was because the last recorded test point was always just below the heat rejection value that caused the dryout and environmental conditions were different for each test. Therefore, the heat rejection values recorded prior to dryout were noted. The maximum heat rejection value and internal temperature that UFRT 2 dried out at were 14.6 W and 323 K, respectively, as shown in Table 7.3. UFRT 5 dried out at a maximum heat rejection of 37 W and 367K in Test Series 3. In all of the test series, UFRT 5 dried out at a higher heat rejection and internal temperature. UFRT 5 had approximately 1.0 g of water more than UFRT 2, which may increase the UFRT dryout temperatures. Also, UFRT 5 had no wick while UFRT 2 had a wick as shown in Figure 6.3. UFRT 5 may have allowed fluid to traverse the entire evaporator while in UFRT 2, the wick would tend to hold the fluid near the top of the evaporator, thereby hindering removal of the heat from the lower clamp heater.

Table 7.3. UFRT Dryout Conditions

Test Series	UFRT2		UFRT5	
	Heat Rejection (W)	Internal Temperature (K)	Heat Rejection (W)	Internal Temperature (K)
1	12.1	320	36.9	367
2	N/A	N/A	18.7	328
3	14.6	323	18.4	337
4	N/A	N/A	22	357
5	N/A	N/A	29.5	328

7.5.2 Operating Characteristics with NCGs

UFRT 4 operated in what seemed to be an acceptable fashion during the test. However, UFRT 4 did not follow the same trends as UFRT 1 or UFRT 3 in any of the test series. UFRT 4 had a shallower surface and internal temperatures with respect to heat rejection than UFRTs 1 and 3. For example, UFRT 4 typically had higher surface and internal temperatures than UFRT 3 at low heat rejection values and surface and internal temperatures lower than UFRT 1 at higher heat rejection values. UFRT 4 did not correspond to the post test math model calculations shown in Appendix F. UFRT 4 also showed abnormally high evaporator to internal temperature differences, similar to UFRTs 1 and 3 when NCGs or vapor void was presumed below the internal temperature probe. Therefore, it is suspected that significant NCGs or vapor void was present in UFRT 4 during the test.

The result of NCGs or vapor void in the UFRT was a high evaporator to internal temperature difference. The presence of the NCGs or vapor made the internal to surface temperature difference falsely low. However, because the evaporator to internal temperature difference was as high as 40°C, the total temperature difference from evaporator to surface exceeded 50°C for most of the test series.

7.5.3 UFRT Normal Operations

UFRTs 1 and 3 performed as expected as shown in post-test model correlation plots in Appendix F. Except for Test Series 3, the model solutions were within ±5°C of the test series results. Also, the test results had a slightly higher temperature difference than the model from the middle to the outside tubes, as shown in Figures F1 through F5. Both UFRTs 1 and 3 had the same trend as the post-test model.

UFRTs 1 and 3 had very small temperature differences from evaporator to internal temperatures. At the low heat rejections, approximately 20 W, both UFRTs had negligible temperature differences that did not exceed 10°C. However, at the higher heat rejections, the wicked UFRT (UFRT 3) never exceeded 7.0°C temperature difference between the evaporator and internal temperatures while UFRT 1, the wickless UFRT, had maximum temperature differences of not more than 14.0°C. The advantage in evaporator to internal temperature differences is associated with the wicked UFRT, UFRT 3.

UFRT 1 had the lower temperature difference from internal to surface between UFRT 3 and UFRT 1. UFRT 1 temperature difference ranged from 17°C to 30°C for all of the test series. The internal to surface temperature difference for UFRT 3 were within 3°C of UFRT 1 in the first test series. However, as the test series progressed, the internal to surface temperature difference increased from 18°C to 32°C at the 18 W heat rejection values to 33°C to 56°C at the 58 W heat rejection values.

UFRT 1 had the smallest evaporator to surface temperature differences of approximately 20°C to 40°C at the 18 W and 48 W heat rejection values, respectively. UFRT 3 had evaporator to surface temperature differences of 20°C to 52°C at 18 W and 58 W heat rejection values, respectively. If we assumed that the internal to surface temperature differences should be approximately the same, then the internal to surface temperature differences of UFRT 1 and evaporator to internal temperature differences of UFRT 3 can be combined to produce a small evaporator to surface temperature difference savings of approximately 5°C. This would result in a wicked UFRT evaporator to surface temperature difference range of approximately 20°C to 35°C.

7.5.4 UFRT Operations in Various Environments

As can be seen in Table 6.2, most of the simulated UFRT environments on the sun side of the moon varied little, less than 14 K, except for the full solar case, Test Series 5. The difference in temperature environments from Test Series 1, 2, and 4 for the middle tube, UFRT 3, was only 14 K while the environments for the outer UFRT, UFRT 1, was only 6 K. Similarly, during the test, the various environments differed by less than 12 K for both UFRTs 1 and 3. The sun side environments did not vary enough to see a significant difference in the UFRTs operating temperatures or in the heat rejection values. Furthermore, both UFRTs 1 and 3 acted nearly the same in Test Series 1, 2, and 4 due to the similarity of the environments. The test confirmed model results that the sun side environments were similar even with the combination of solar and IR heat input.

The full solar case produced a much lower temperature environment of 232 K. This environment was approximately 70 K lower than any of the cases that used a combination of solar and IR fluxes (Test Series 1-4). This test series confirmed that the UFRTs ran at an acceptable sink temperature in a full solar environment. This case also shows that the IR flux had a much greater influence on the environmental temperatures than did the solar flux, due to the UFRTs' high value of emissivity.

8.0 BENEFIT OF THE UFRT IN A LUNAR BASE THERMAL CONTROL SYSTEM

To assess the potential benefit of the UFRT for future NASA missions, a simple trade study was performed. Total heat rejection system masses were computed for a UFRT radiator and for a state-of-the-art aluminum radiator for the case of a 50 kW lunar base at the equator. This study was a variation on the trade study documented in Ewert, 1993. Since the UFRT could be used alone or in conjunction with other advanced thermal control system (TCS) hardware, four different TCS configurations were considered: heat pump, radiator shade, heat pump plus shade and neither (horizontal low alpha radiator by itself). For each case, the total heat rejection system mass was computed including a "power mass penalty" for power consumed by the system.

8.1 ASSUMPTIONS

Key assumptions in the study were:

- Internal TCS set point is 275 K and there is a 3 K temperature drop at each interface heat exchanger. For example, in the heat pump system, the heat pump evaporator operates at 272 K and lifts the temperature to 377 K in the condenser. Heat is then transferred to the rejection loop fluid at 374 K and to the metal in the radiator at 371 K. The radiator surface temperature, or operating temperature, is the radiator metal temperature minus the "radiator DT" as seen in Figure 8.1. In the systems without heat pump, the rejection loop fluid is 272 K and the metal in the radiator is 269 K.
- Evaporator-to-condenser temperature drop, or "radiator DT," for the current UFRT is 20 K based on test data. Temperature drop for an improved UFRT was assumed to be 3 K. The temperature drop for the state-of-the art flow-through radiator is 1 K. These temperature drops reduce radiator operating temperature and thus reduce heat rejection per unit area.
- 50 kW lunar base located at the equator (worst thermal environment).
- Radiator shade is parabolic and half as tall as the vertical radiator. It has a mass of 1.7 kg/m^2 of radiator area.
- Heat acquisition and transport system masses are not included; they are assumed to be equal for all cases.
- Maximum (and optimum) heat pump lift is 105 K. Heat pump efficiency is 45% of the Carnot efficiency and mass is 8 kg/kW of capacity.
- Effective heat sink temperatures for each case were computed using thermal math models.
- Vertical radiators are two-sided and their mass is computed from the International Space Station Alpha central TCS radiators (9/93 estimates). State-

of-the-art radiator mass is equal to the space station radiator mass which is 16 kg/m^2 of projected (not radiating) area. A breakdown of this mass between panels, manifold, and structure is shown below. It is assumed that the decreased structural requirements due to the availability of the lunar surface for bracing and the increased requirements due to increased gravity cancel each other out. The radiator is deployable; missions which allow an erectable radiator would probably have a lower mass.

- Current UFRT radiator mass is equal to state-of-the-art radiator mass with the radiator panel mass replaced by the UFRT mass of 0.13 kg/tube or 3.11 kg/m^2 of projected area. Improved UFRT mass is based on concepts by Battelle which would eliminate the ceramic fabric and decrease the tube size to reduce mass to 1.12 kg/m^2 of projected area. Mass breakdown is (kg/m^2):

	State-of-the-art	Current UFRT	Improved UFRT
panel without manifolds	5.08	3.11	1.12
panel manifolds	1.19	1.19	1.19
deployment structure & base	9.72	9.72	9.72
Total	16.00	14.00	12.00

No credit was given to the UFRT structure mass due to the lower panel mass since deployment structure mass is driven more by its own mass and stiffness requirements than it is by panel mass. Improved structures are not considered here as they are a separate development effort which could be applied to either an aluminum or UFRT radiator panel. There may be some additional structural benefit with the lighter UFRT panels, but that is beyond the scope of this study.

- The "neither" case uses a one-sided horizontal low alpha radiator with absorptivity (α) = 0.1. Since this radiator is one-sided, it can be closer to the ground and it should require less support structure than the vertical radiators. Therefore, its mass was arbitrarily assumed to be 3 kg/m^2 less than the vertical radiators.
- Emissivity is 0.89 for the UFRT as measured at JSC in July 1994. Emissivity and fin efficiency are 0.90 and 0.92 respectively for the state-of-the-art radiator.
- UFRT view factor to space (no fins) for the tested spacing is 0.93 which takes the place of the fin efficiency for the state-of-the-art radiator.
- The power mass penalty used for the heat pump is 22 kg/kW per Lewis Research Center for daytime power using an advanced solar photovoltaic power system.

Other assumptions can be found in Ewert, 1993.

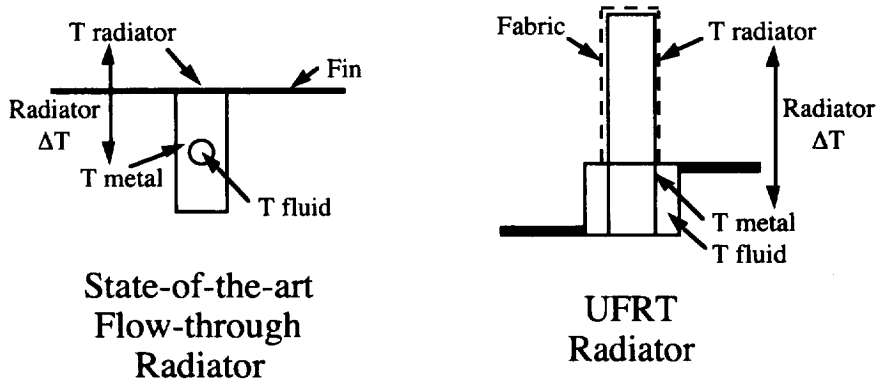

Figure 8.1. Radiator Surface Temperature.

8.2 TRADE STUDY RESULTS AND DISCUSSION

Table 8.1 shows the result of the trade study for the heat pump (H/P), radiator shade, heat pump plus shade (both) and radiator alone (neither) cases. The current UFRT increases, rather than decreases, the heat rejection system mass compared to the state-of-the-art radiator for all 4 cases considered. The primary reason for this is the large temperature drop through the UFRT which reduces radiator operating temperature. In a hot thermal environment such as the moon, this is a substantial penalty. The mass savings due to the UFRT were not enough to outweigh the increased radiator area required. While the reduction in radiator panel mass was 39% due to the UFRT, the reduction in overall radiator mass (including structure) was only 13%, pointing out the need to work on improving the radiator structure as well as the panels.

Table 8.1. Results of Trade Study

HEAT REJECTION SYSTEM MASS SUMMARY(KG)	50 kW SYSTEM			
	H/P	SHADE	BOTH	NEITHER
STATE OF THE ART	3320	3490	2553	6468
CURRENT UFRT	4464	5963	2767	13965
IMPROVED UFRT	2904	2863	2306	4820

Assuming that the conductance between the titanium liner and the radiator surface can be reduced, an overall temperature drop through the UFRT of 3K would be reasonable. Using this assumption along with projections for lower mass tubes, the trade study results for an improved UFRT do show a mass savings compared to the state-of-the-art radiator for all 4 cases. The heat rejection mass savings range from 10% for the "both" case to 25% for the "neither" case.

9.0 CONCLUSIONS

This report documents that the major objectives for the FY94 UFRT program have been successfully accomplished. Six UFRTs, with the titanium liners, were manufactured and provided to JSC in July 1994. Five of the delivered tubes were tested successfully in a thermal/vacuum chamber under simulated lunar conditions in September 1994.

The thermal/vacuum chamber testing explored three different operating characteristics of the UFRT: dryout, operations with NCGs or vapor void, and normal operations. The UFRT dryout characteristic was defined as a rapid evaporator temperature rise while the internal and surface temperatures remained constant. In the dryout comparison of UFRTs 2 and 5, it can be seen that the wicked UFRT (UFRT 2) dried out at a lower heat rejection and internal temperature than UFRT 5. The results of this test also showed that the wickless UFRT (UFRT 5), with a slightly higher water charge, had better dryout characteristics than the wicked UFRT.

When NCGs or vapor void were present in the UFRTs, a high temperature difference existed between the evaporator and internal temperatures. The UFRTs still operated with the NCGs or vapor void present. However, the penalty for UFRT operation with NCGs or vapor void was a high temperature difference between the evaporator to surface temperature of approximately 70°C at the high power settings.

UFRTs 1 and 3 operated as expected and correlated well with the post-test model. The overall evaporator to condenser surface temperature difference was smallest for UFRT 1 (no wick), which was 20°C to 40°C at the 18 W and 48 W heat rejection values, respectively. The wicked UFRT (UFRT 3) had evaporator to surface temperature differences of 20°C to 50°C at the 18 W and 58 W heat rejection values, respectively. Combining the best characteristics from both UFRTs (UFRT 1 - internal to surface; UFRT 3 - evaporator to internal), the best evaporator to surface temperature difference can be as low as 20°C to 35°C at the 18 W and 48 W heat rejection values, respectively.

In addition to characterizing the UFRTs, the thermal/vacuum chamber testing demonstrated the successful buildup and operation of a test stand for this purpose. However, the test team did compile a list of "lessons learned," included in Appendix M, to be considered for future UFRT tests.

The test data obtained in this program also supported a trade study to compare a UFRT radiator to a state-of-the-art aluminum radiator (Section 8.0). The study did show that the UFRT design could achieve as much as a 25% mass savings in the heat rejection subsystem of future planetary-type TCSs.

10.0 REFERENCES

Ewert, M. K., 1993, "Investigation of Lunar Base Thermal Control System Options," 23rd International Conference on Environmental Systems, Colorado Springs, Colorado, SAE Technical Paper #932112.

Graf, J.P., and Keller J.R., 1994, "UT Lunar Radiator Shade Concept Chamber E Thermal Vacuum Test Final Report," report submitted to NASA Johnson Space Center, JSC-38083, ADV-122.

Guenther, R. J. et al., 1992, "Fiscal Year 1992 Annual Report for the Bubble Membrane Radiator Project," report submitted to NASA Johnson Space Center under Contract DE-AC06-76RLO 1830.

Incropera, F.P., and DeWitt, D.P., 1985, Fundamentals of Heat and Mass Transfer, John Wiley and Sons, New York.

Paul, T.H., 1994, "Lunar Radiator Parabolic Shade Experimental Sink Temperature Uncertainty Analysis," report submitted to NASA Johnson Space Center, LESC-31112, CTSD-1736.

Pauley, K. A. et al., 1993, "Design and Test of Ultralight Fabric Reflux Tubes," Proceedings of the Tenth Symposium on Space Nuclear Power and Propulsion, Institute for Space Nuclear Power Studies, University of New Mexico, Albuquerque, New Mexico.

APPENDIX A
BATTELLE DESIGN DRAWINGS FOR UFRT WITH TITANIUM LINERS

Part Name	Number	Battelle Drawing No. and Description	Material
UFRT Overall Design	1	Titanium Ultralight Reflux Tubes for August 1994 Testing at NASA Johnson Space Center, DV Archer, 7/2/94	See Below
Preform	1	Copper Preform for Heat Pipe, LL King, 11/7/91	Titanium, ASTM B338, Grade 2
Liner	1	Titanium Liner for UFRT, DV Archer, 6/25/94	Titanium as formed from ASTM B338, Grade 2
Inner Copper Sleeve	2	SK No. 1044, Reflux Tube Crimping Rings, 1/21/92	Copper
Outer Copper Sleeve	2	SK No. 1044, Reflux Tube Crimping Rings, 1/21/92	Copper
End Cap	1	Titanium UFRT End Caps, DV Archer, 7/3/94	Titanium
End Cap with Port	1	Titanium End Cap (With Hole), DV Archer, 3/14/94	Titanium
Ceramic Fabric	1	Titanium Ultra-light Reflux Tubes for August 1994 Testing at NASA Johnson Space Center, DV Archer, 7/2/94	Nextel 312
Internal Wick	1 or 0	NA	SiO_2
Spring	1 or 0	NA	Spring steel

APPENDIX B
QUALIFICATION TEST PLAN FOR THE FY94 UFRT DESIGN

TEST PURPOSE

The qualification test will be conducted to:

- verify the FY94 UFRT design capabilities, including operating pressure, condenser and evaporator temperatures, and power through-put
- provide test experience which may improve the operability of the thermal/vacuum testing of the UFRT design
- quantify individual thermal phenomena during the operation of the UFRT design which may aid in the interpretation of data collected during thermal/vacuum testing

A successful test would include the following elements:

- successful charging and startup
- operation of the URFT up to the minimum ambient atmospheric operating temperature 377K (104°C)
- general isothermicity over the condenser length during steady state operation
- pressure containment throughout the test
- successful shutdown without pressure anomalies at the conclusion of the test

TEST DESCRIPTION

The following procedures have been developed to conduct the qualification testing of a single UFRT prototype. This design does not incorporate a wick structure in the evaporator region. The current design specifications are summarized in Table B.1.

Table B.1. FY94 UFRT Design

Evaporator		Condenser	
Length	5.1 cm	Length	101.92 cm
Inner Diameter	2.54 cm	Inner Diameter	2.54 cm
Wall Thickness	304.8 μm	Liner Wall Thickness	63.5 μm
Material	Titanium	Fabric Wall Thickness	560 μm
Evaporator Surface	////////////////////	Liner Material	Titanium
Length	7.62 cm	Fabric Material	AlB_2SiO_2
Outer Diameter	2.54 cm	Working Fluid	////////////////////
Surface Roughness	Smooth	Fluid	Water
Material	N/A	Volume	20 cc

Test Equipment

The qualification test will require a single instrumented prototypic UFRT. The required instrumentation includes bare-wire thermocouples, a sheathed thermocouple, a pressure transducer, and two 100-watt clamp heaters. An infrared camera with a liquid nitrogen feed will also be used to image the test article. The digital data will be collected using a personal computer-based data acquisition system. A 1/3 psi check valve will be used to prevent UFRT collapse during the test.

Test Procedure

The test will map the performance of the UFRT test article between 104°C (220°F) and 166°C (330°F). An outline of the test procedures will consist of the following activities:

- Set up IR camera with liquid N_2 feed.
- Install 5 thermocouples: 2 at evaporator, 1 at condenser tip (insulate), 1 internal at condenser end, and 1 placed on the condenser fabric.
- Install heaters and insulate evaporator.
- Estimate/calculate amount of water required for fill.
- Obtain about 100 cc of distilled/deionized/degassed water.
- Set up reflux tube in vertical position using the Chamber E mounting bracket, with the evaporator region on the bottom.

- Use the following procedure to charge the tubes: (1) fill the UFRT will an argon cover gas; (2) place 25 cc of water in the UFRT; (3) add heat to the heater clamps until boiling occurs; (4) vent water vapor until solid vapor is sustained at the end port; and (5) close fitting on end port.
- Determine the final charge amount by weighing the UFRT (plus instrumentation) both before and after the completion of the charging procedure.
- Test between 104°C (220°F) and 166°C (330°F), evaluating the temperature profile with both thermocouples and IR camera (use the latter for axial as well as circumfrential temperature profile measurements, and record on VHS tape) to ensure isothermal performance. Also use the data acquisition system to record power, pressure, and temperatures measured with thermocouples.
- After testing, turn off heater power and again crack condenser fitting to prevent collapse of tube as temperature/pressure drops below about 110°C (230°F).
- Drain water (options: check reflux tube internals with boroscope; remove all water and pressurize with dry inert gas for shipment to JSC).
- The procedure will be repeated for the second UFRT design.

Data Collection

Data will be collected using a personal computer-based data acquisition system. The parameters of interest include temperatures at various locations, internal pressure, and heater power. The temperatures will be measured at the evaporator endcap, the evaporator surface, the condenser internal, and the condenser surface.

The infrared camera will also be used to determine the temperature of various surfaces by inputting an assumed emittance for the material. This feature will be used to calibrate the condenser surface thermocouple.

TEST LOCATION

The test will be conducted in the 306W Building, 300 Area, Pacific Northwest Laboratory. The room is a high bay, which creates difficulties in maintaining a constant heat transfer coefficient during the operation of the UFRT prototype. This issue will be addressed by the use of shields to minimize the effects as much as possible.

Other test locations were explored at the Pacific Northwest Laboratory. Several vacuum chambers were visited with the intention of providing minor modifications to accommodate the UFRT test article. However, it was determined that the cost of modifications would exceed the budget allocated for this task.

APPENDIX C
QUALIFICATION TEST RESULTS FOR THE FY94 UFRT DESIGN

The thermal qualification test was conducted on a prototypic UFRT (UFRT 1) in order to insure both the integrity and functionality of design. The test was considered successful if the following criteria were met:

- Successful charging and startup
- Operation of the UFRT up to the minimum ambient atmospheric operating temperature (104°C (220°F))
- General isothermicity over the condenser length during steady-state operation
- Pressure containment throughout the test
- Successful shutdown without pressure anomalies at the conclusion of the test

UFRT 1 was tested at Battelle in air in a vertical position on June 17, 1994 using two clamp-on heaters. The test sequence consisted of heating the UFRT in a vertical (thermosyphon) orientation to establish power capabilities and ensure pressure containment. Power was increased in 25 W increments, starting with 125 W and increased to a maximum of 175 W. At the maximum power level of 175 W, the UFRT temperatures were close to 411 K (280°F) and the corresponding pressure should have been about 0.3 MPa (50 psia). The pressure transducer did not function properly. Power was thereafter decreased to 50 W, and the pressure sensor connection attachment fitting was cracked open to prevent reflux tube collapse from ambient atmospheric pressure. Power was then completely turned off and data acquisition terminated. Throughout the test, an infrared (IR) camera was used to determine whether the heat rejection was isothermal along the condenser region. Total testing time was about 80 minutes. Following a cool-down period, the water was removed, the UFRT was filled with argon gas to 0.3 MPa (45 psia), and it was packaged for shipment to JSC. The thermocouple and power response for the qualification test is shown in Figure C.1.

- The non-condensable gas venting procedure during startup worked well (IR photography showed uniform temperatures along entire condenser length during operation). It is estimated that << 1 g of fluid was lost from the tube during the 1 to 2 minutes of "steaming" with the tube open to atmosphere. The UFRT was weighed before final assembly and addition of water, but was not reweighed after the test.

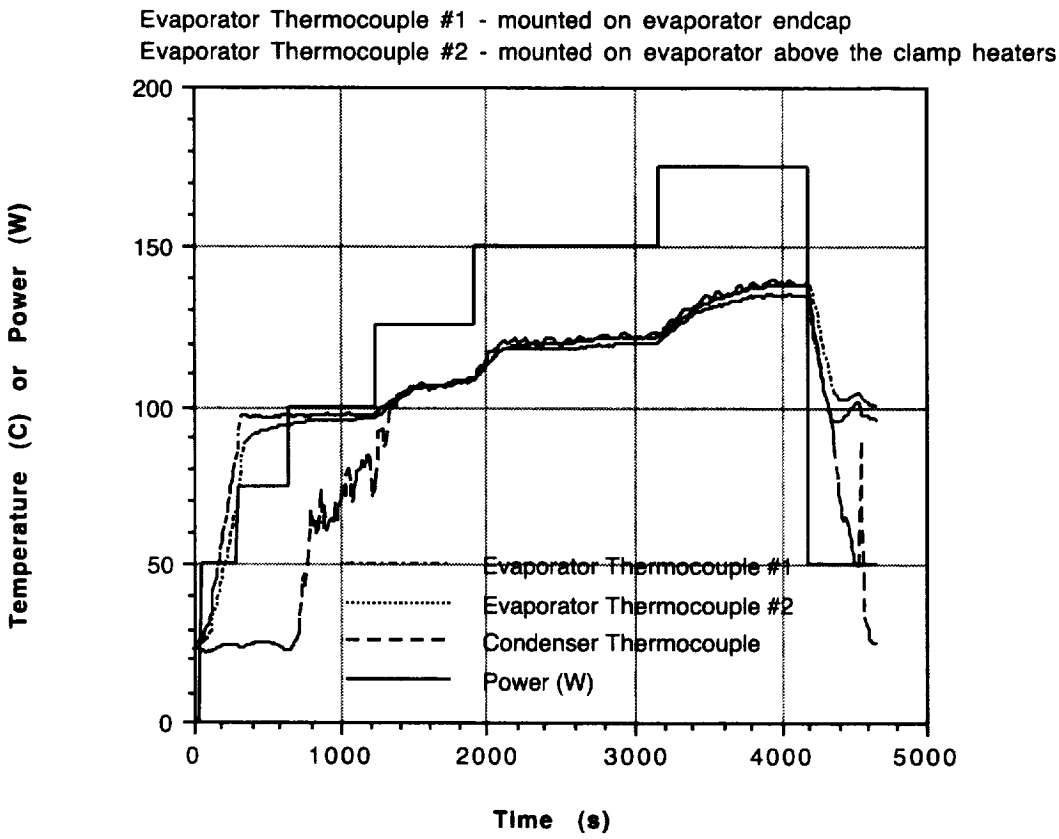

Figure C.1. Thermocouple and Power Data From the UFRT Qualification Test.

- At the highest power lever (175 W) the fabric surface temperatures were about 22 K (36°F) less than the condenser vapor temperatures. This temperature drop is based on an assumed emittance for the Nextel fabric of 0.93 (used by the IR camera) that was well matched by thermocouple readings. For example, at 150 W, the condenser thermocouple indicated 375.6 K (216.7°F), while the IR camera showed 375.0 K. In tests conducted by Battelle on previous UFRTs with copper liners, the temperature drop was less than 10K under similar conditions. This increase in temperature difference is ascribed to the increased thermal resistance from the uneven quality of the Nextel sleeve, and poorer contact with the condenser from a looser fit of the fabric over the liner and/or the expected lower yielding of the titanium into the fabric after pressurization. This is an area for further investigation and optimization.

The UFRT design was tested to 175 W without failure or loss of heat rejection capability. No problems were encountered with the Nextel/Ti heat pipe operating in the vertical (reflux) mode other than some evaporator liquid dryout. Test data indicate that this heat pipe, operating in a space (non-convective) environment will not be performance-limited, but will reach radiative limits well before reaching other thermodynamic limits.

APPENDIX D
UFRT VENTING PROCEDURE DESCRIPTION

Since the UFRTs were filled in atmospheric conditions, air may have been trapped inside the tubes. If this non-condensable gas (NCG) is not removed before testing is begun, the heat rejection performance of the UFRTs may be severely degraded. Therefore, a venting procedure was developed and is shown below. The equations used to determine venting time are listed in the second section of this Appendix.

1) Open UFRT vent valves to the chamber.
2) Heat the UFRT to 25°C, as indicated by the evaporator thermocouple temperatures.
3) With the vent valves open to the chamber, begin pump down. Maintain the UFRT temperatures at 25°C.
4) When the chamber pressure reaches 10.4 kPa (1.5 psia), the UFRT vent valves are shut while the pump down of the chamber continues. It is essential that the pressure in the UFRTs always be greater than the chamber pressure. While the saturation temperature associated with 25°C is only 3.2 kPa, this higher pressure will ensure that boiling does not occur allowing a substantial amount of working fluid to be lost.

Steps 1 through 4 are used to reduce the amount of air in each UFRT tube by removing air and by reducing the pressure of the air above the liquid water. By reducing the overall pressure of the tube, the amount of air in solution will be reduced.

5) Once the chamber pressure drops below 3.5 kPa (0.5 psia), turn the UFRT heaters off and continue pump down to vacuum conditions.
6) Allow the water in the UFRTs to freeze. From Battelle calculations, freezing will be completed when the end cap temperature drops below 255.2 K.
7) Once freezing has occurred, open each UFRT one at a time and vent for 20 minutes.

Steps 5 through 7 are used to eliminate the air above the frozen solid. After these steps, the only air remaining is that air which is trapped in the solid matrix.

8) Turn of the heaters and melt the ice. The ice will be melted when the internal temperature probe reaches 20 to 25°C.
9) Once the internal temperatures reaches 20 to 25°C, hold the water at this temperature for one hour.

Step 8 and 9 are used to liberate the air remaining in the solid and liquid and ensure it is in the top portion of the condenser section. In other words, this vigorous boiling and condensation process pushes all the NCGs to the top of the condenser section.

10) Vent each UFRT for one second.

Since all the air in each UFRT is at the top of the condenser section, the venting associated with step 10 eliminates the final NCGs.

The concentration of the air in the water (in ppm) can be calculated by the following equation (Paul, T. H., 1994):

$$x = P/H \qquad (D.1)$$

where P is the pressure of the gas above the liquid in atmospheres and H is Henry's constant. Henry's constant varies with temperature and the value of this constant for various temperatures is listed in Table D.1. Equation D.1 indicates the lower the pressure of the gas above the liquid the lower the concentration of water in the gas.

Table D.1. Values of Henry's Constant at Different Temperatures

Temperature (°C)	H
0	43200
50	94600
100	107000

Once freezing has been completed and the air above the solid vented, the only air remaining in the system is that which is trapped in the solid. After the solid is melted and vigorous boiling is present, the NCGs will be pushed to the top of the UFRTs. The volume occupied by the NCGs can be calculated from the ideal gas law.

$$PV = nRT \qquad (D.2)$$

where P, V, n, R, and T are the pressure, volume, number of moles, ideal gas constant, and temperature, respectively. The pressure and temperature will correspond to those of the saturation condition in the UFRT.

Once the volume of the tube occupied by the NCGs is determined, the final vent time can be determined. Since the UFRTs vent to a vacuum and the pressure in the UFRTs will be nearly constant due to the heater input, the flow process can be described by the choked flow equation found in any standard thermodynamics textbook [2] and the vent time is simply the volume divided by the volumetric flow rate. For the problem at hand the vent time is approximately 0.2 sec; however, since the pneumatic valves can only cycle in one second, this time was chosen as the vent time.

APPENDIX E
UFRT TSS/SINDA THERMAL MODEL DESCRIPTION

Geometric modeling of the test was performed using the TSS. Chamber E was modeled as a closed cylinder. A parallel light source entered through a one-way transparent surface at the end opposite from the chamber door as shown in Figure E.1. The UFRTs were placed side to side in an array as shown in the figure. The UFRTs were placed on 10.16-cm centers with the entire UFRT array being 43.18 cm across. The UFRTs were placed near the chamber E door as shown. The model included the test stand that held the UFRTs in place. The mylar that covered the pneumatic valves was simulated using a flat plate located above the UFRTs and between the UFRT and the chamber door as shown in Figure E.2. The IR was input from eight 40.6-cm x 1.6-cm plates arranged four between the UFRTs and the solar beam and four between the UFRTs and the Chamber E door as shown in Figure E.2. The location of these lamps also simulated the solar shadowing that existed during the test. An additional four 12.7-cm x 1.6-cm IR plates were located at on both edges of the UFRT array as shown. The optical properties of the materials used in the TSS solid model are listed in Table E.1.

Table E.1. Material Optical Properties

Material	Absorptivity	Emissivity
Nextel fabric	0.20	0.89
Titanium	0.50	0.14
Copper	0.35	0.04
Chamber walls	0.95	0.95
IR surfaces	1.00	1.00
Steel	0.50	0.15
Aluminum	0.22	0.47

The UFRT model environment was adjusted to mirror the conditions and chamber E test environment as shown previously in Tables 6.1 and 6.2. To simulate the chamber E cold walls, the simulated cold walls were set to 120K. The IR panels provided IR to the UFRTs and were varied for each test series as shown in Table E.2. To simulate the planetary conditions, a diffuse IR was emitted from the flat plates that simulated the IR lamps. The maximum IR applied to the main and side flat plates was 22.63 W/m^2 and 56.58 W/m^2, respectively. The parallel light source simulated the solar heat impinging on the UFRTs and was set as shown in Table E.2. The maximum solar constant (solar = 1.0) used was 1,370 W/m^2.

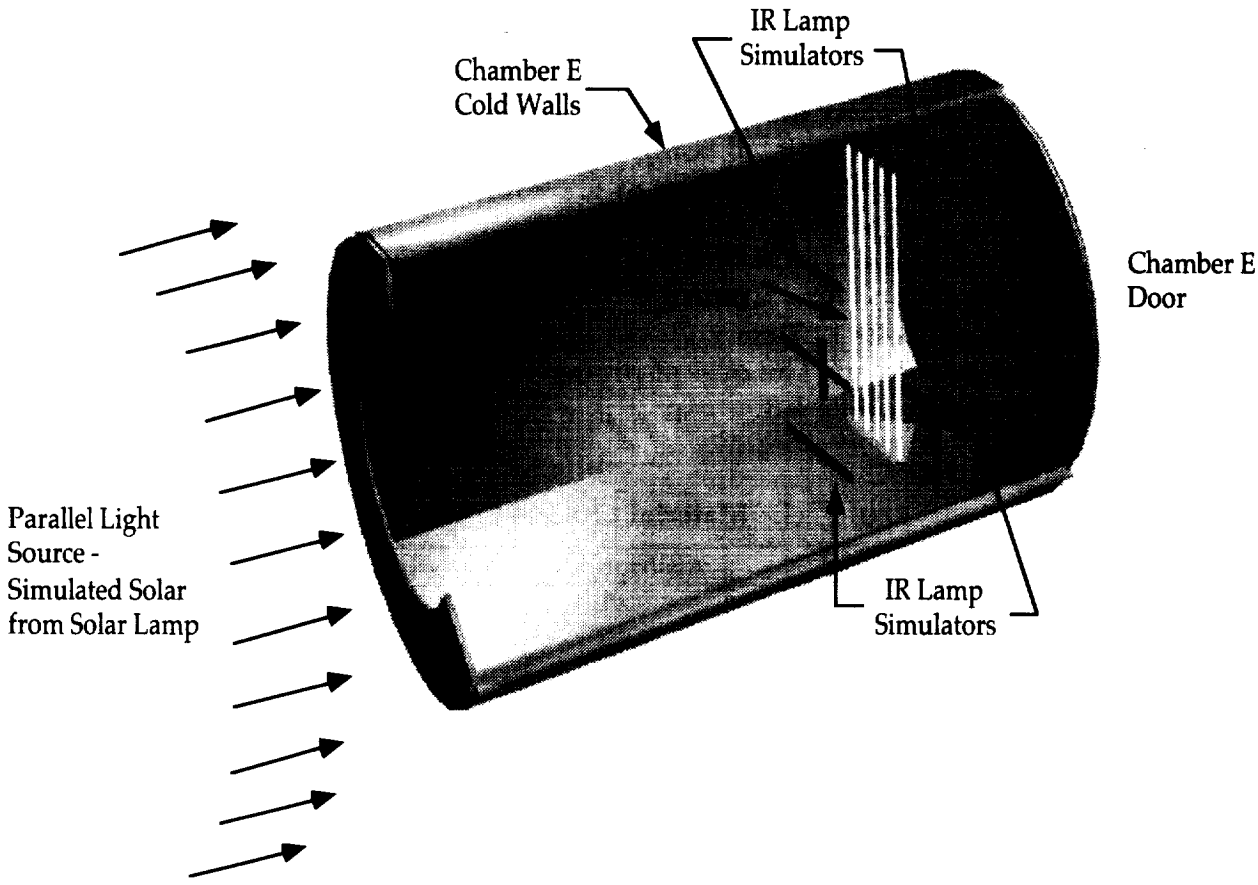

Figure E.1. UFRT Post-Test Thermal Model.

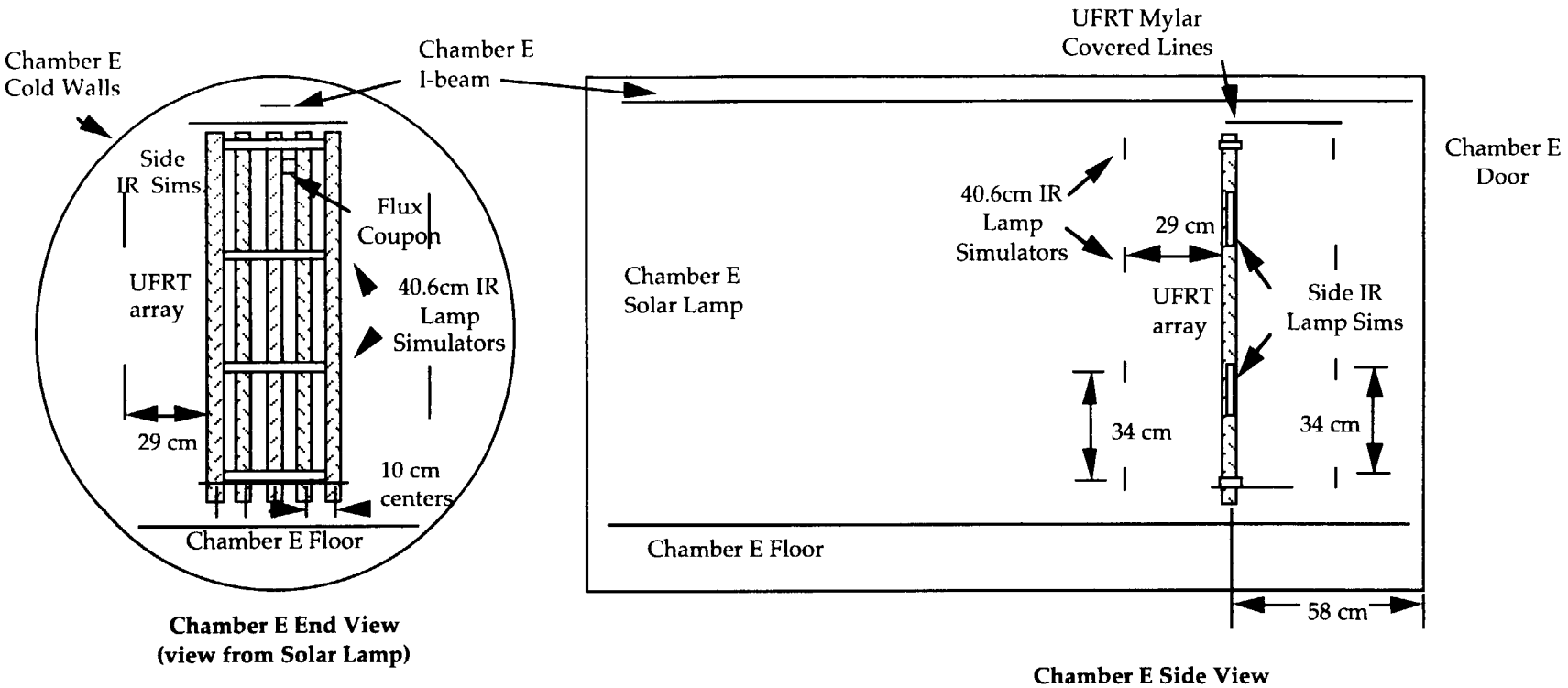

Figure E.2. UFRT Model Chamber E Configuration

Table E.2. Chamber E IR Lamp and Solar Settings in Thermal Model

Test Series	Sim. Solar (W/m2)	Flat Plate IR Output (W/m2)	
		Main	Side
1	0.00	22,630	16,972
2	0.00	18,135	33,944/56,575
3	685.00	33,945	33,945
4	973.00	16,120	16,972
5	1370.00	0	0
6	0.00	0	0

Each UFRT condenser section was divided into 16 nodes, 4 lengthwise and 4 circumfrentially. These 16 surface nodes were connected in the SINDA model to one center node. Because of the titanium's high conductivity and 2-mil thickness, no discernible temperature difference would be seen between the inner and outer titanium wall. Therefore, the heater node of each UFRT was attached to the Nextel fabric. The Nextel fabric conductivity of $0.015 \frac{W}{m\text{-}K}$ was used to connect the interior of the Nextel fabric to the UFRT surface nodes. This conductivity represented the contact conductance between the titanium and the Nextel fabric in addition to the Nextel conductance.

Heat was applied to the central node until the assigned temperature of the node was reached. Then, the steady state temperature condition of the tube was known. The sink and surface temperatures of the Nextel fabric were extracted from the SINDA model. The sink temperature was obtained using the heat input into the heater node, Q, and the Nextel surface temperature in the following equation:

$$T_{sink} = (T^4_{surf} - \frac{Q}{\sigma \varepsilon A})^{0.25} \qquad \text{(E.1)}$$

The model containing a 7.6-cm x 7.6-cm flux coupon was placed between UFRTs 2 and 3 as shown in Figure E.2 to give an indication of how the UFRT environments compared to the flux coupon temperatures. The flux coupon had a Nextel fabric facing the solar lamp and an aluminum side facing the Chamber E door in the TSS model. In the SINDA model, a node was placed in between the two surface nodes and the temperature of that node was allowed to reach steady state without any heat input. The conductivity of the Nextel fabric was used to connect the surface of the Nextel to the central node, while a high conductivity was assigned to the aluminum side due to its negligible thermal resistance.

Only the condenser section was analyzed for the heat rejection paths. The exposed area of the copper band and titanium end cap at the top represented only 3% of the entire exposed area. The evaporator section was also excluded because its portion of the UFRT was covered with heaters and MLI and was not exposed to the chamber during the test.

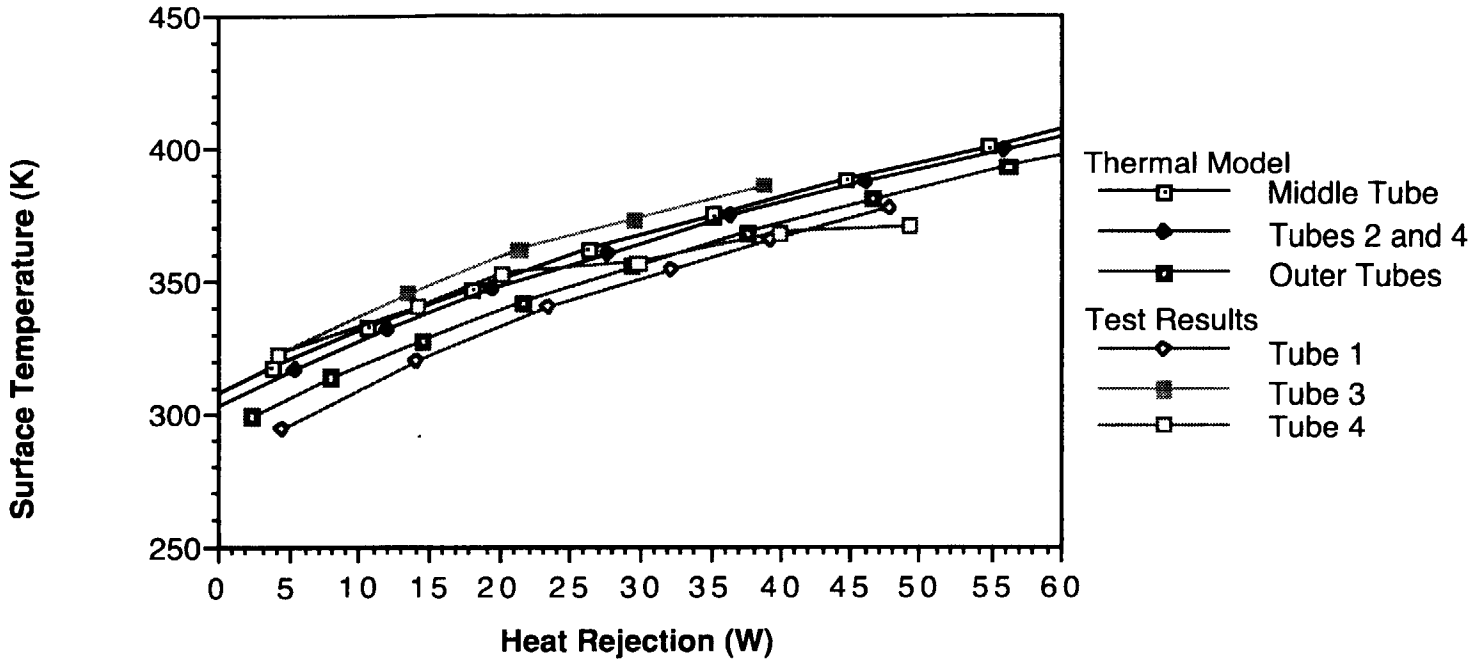

Figure E.3. UFRT Surface Temperatures, Series 1.

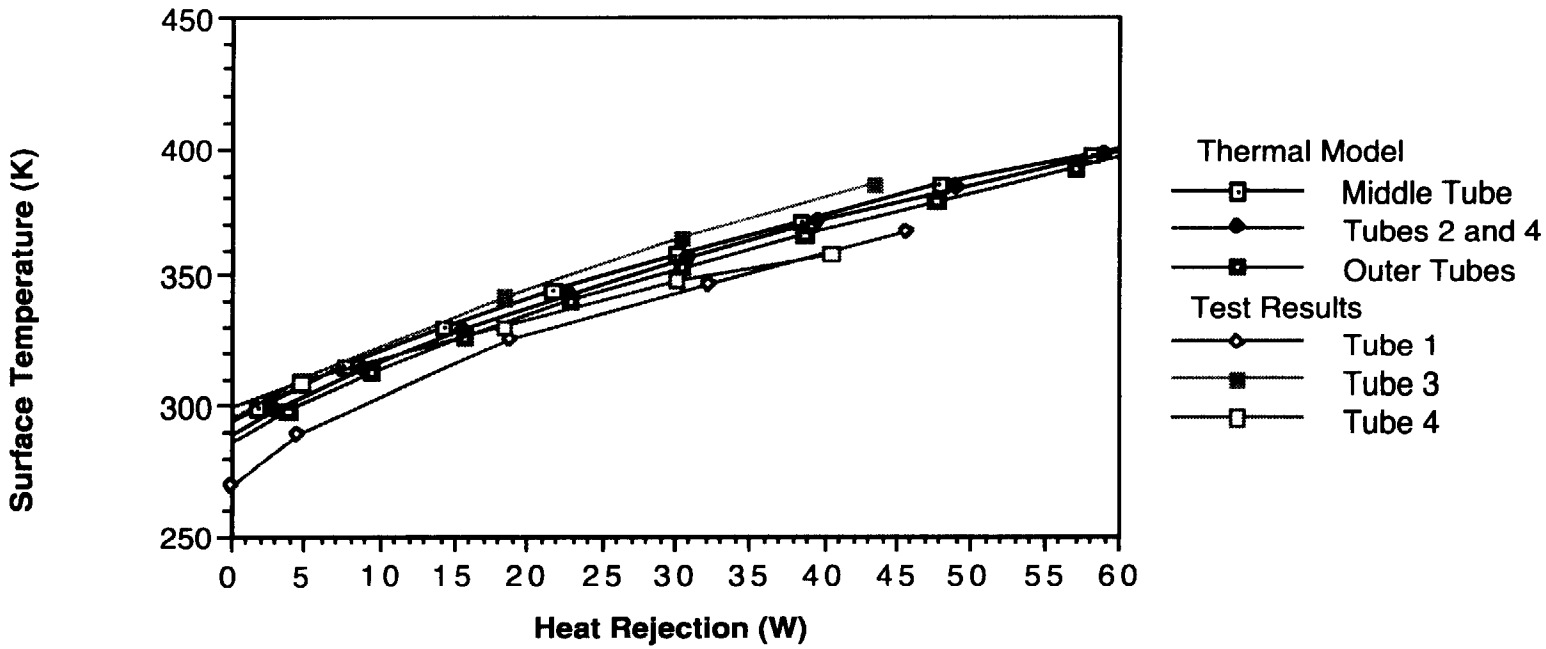

Figure E.4. UFRT Surface Temperatures, Test Series 2.

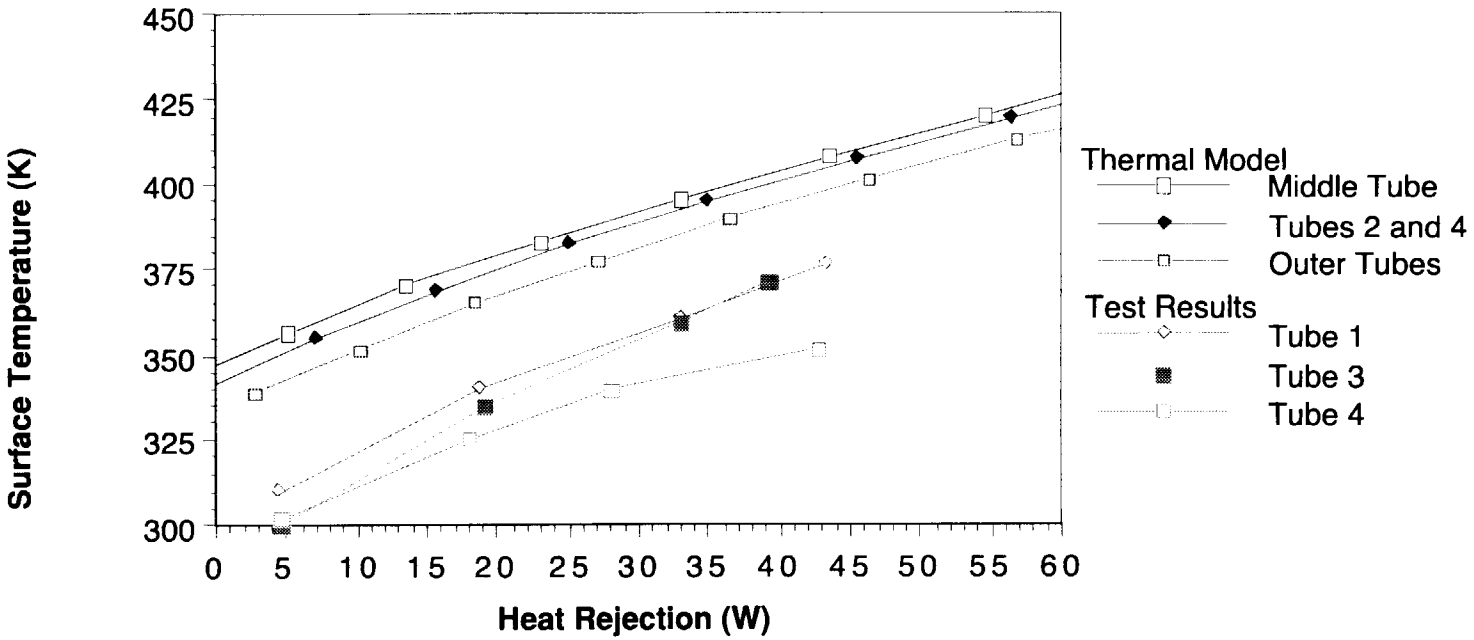

Figure E.5. UFRT Surface Temperatures, Test Series 3.

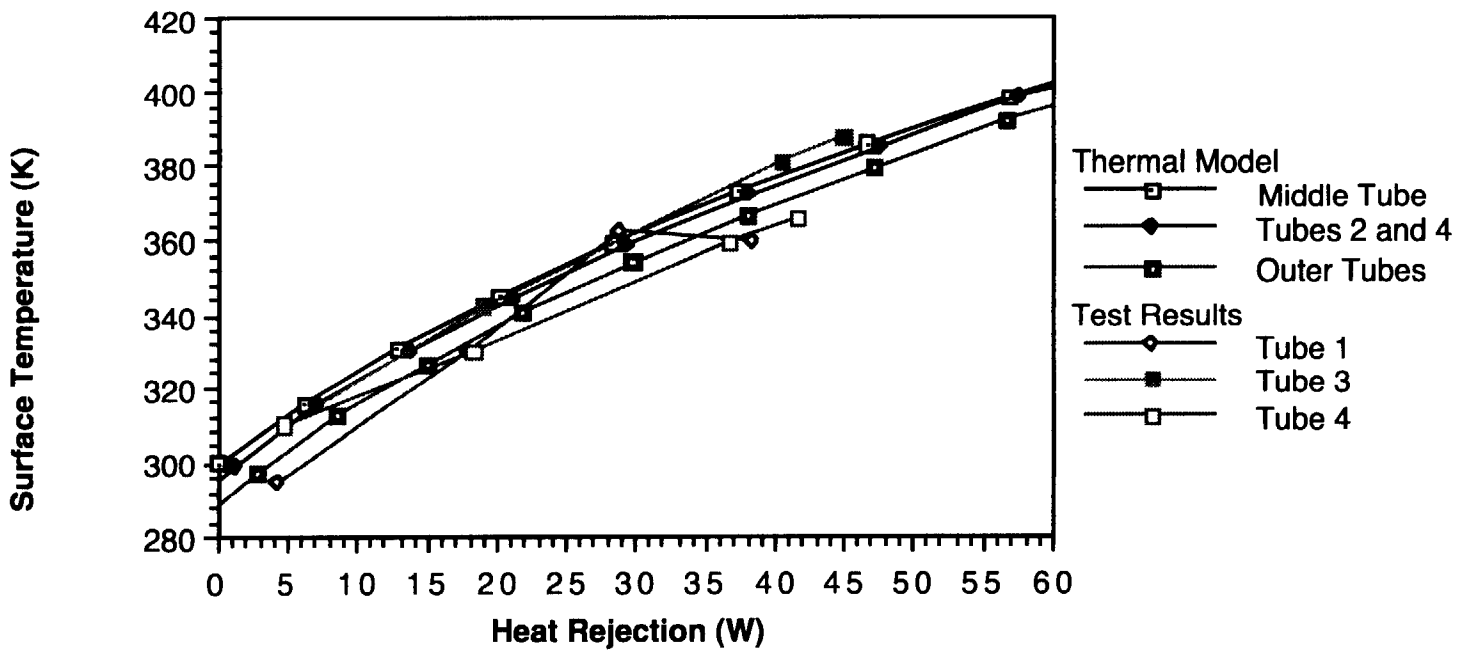

Figure E.6. UFRT Surface Temperatures, Test Series 4.

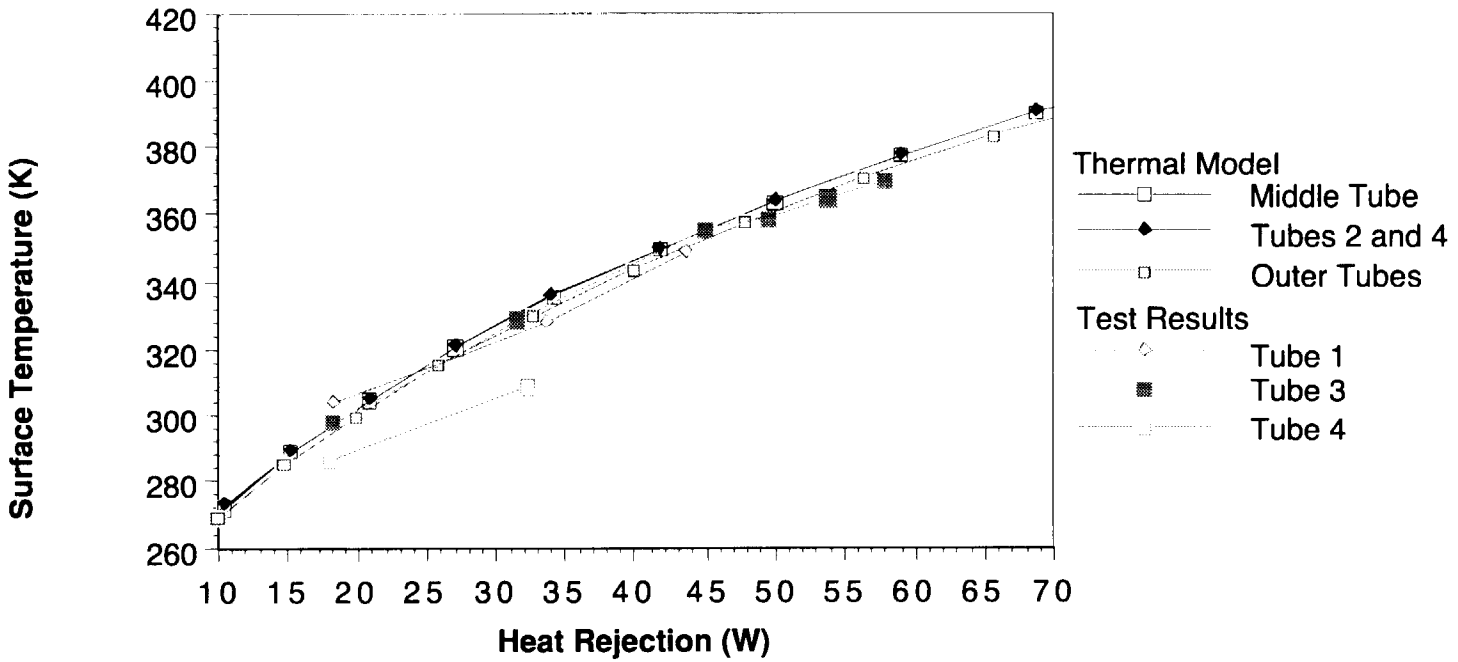

Figure E.7. UFRT Surface Temperatures, Test Series 5.

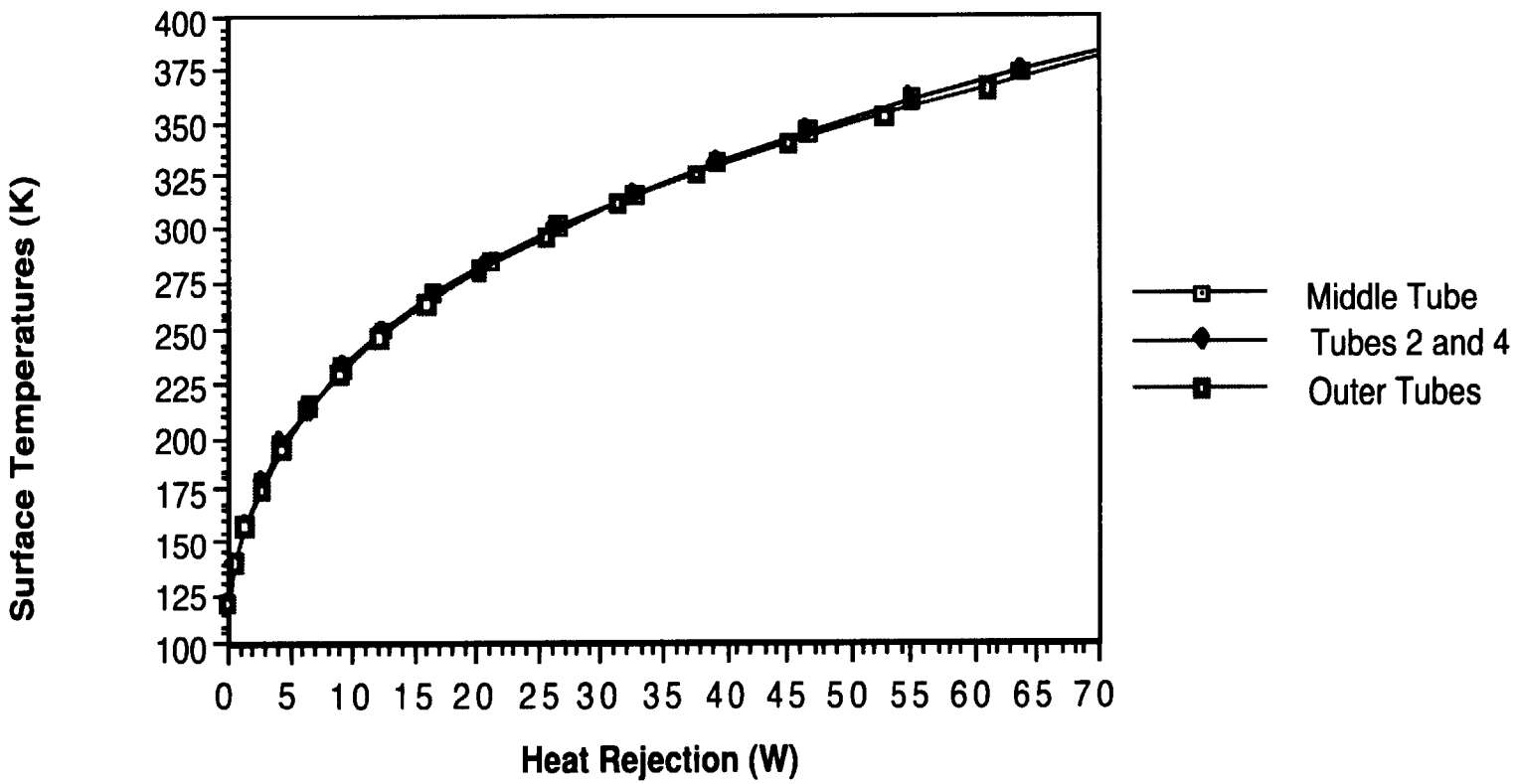

Figure E.8. UFRT Surface Temperatures, Test Series 6.

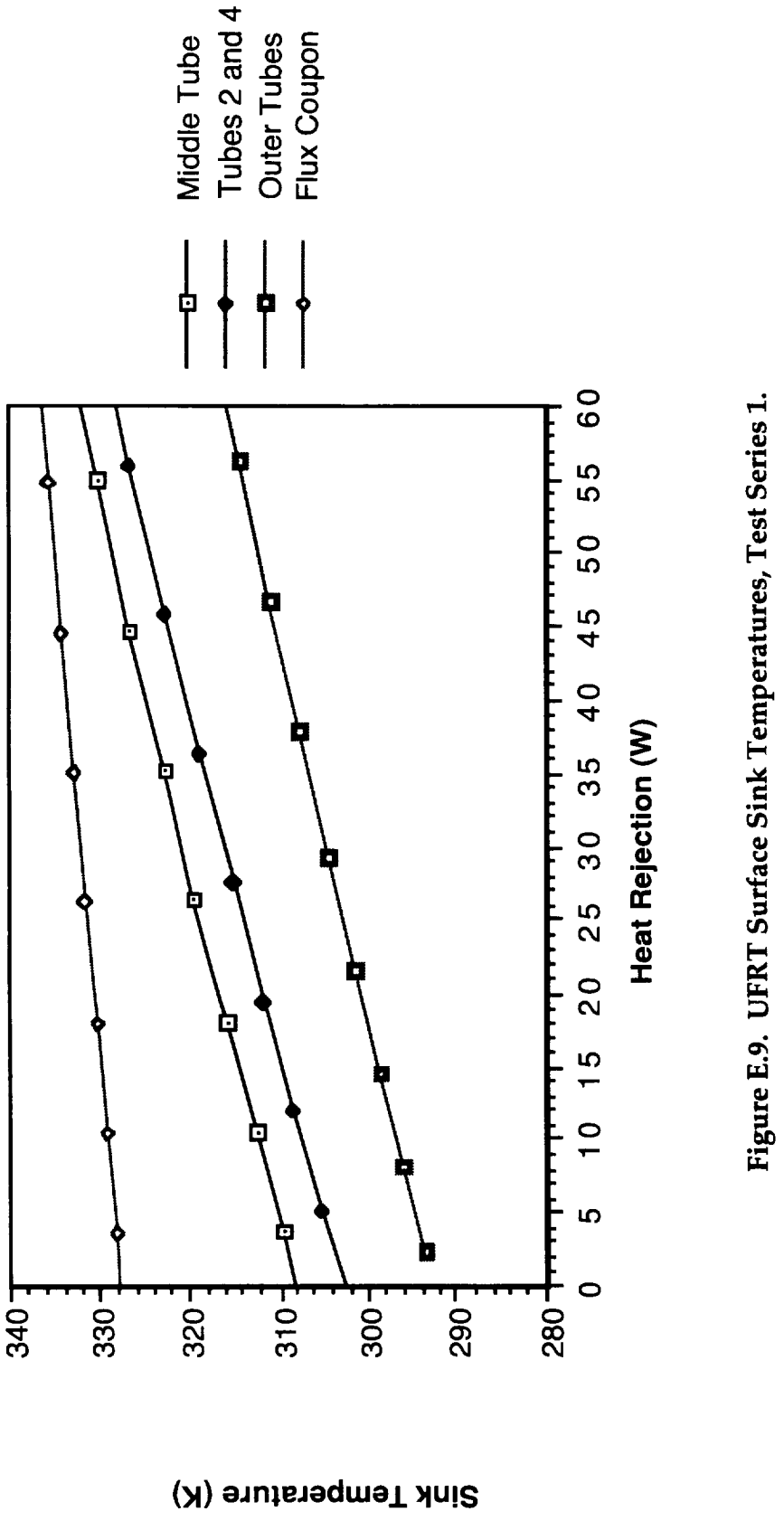

Figure E.9. UFRT Surface Sink Temperatures, Test Series 1.

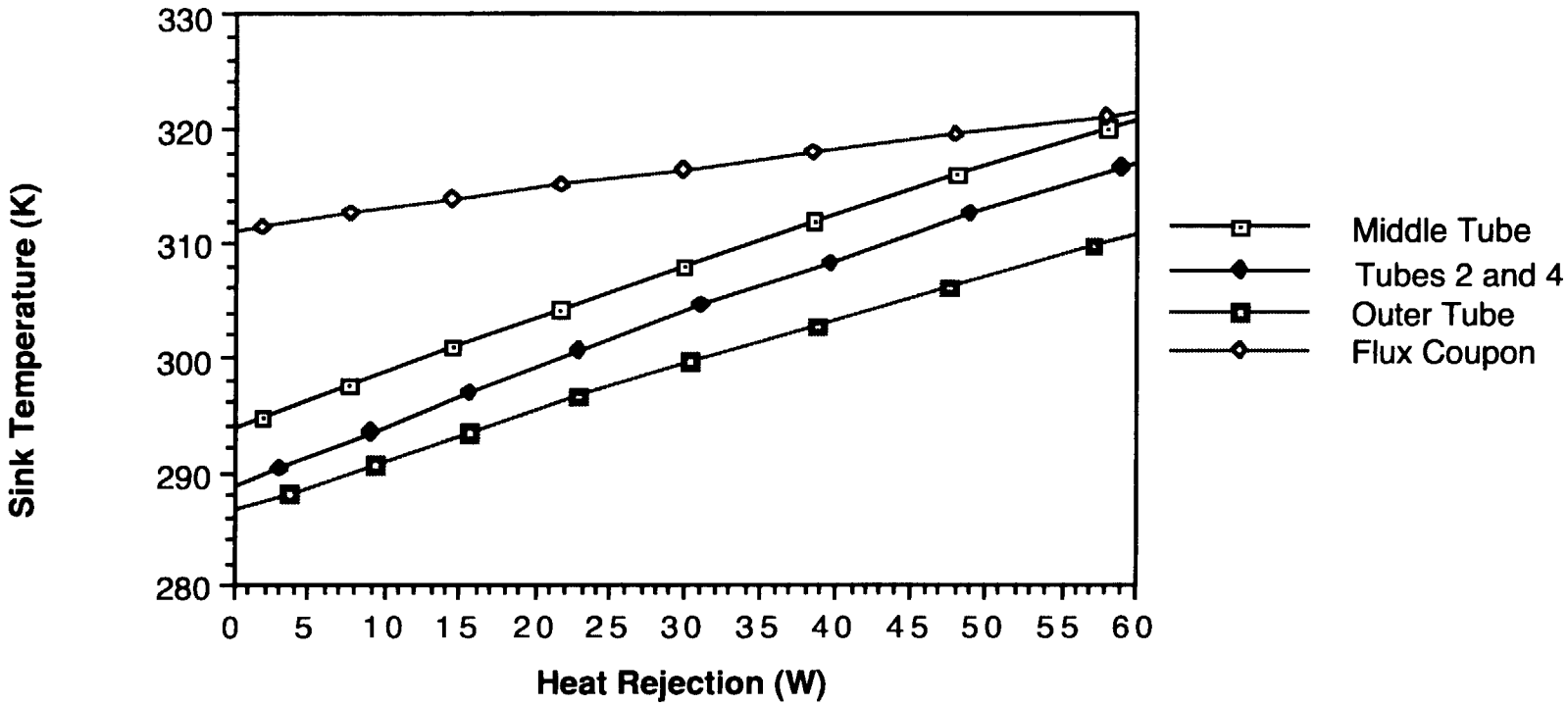

Figure E.10. UFRT Surface Sink Temperatures, Test Series 2.

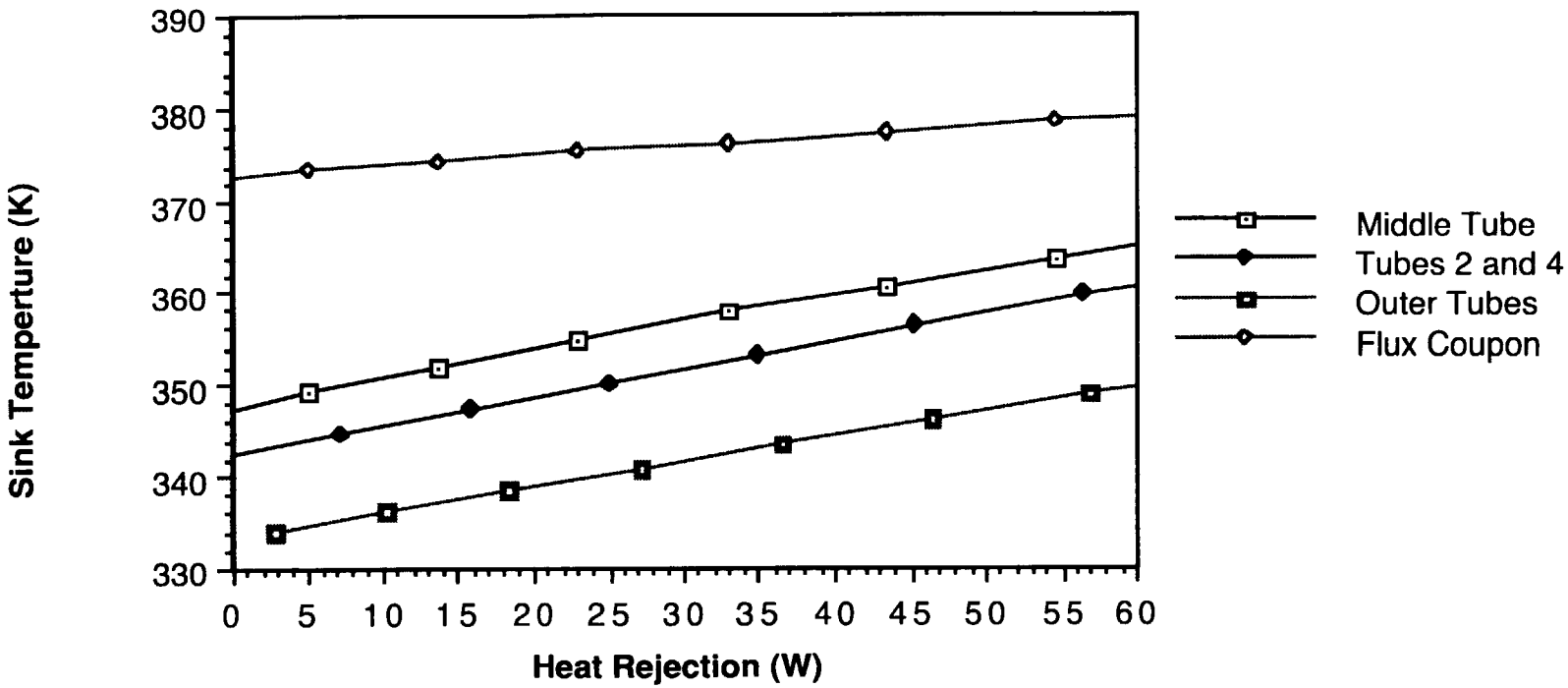

Figure E.11. UFRT Surface Sink Temperatures, Test Series 3.

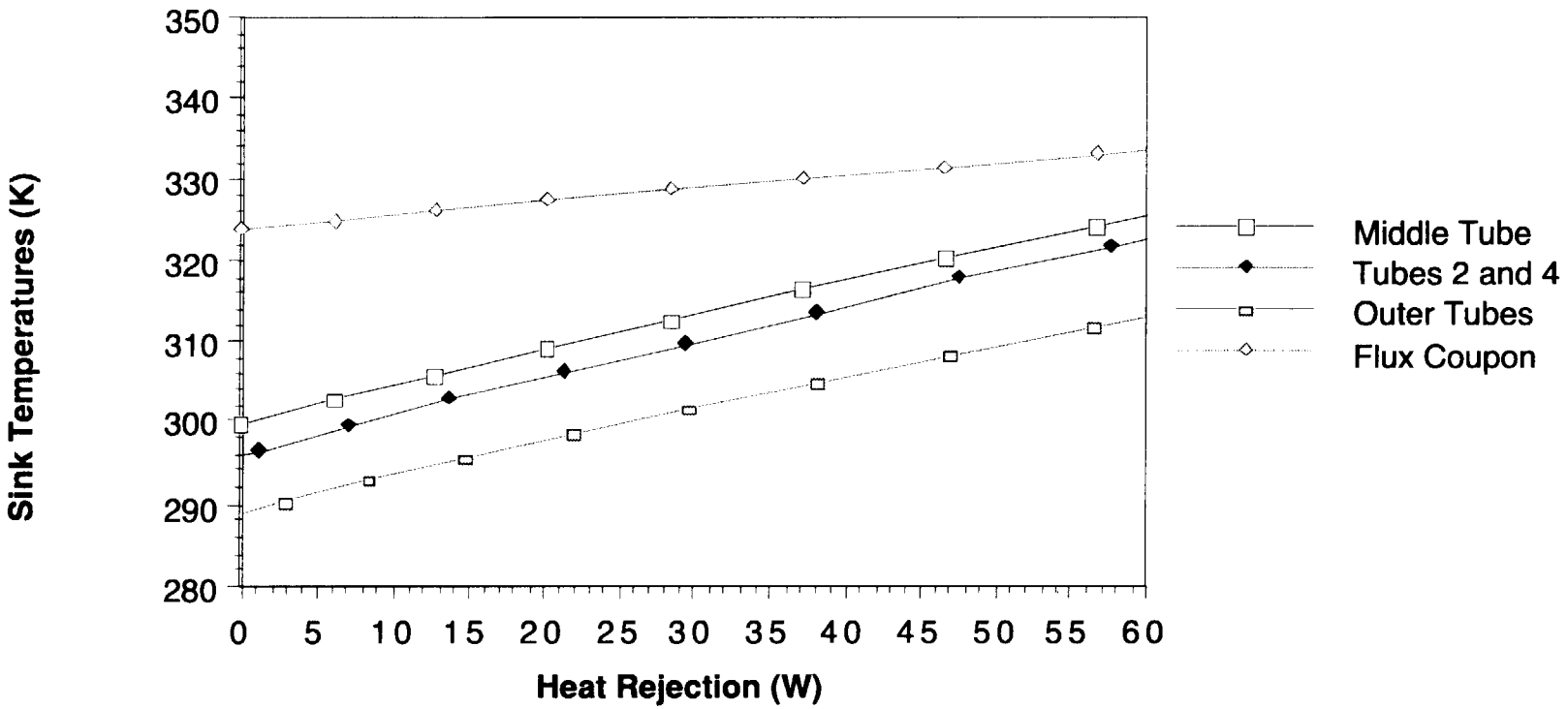

Figure E.12. UFRT Surface Sink Temperatures, Test Series 4.

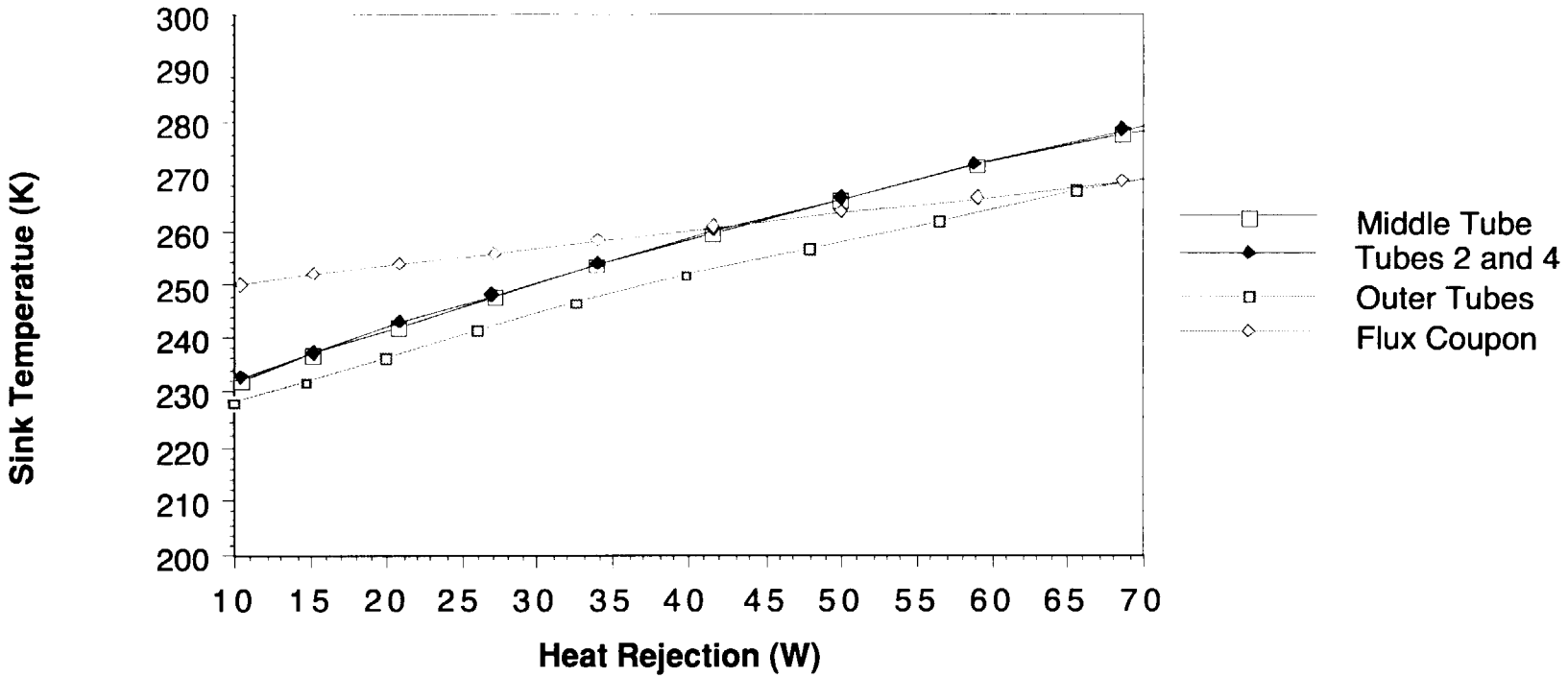

Figure E.13. UFRT Surface Sink Temperatures, Test Series 5.

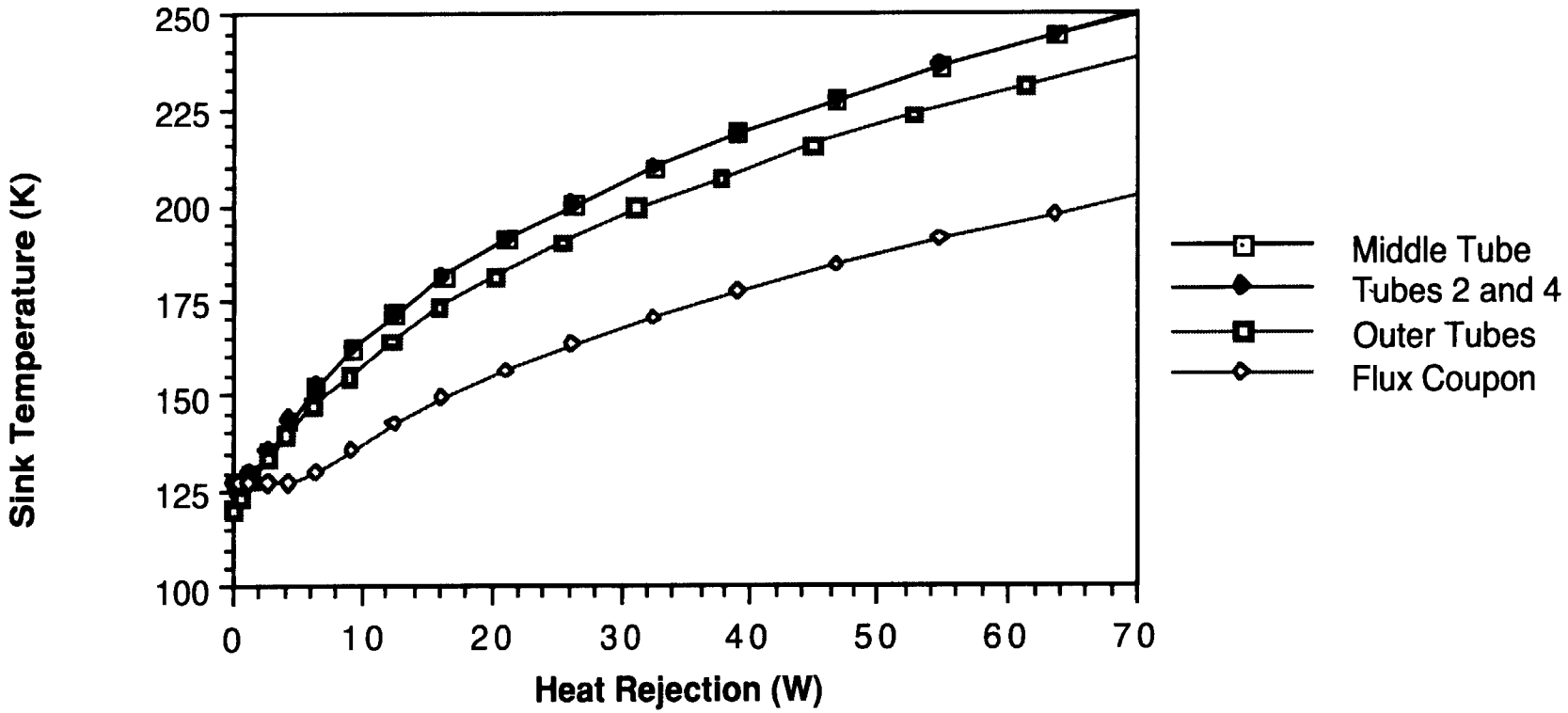

Figure E.14. UFRT Surface Sink Temperatures, Test Series 6.

APPENDIX F
ANALYSIS OF UFRTS USING HEAT PIPE THEORY

Two important performance parameters may be calculated to assess the performance of UFRTs during the thermal/vacuum tests. These are the radiative heat transfer and the overall temperature drop along each UFRT. These performance parameters may be determined directly from the experimental data measured during the tests. These parameters will be explicitly defined below.

The actual power input into each UFRT may be compared with the calculated radiated power from the UFRT condenser region. The calculated radiated power is determined by gray-body heat transfer to the environment and to the adjacent UFRTs. This heat transfer may be calculated, in its most basic form, using Equation F.1.

$$Q = \varepsilon\sigma\pi LD(T^4 - T_{env}^4) \qquad (F.1)$$

where Q is the radiated power in Watts, ε is the dimensionless emissivity, σ is the Stefan-Boltzmann constant (5.729×10^{-8} W/(m^2-K^4)), L is the length of the condenser region of the UFRT, D is the outer diameter of the condenser region of the UFRT, T is the outer surface temperature of the condenser region of the UFRT, and the T_{env} is the effective environmental sink temperature as viewed by the UFRT condenser.

However, equation F.1 does not include a separate formulation for the heat transfer from the UFRT to the environment and the UFRT to any adjacent UFRTs. If all of the UFRTs are operating at the same temperature, the net heat transfer between UFRTs will be zero. However, since the UFRTs were often operated at different temperatures (including zero power input during some test points), this heat transfer must be accounted for. Therefore, a view factor must be included in the radiation heat transfer equation.

Assuming the UFRTs are infinitely long parallel cylinders, the view factor between each UFRT can be found using Equations F.2 and F.3:

$$F_{1-2} = F_{2-1} = \pi^{-1} [(X^2-1)^{1/2} + \sin^{-1}(1/X) - X] \qquad (F.2)$$

where

$$X = 1 + (s/2r) \qquad (F.3)$$

where F_{1-2} and F_{2-1} are the view factors from surface 1 to surface 2 and from surface 2 to surface 1, s is the edge to edge spacing between adjacent UFRTs in cm, and r is the outer radius of a UFRT condenser region.

In the thermal/vacuum tests, the UFRTs were placed in an array of five parallel cylinders. The view factor between UFRTs for this configuration has been determined to be 0.04. This means that 4 percent of the solid angle from each UFRT "views" the adjacent UFRT.

The calculated power for the edge UFRTs, tubes 1 and 5, may therefore be found by employing Equation F.4:

$$Q = F_{ufrt-env} * \varepsilon\sigma\pi LD(T^4-T_{env}^4) + F_{ufrt-ufrt} *\varepsilon\sigma\pi LD(T^4-T_{ufrt}^4) \qquad (F.4)$$

The calculated power for the middle UFRTs—tubes 2, 3, and 4—may be determined by using Equation F.5:

$$Q = F_{urft-env}* \varepsilon\sigma LD(T^4-T_{env}^4) + F_{ufrt-ufrt_a} * \varepsilon\sigma LD(T^4-T_{ufrt_a}^4) + F_{urft-ufrt_b} * \varepsilon\sigma LD(T^4-T_{ufrt_b}^4) \qquad (F.5)$$

where the two adjacent UFRTs are designated $UFRT_a$ and $UFRT_b$.

The temperature drop is a measure of the heat transfer efficiency of the UFRT. For a low temperature drop, the condenser radiates at approximately the same temperature as the primary working fluid at the exterior of the evaporator. However, for a large temperature drop the radiating temperature from the surface of the condenser may be much less than that of the exterior of the evaporator. This condition necessarily requires additional radiating surface area to reject the same amount of heat as a thermal management device with a low temperature drop. It may be calculated simply from the thermocouple data by Equation F.6:

$$\Delta T = T_{evaporator} - T_{condenser} \qquad (F.6)$$

The heat pipe code, HTPIPE (Woloshun, 1988), was used to model the performance limits of the current UFRT design. HTPIPE is a one-dimensional steady-state heat pipe analysis code. The results of the code have been validated with some experimental data developed at the Los Alamos National Laboratory.

The HTPIPE code calculates the six heat pipe performance limits: capillary, viscous, sonic, entrainment, and boiling limits. These maximum power limits are based upon a specified evaporator exit temperature and assume a constant power boundary condition. Each of these limits will be discussed below.

The capillary limit of the UFRT is based on the pressure gradient limitations across the vapor/liquid interface. If the pressure in the liquid is greater than the pressure in the vapor, an unstable condition would exist. However, this generally does not occur and a wet point is generated at some axial location; i.e. other than at the end of the condenser. The capillary limiting condition is defined in Equation F.7:

$$\Delta P_{cap} = 2\sigma_1 \cos\theta / r_c \qquad (F.7)$$

where ΔP_{cap} is the capillary pressure, σ_1 is the liquid surface tension of the water, and r_c is the capillary pore radius.

The viscous limit is defined by the condition that the vapor pressure cannot be negative. When the overall vapor pressure is very low, the total pressure drop along the condenser may be essentially zero. Since this pressure drop drives the overall fluid transport, a power limit can be derived based on the vapor pressure. Typically, however, this limit is only approached during initial startup. The viscous limit is defined in Equation F.8:

$$Q_{visc} = (r_v^2 \, h_{fg} \, \rho_v \, \Delta P_v)/(1.6 \, \mu_v \, l_{eff}) \qquad (F.8)$$

where r_v is the radius of the vapor region, h_{fg} is the latent heat of vaporization, ρ_v is the density of the vapor, ΔP_v is the overall pressure drop, μ_v is the viscosity, and l_{eff} is the effective length of the condenser region.

The UFRT power transport capacity may also be limited by sonic vapor flow. The choked flow condition in the UFRT is defined in Equation F.9:

$$Q_{sonic} = 0.474 h_{fg} \, (\rho_v P_v)^{0.5} \qquad (F.9)$$

where h_{fg} is the latent heat of vaporization, ρ_v is the density of the vapor, and P_v is the pressure of the vapor.

The entrainment limit in the UFRT is a result of the surface shear between the counter-flowing vapor and liquid. The shear stress exerted by the vapor on the liquid prevents the liquid from returning to the evaporator, causing a dry-out in the evaporator. The entrainment limit is defined in Equations F.10 and F.11:

$$Q_{ent} = 2.99 \, \rho_v \, A_v \, h_{fg}^{1.5} \, [\sigma/(\rho_v \, h_{fg} \, \delta)]^{0.545} \qquad (F.10)$$

where

$$\delta = [\sigma/(\rho_l - \rho_v)g]^{0.5} \qquad (F.11)$$

where ρ_v is the density of the vapor, A_v is the cross-sectional area of the vapor region, h_{fg} is the latent heat of vaporization, σ is the surface tension, ρ_l is the density of the liquid, and g is the gravitational acceleration.

The boiling limit in the UFRT occurs at the departure from nucleate boiling within the evaporator. Additionally, boiling can result in a local dry-out condition, which may result in the overheating of the UFRT. The boiling limit is defined in Equation F.12:

$$Q_{boil} = 2\sigma T_s / \left(\rho_v h_{fg} r_{nuc} / [\delta_w / (\pi D L_e k) + (2\pi R T_S)^{0.5} R T_s^2 / (A_{l\text{-}v} P h_{fg}^2)]\right) \qquad (F.12)$$

where σ is the surface tension, T_s is the saturation temperature, ρ_v is the density of the vapor, h_{fg} is the latent heat of vaporization, r_{nuc} is the nucleation site radius, δ_w is the thickness of the wick, D is the outer diameter of the wick, L_e is the length of the evaporator, k is the thermal conductivity of the wick, R is the inner radius of the evaporator, $A_{l\text{-}v}$ is the area of the liquid-vapor interface in the evaporator region, and P is operating pressure.

APPENDIX G
TEST SERIES 1 -RAW DATA

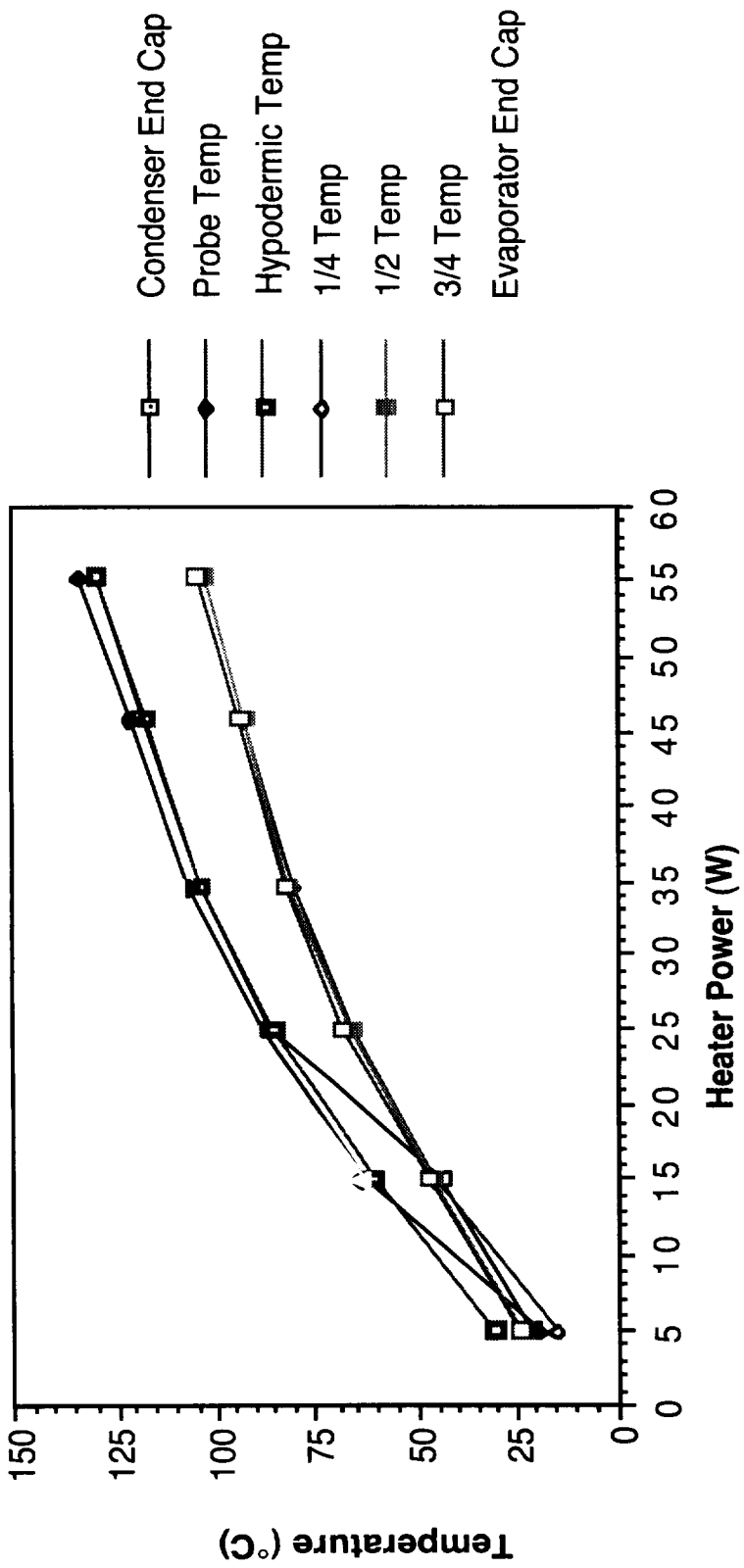

Figure G.1. Test Series 1 - Tube 1 Raw Data

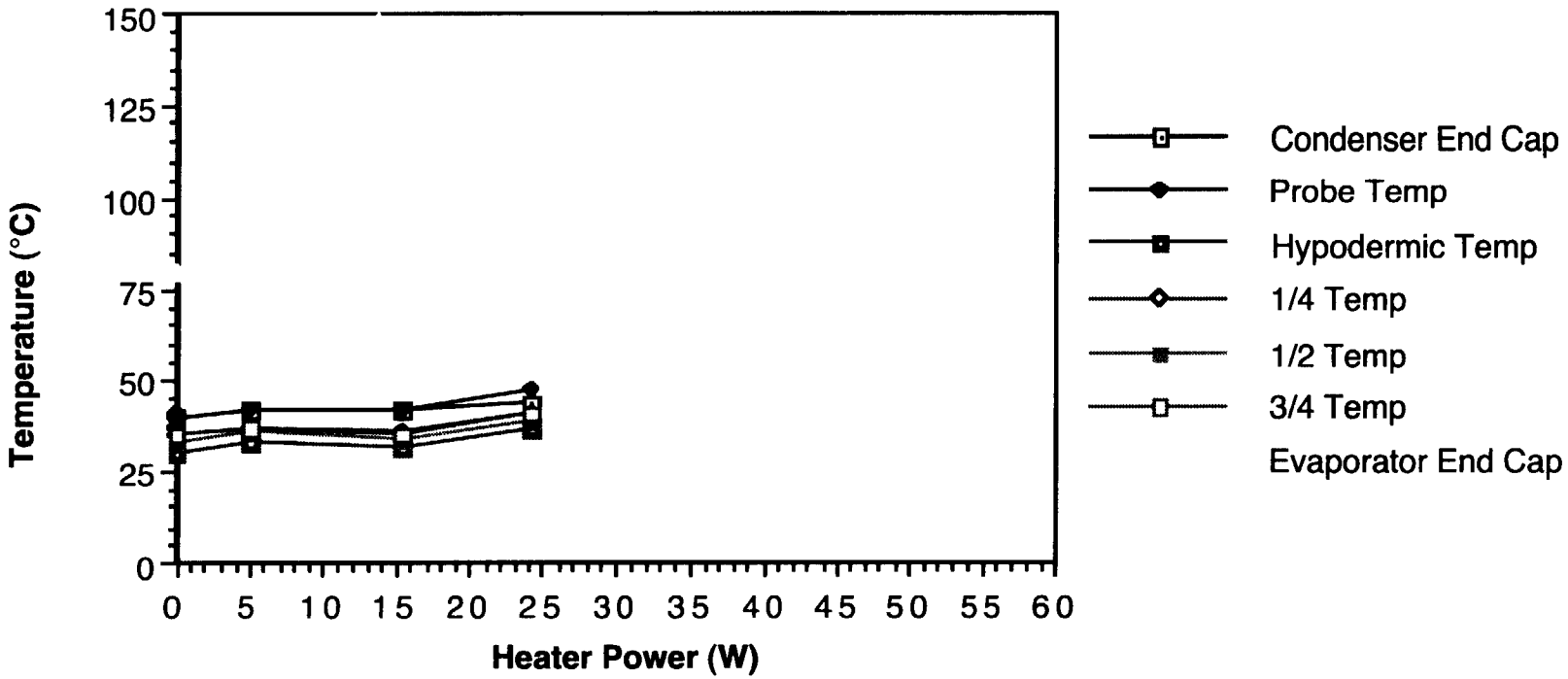

Figure G.2. Test Series 1 - Tube 2 Raw Data.

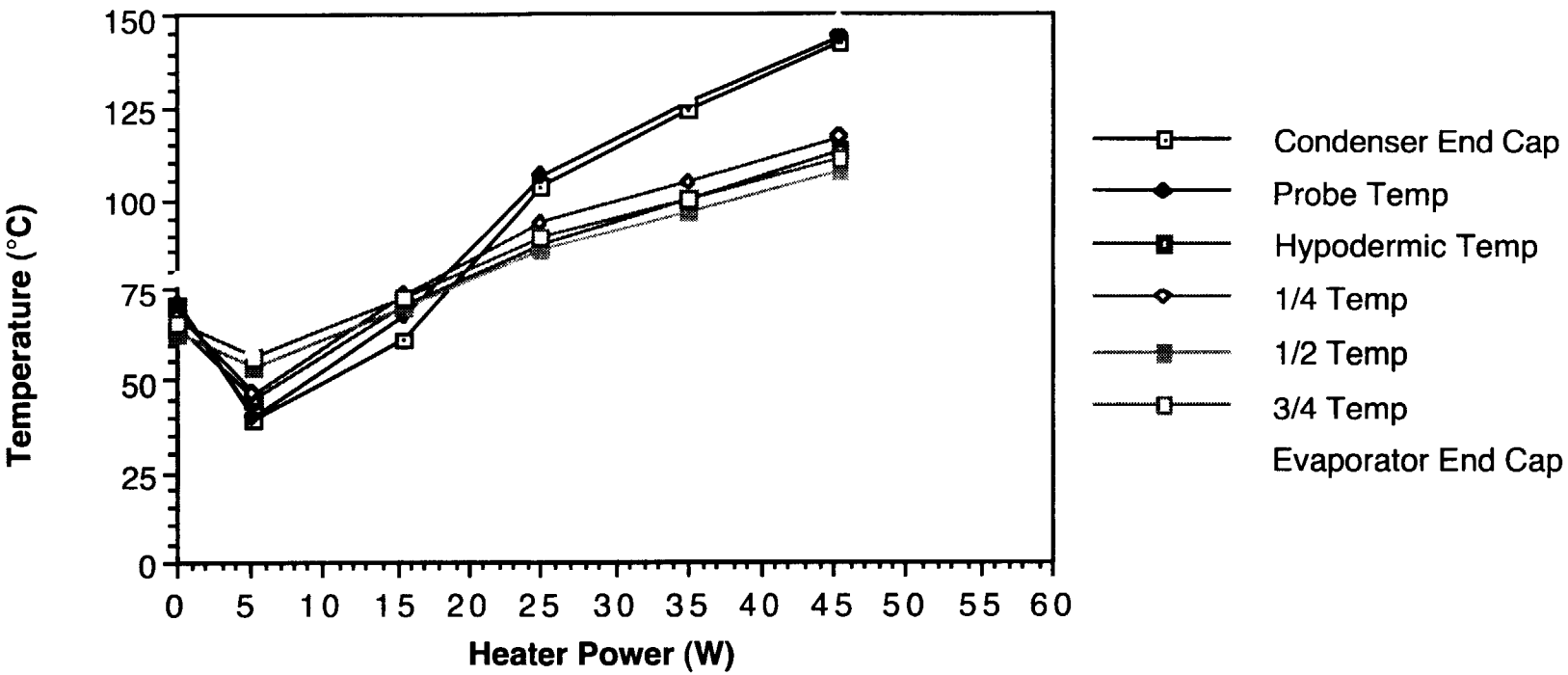

Figure G.3. Test Series 1 - Tube 3 Raw Data.

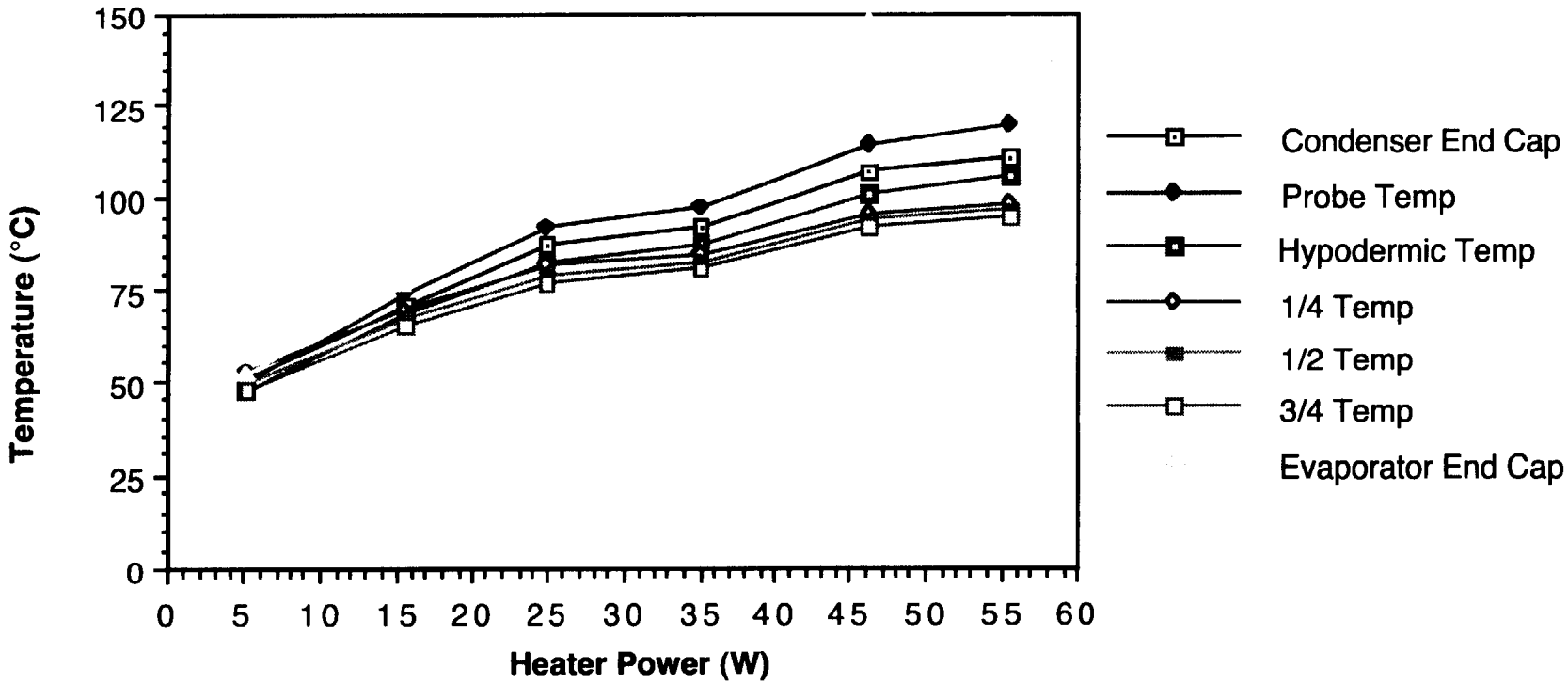

Figure G.4. Test Series 1 - Tube 4 Raw Data.

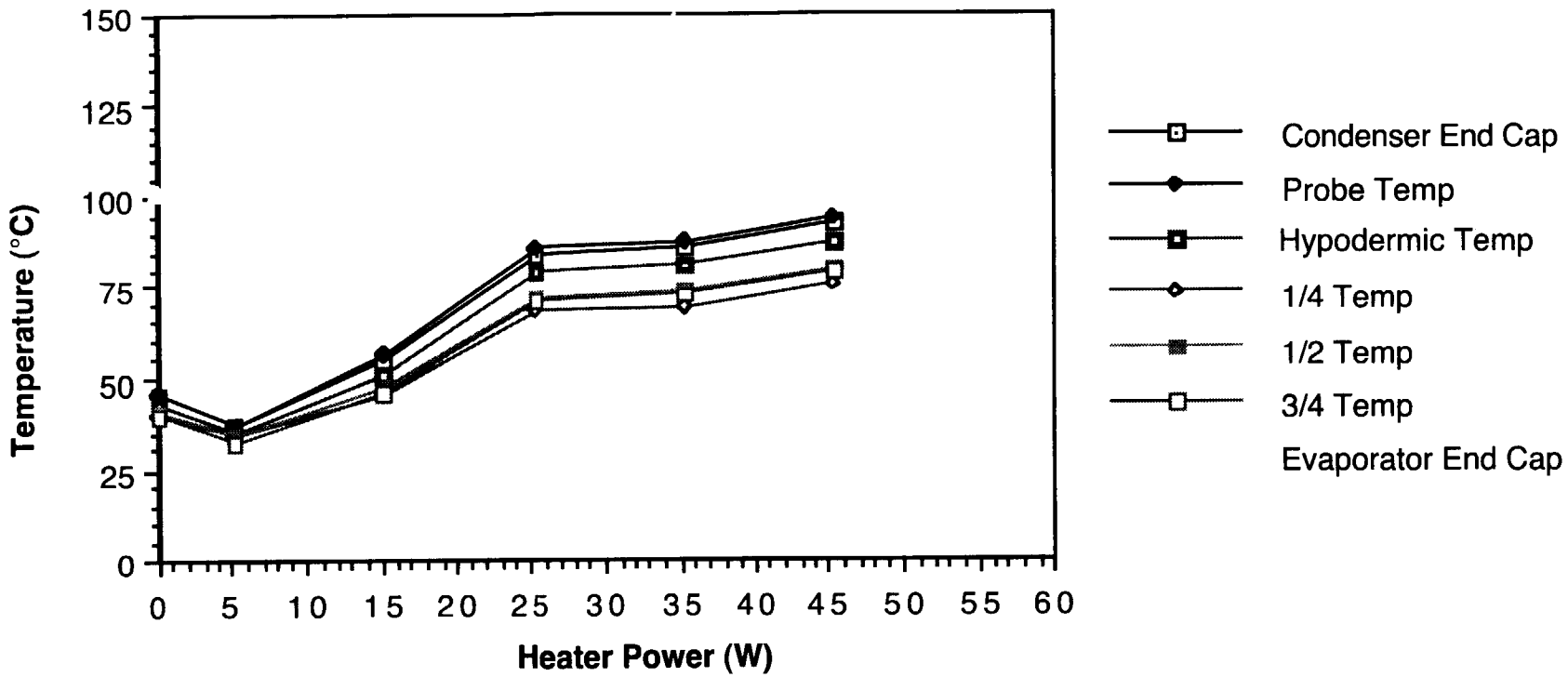

Figure G.5. Test Series 1 - Tube 5 Raw Data.

APPENDIX H
TEST SERIES 2 - RAW DATA

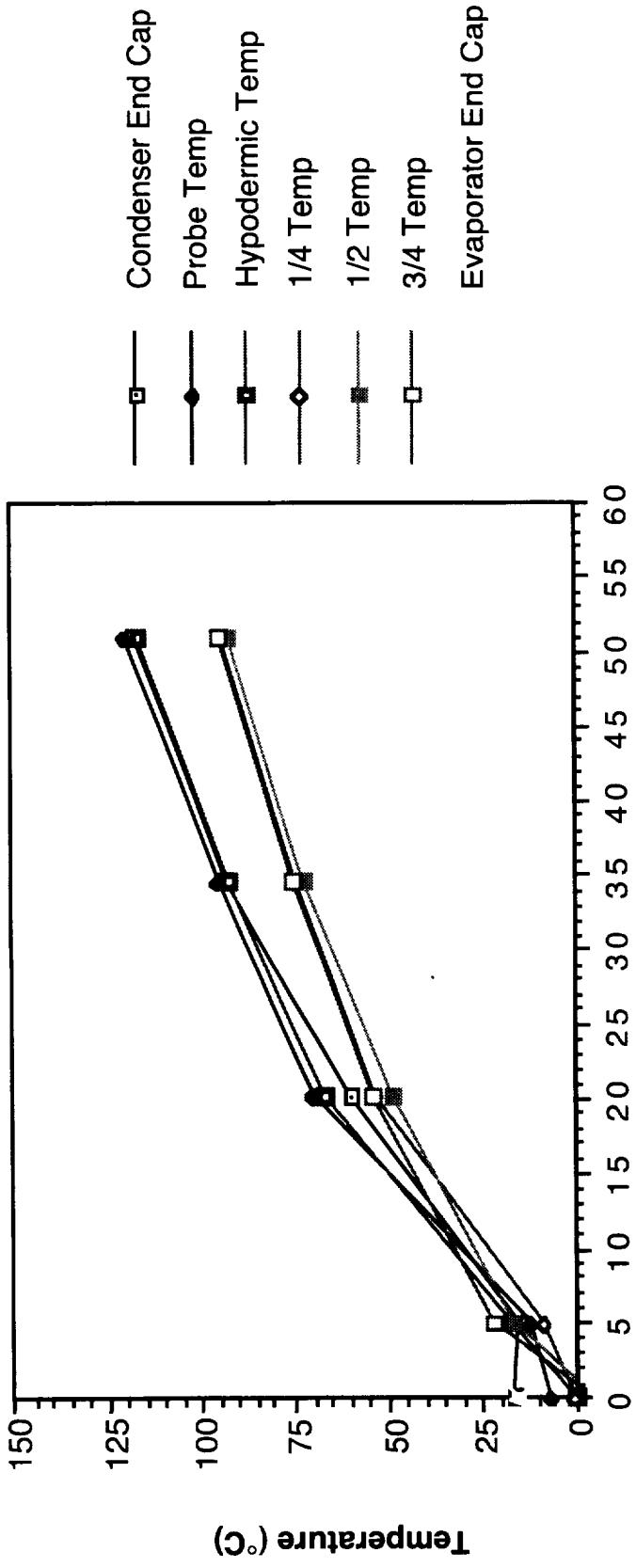

Figure H.1. Test Series 2 - Tube 1 Raw Data.

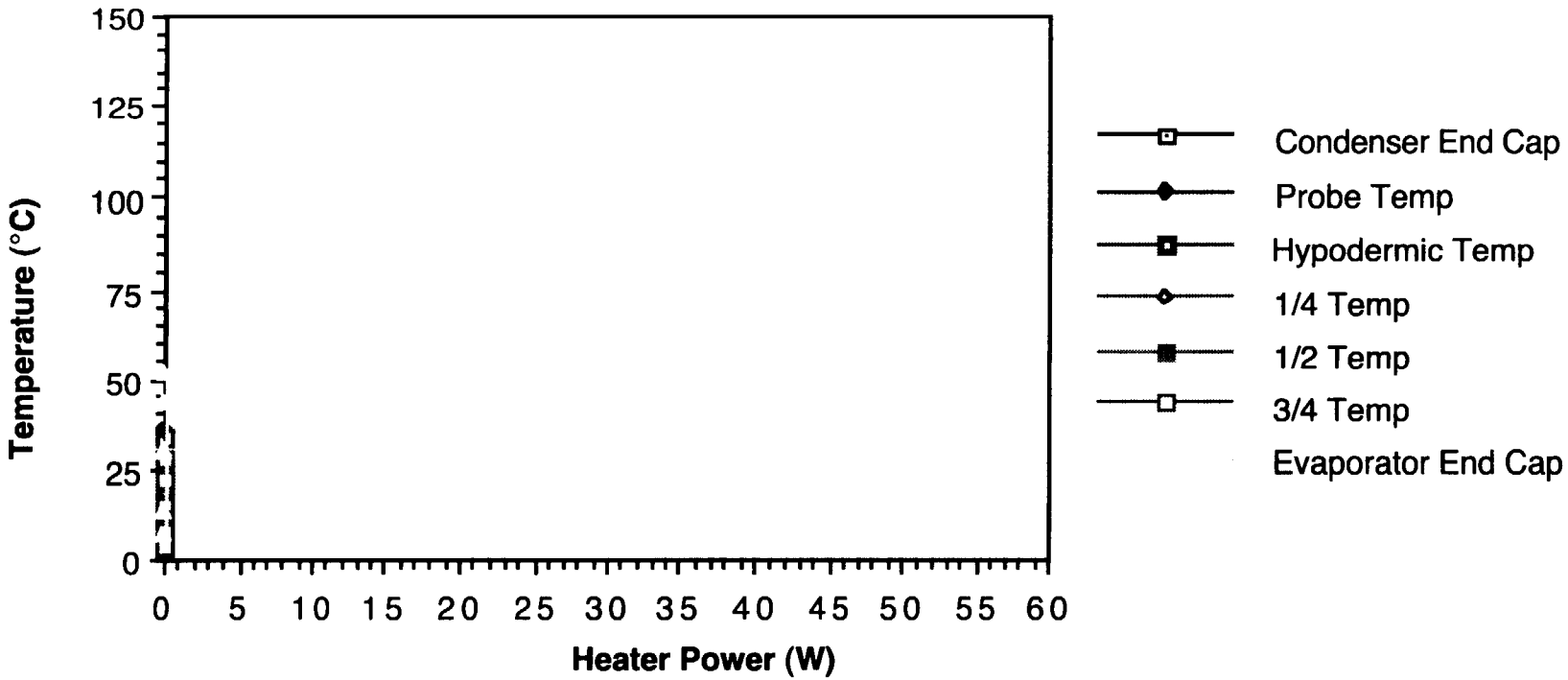

Figure H.2. Test Series 2 - Tube 2 Raw Data.

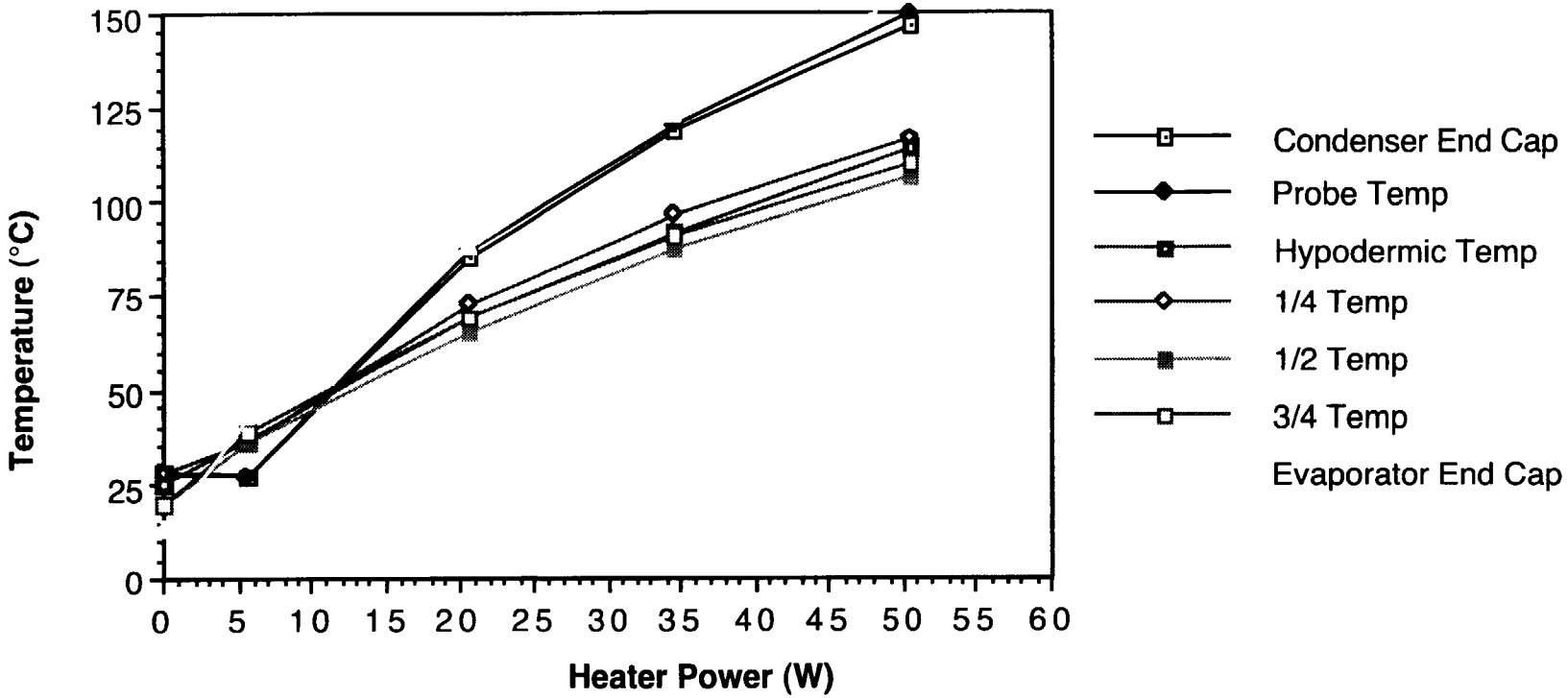

Figure H.3. Test Series 2 - Tube 3 Raw Data.

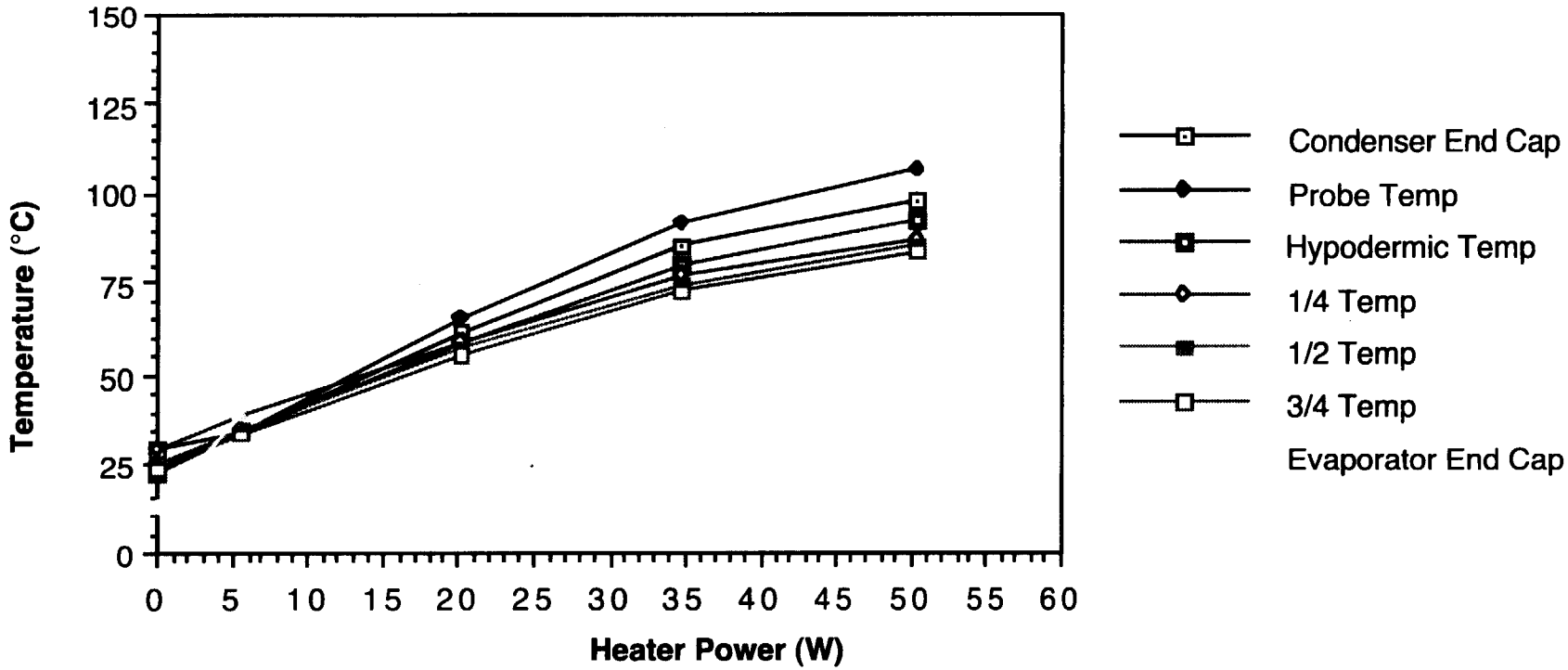

Figure H.4. Test Series 2 - Tube 4 Raw Data.

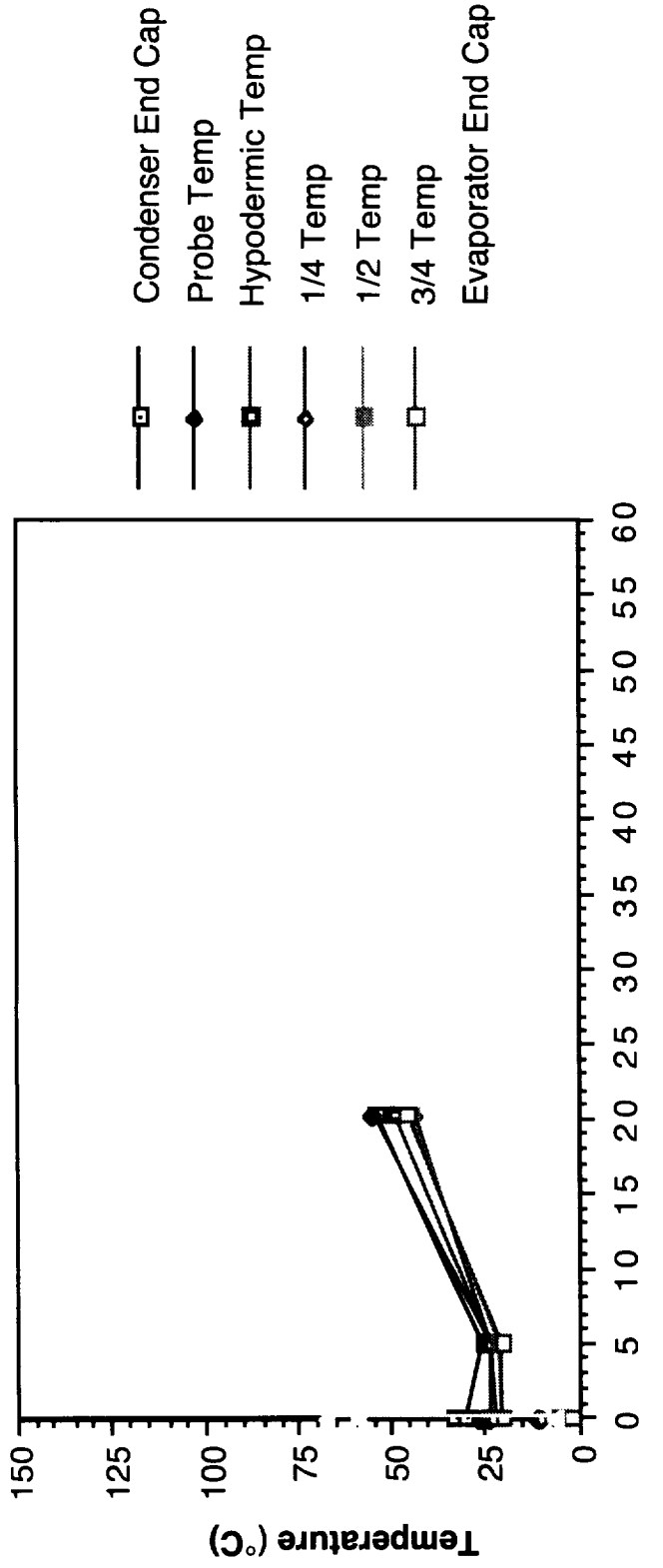

Figure H.5. Test Series 2 - Tube 5 Raw Data.

APPENDIX I
TEST SERIES 3 - RAW DATA

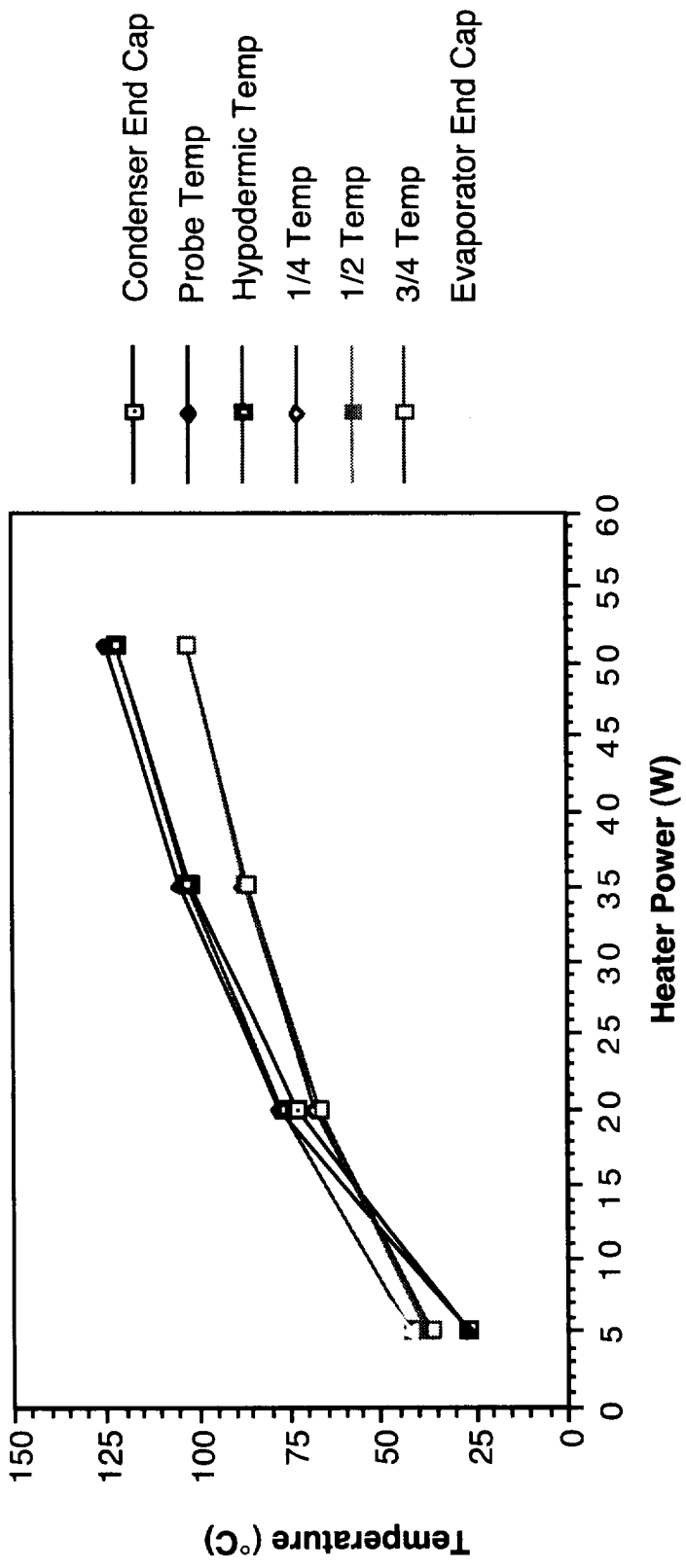

Figure I.1. Test Series 3 - Tube 1 Raw Data.

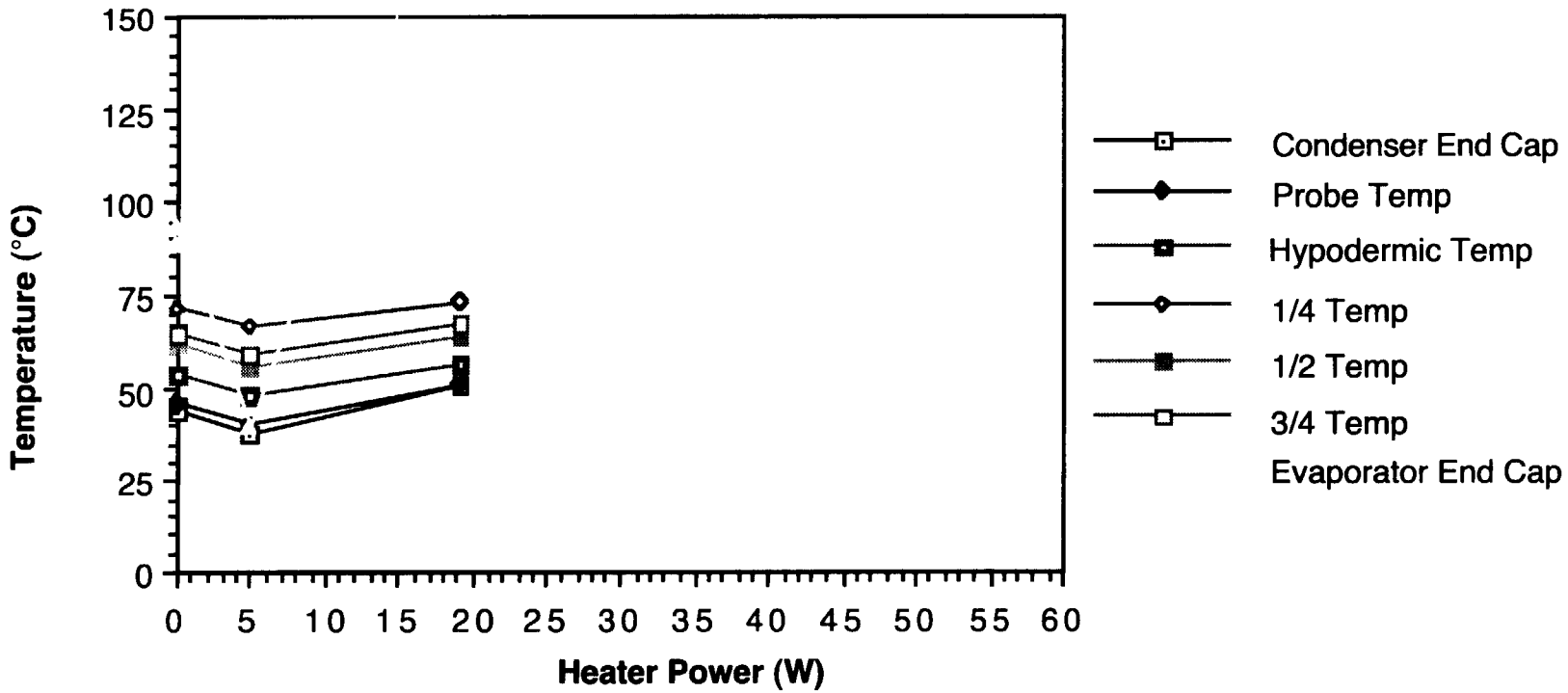

Figure I.2. Test Series 3 - Tube 2 Raw Data.

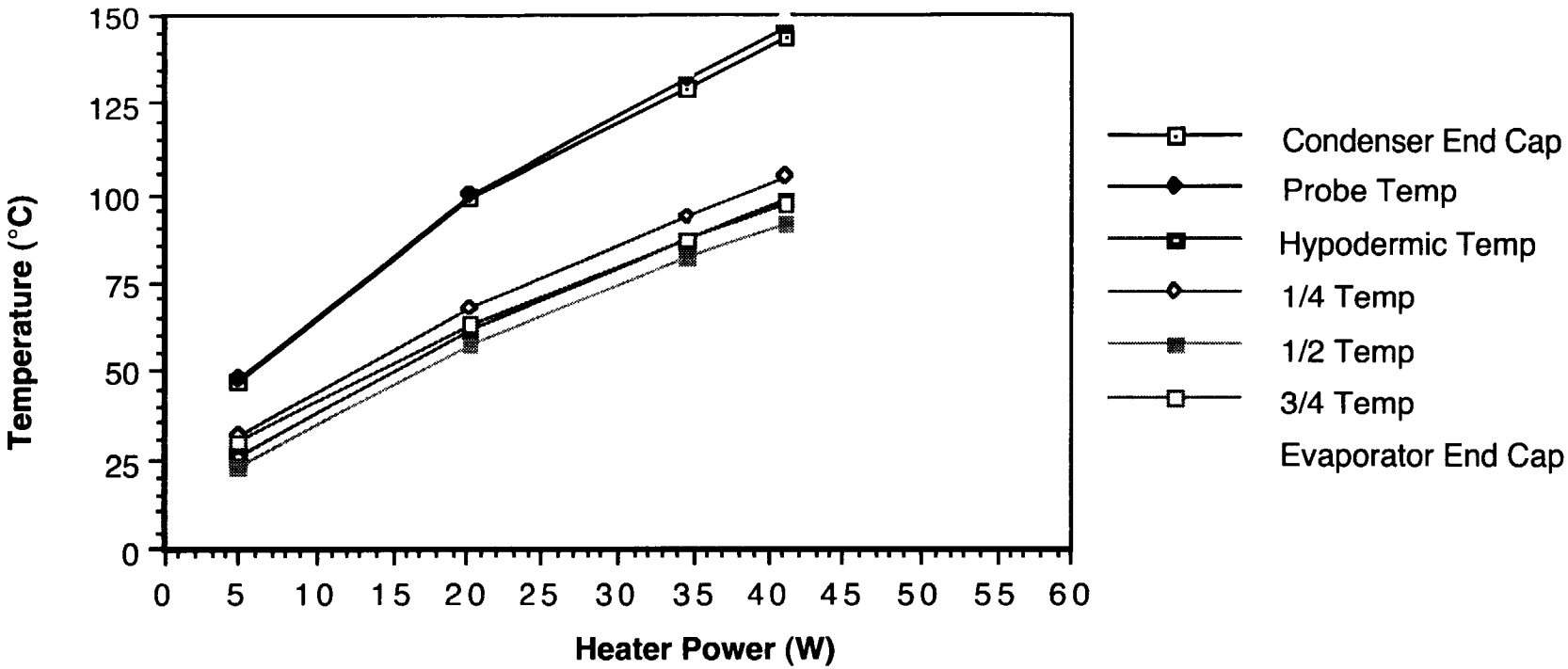

Figure I.3. Test Series 3 - Tube 3 Raw Data.

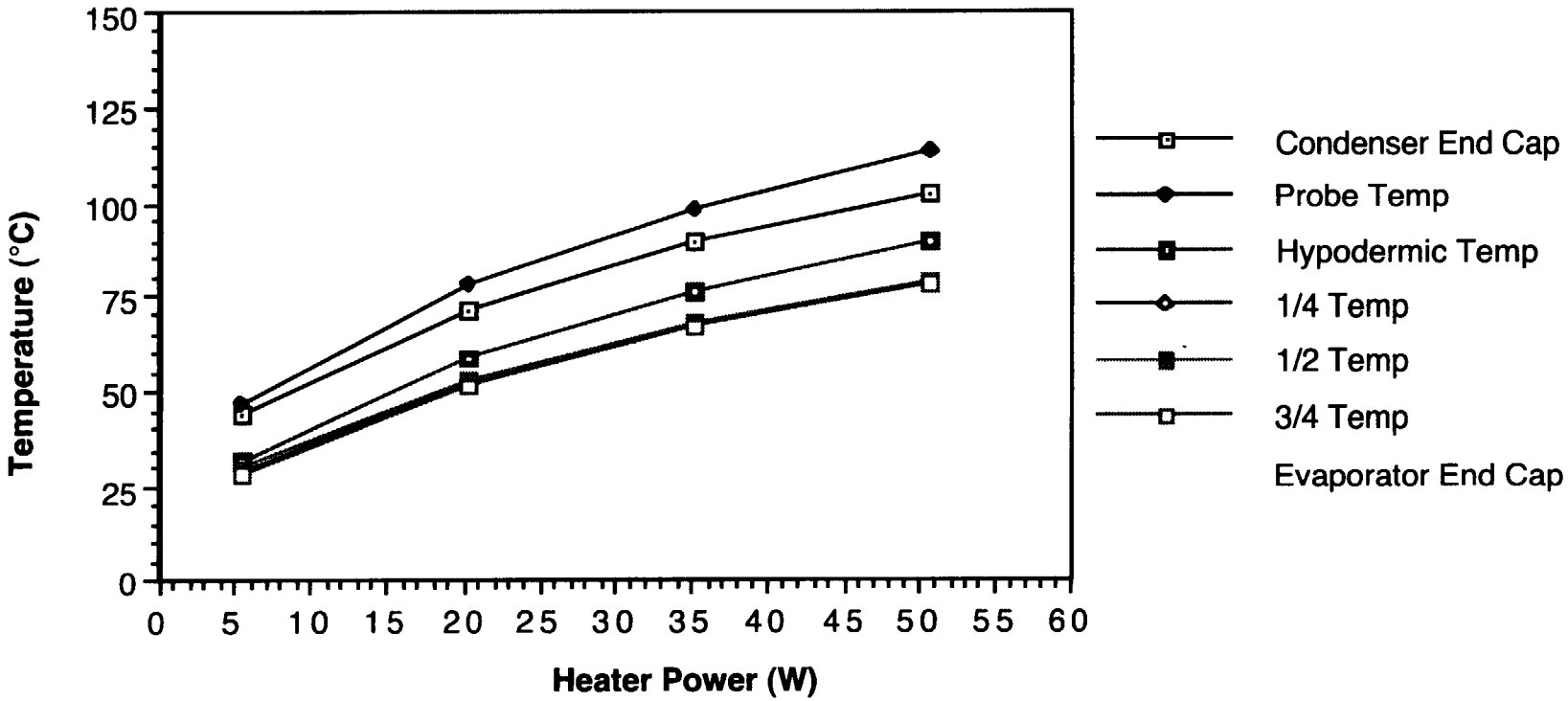

Figure I.4. Test Series 3 - Tube Raw Data.

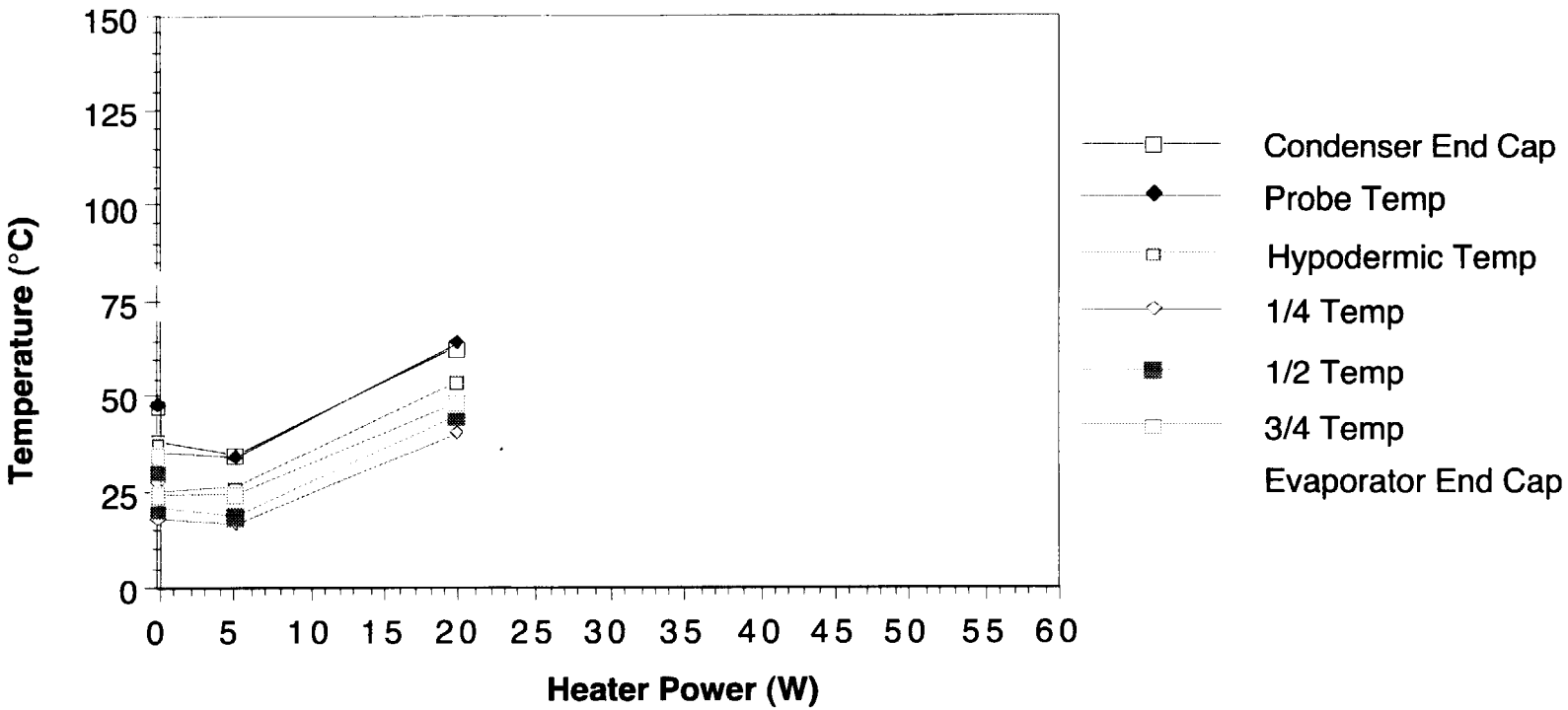

Figure I.5. Test Series 3 - Tube 5 Raw Data.

APPENDIX J
TEST SERIES 4 - RAW DATA

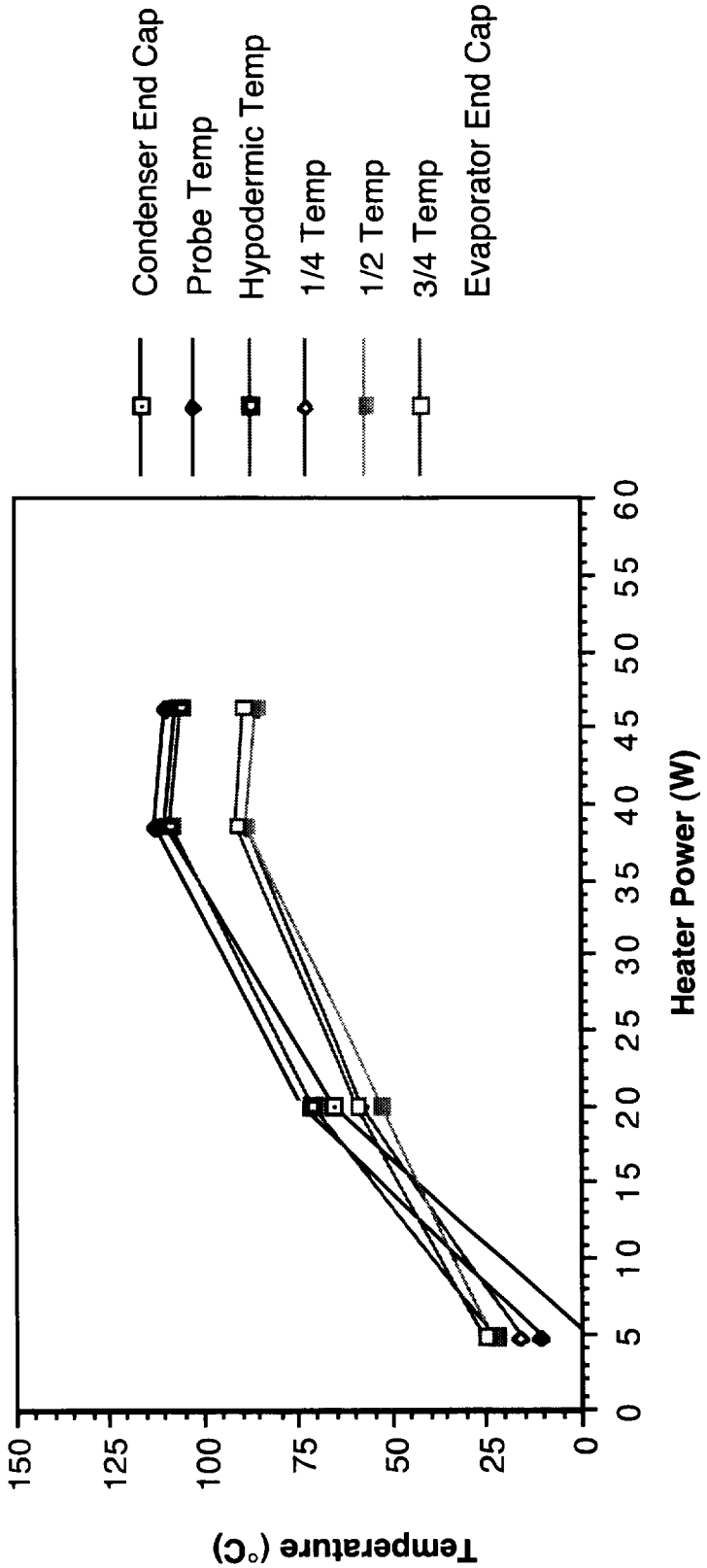

Figure J.1. Test Series 4 - Tube 1 Raw Data.

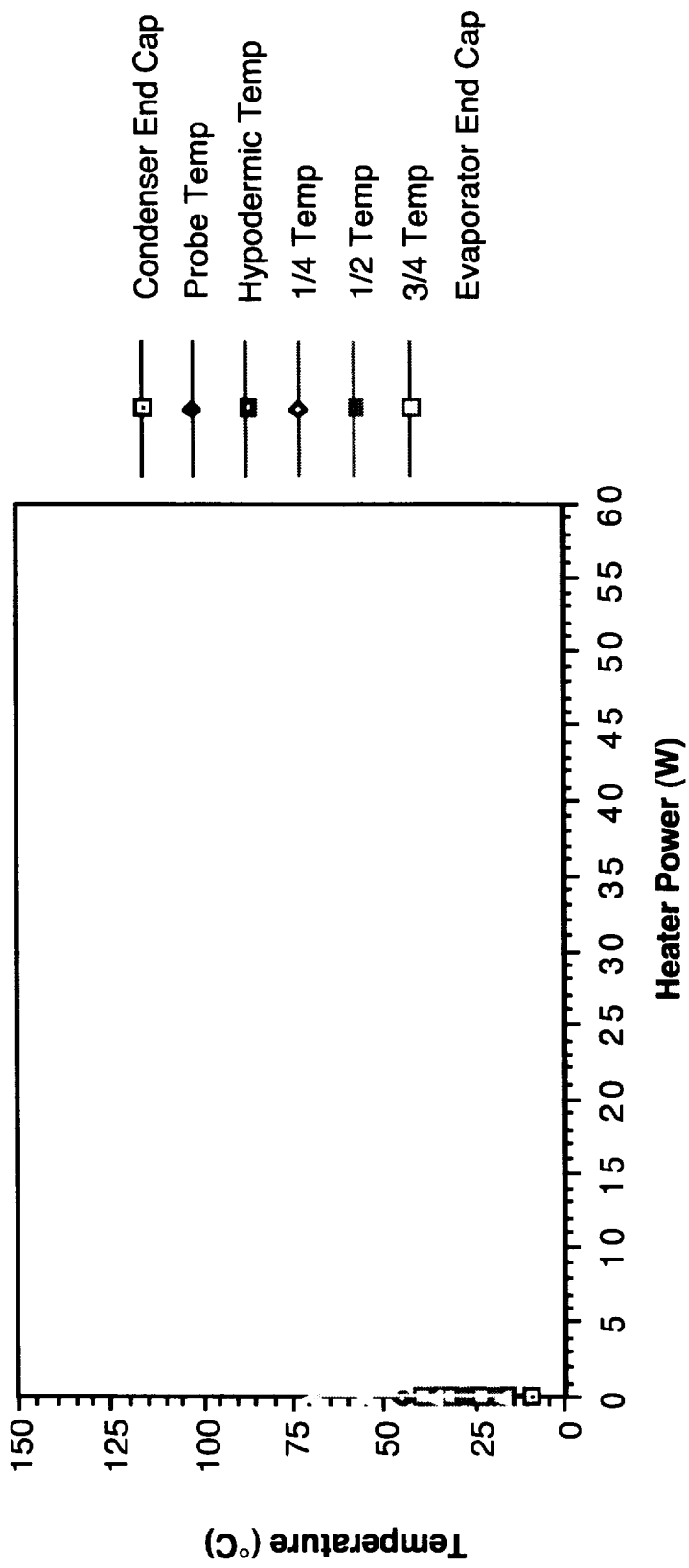

Figure J.2. Test Series 4 - Tube 2 Raw Data.

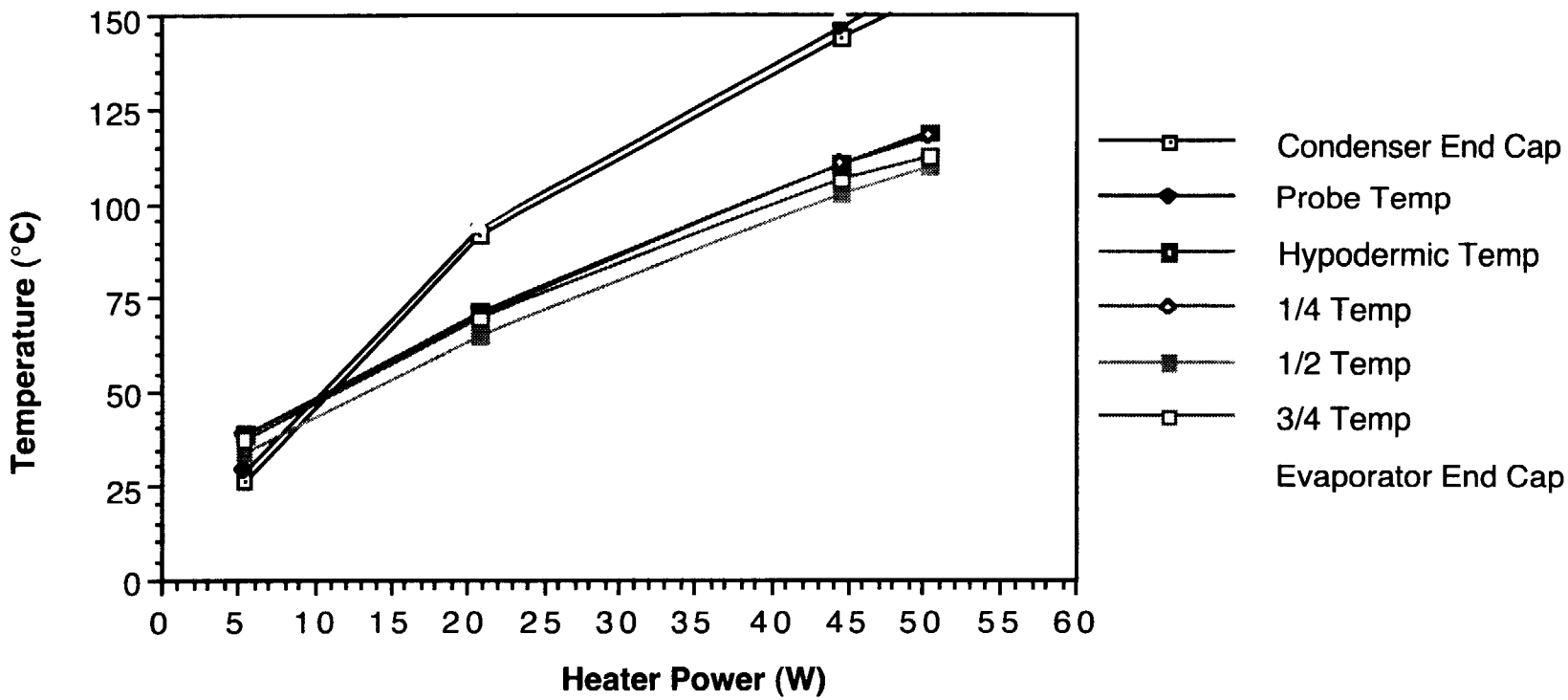

Figure J.3. Test Series 4 - Tube 3 Raw Data.

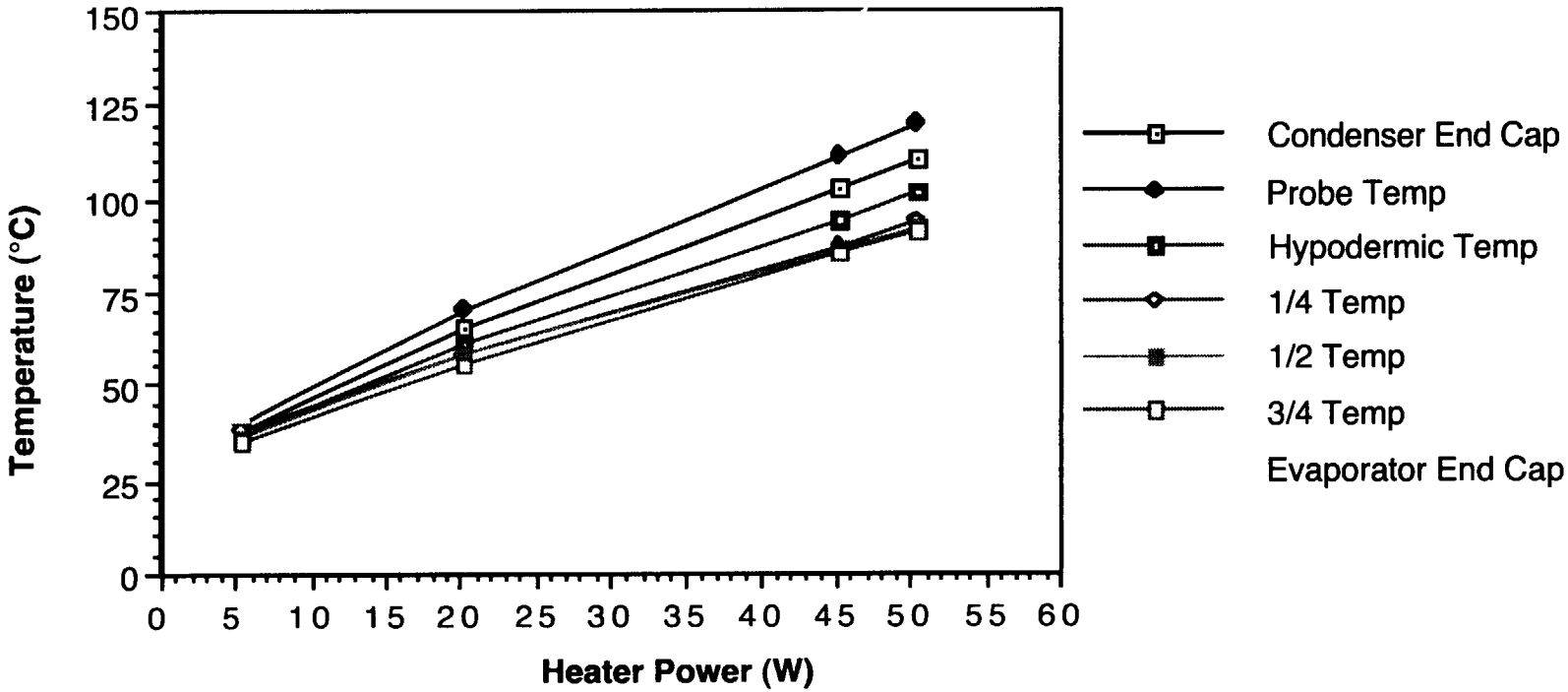

Figure J.4. Test Series 4 - Tube 4 Raw Data.

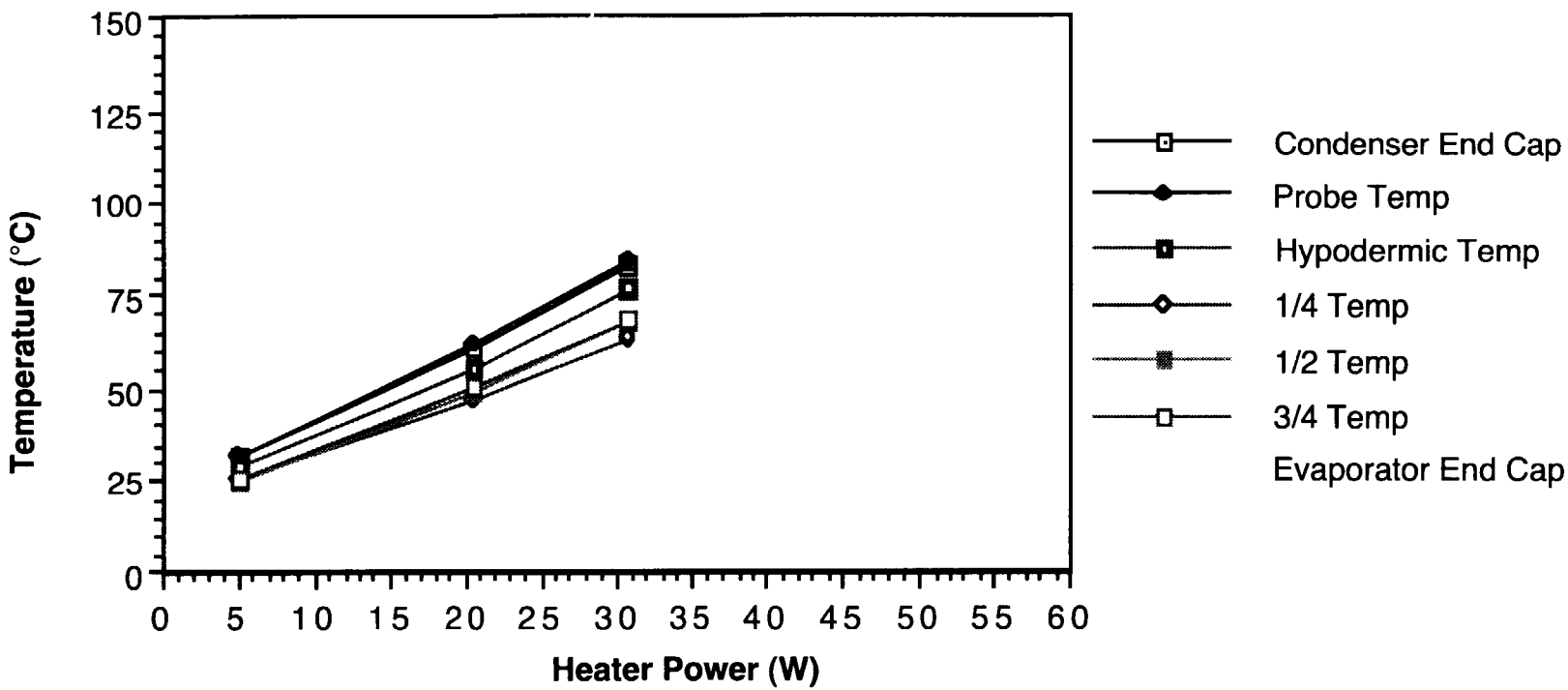

Figure J.5. Test Series 4 - Tube 5 Raw Data.

APPENDIX K
TEST SERIES 5 - RAW DATA

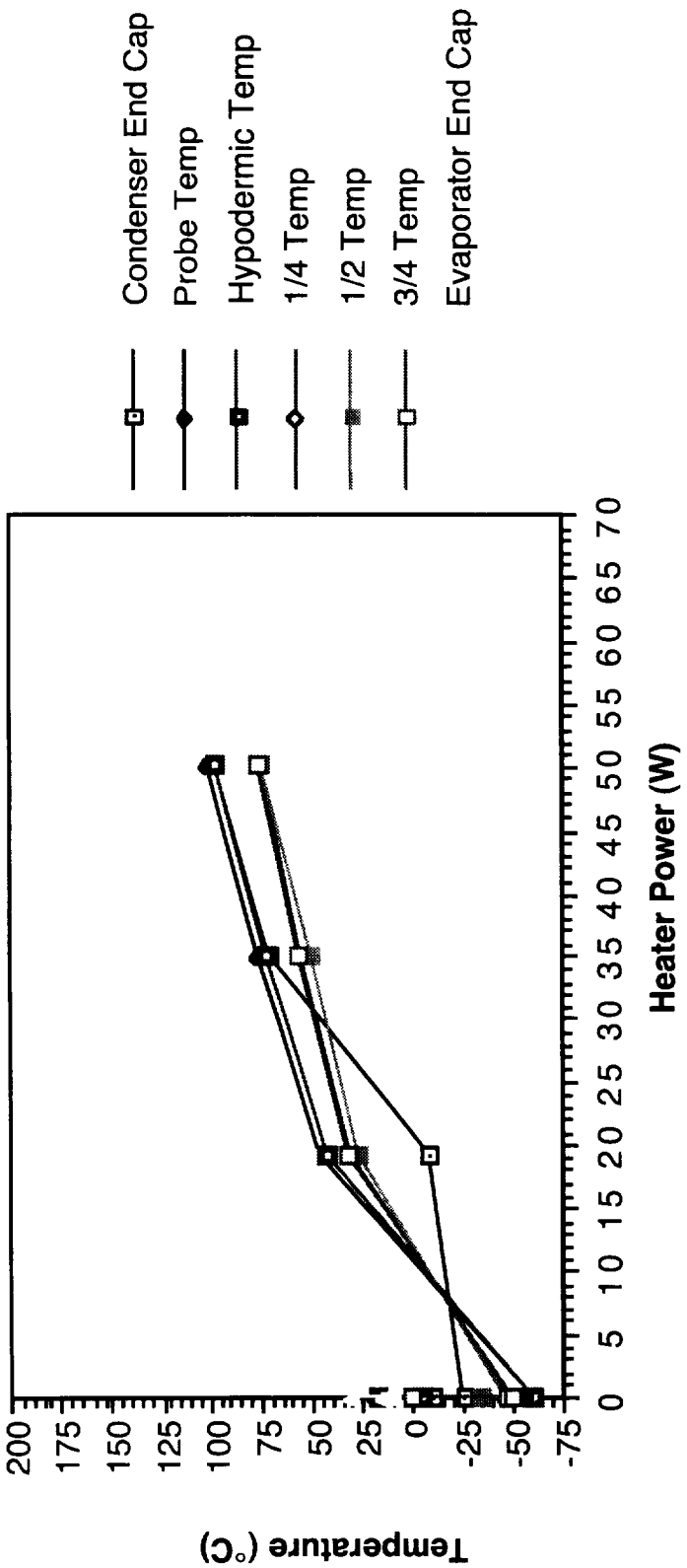

Figure K.1. Test Series 5 - Tube 1 Raw Data.

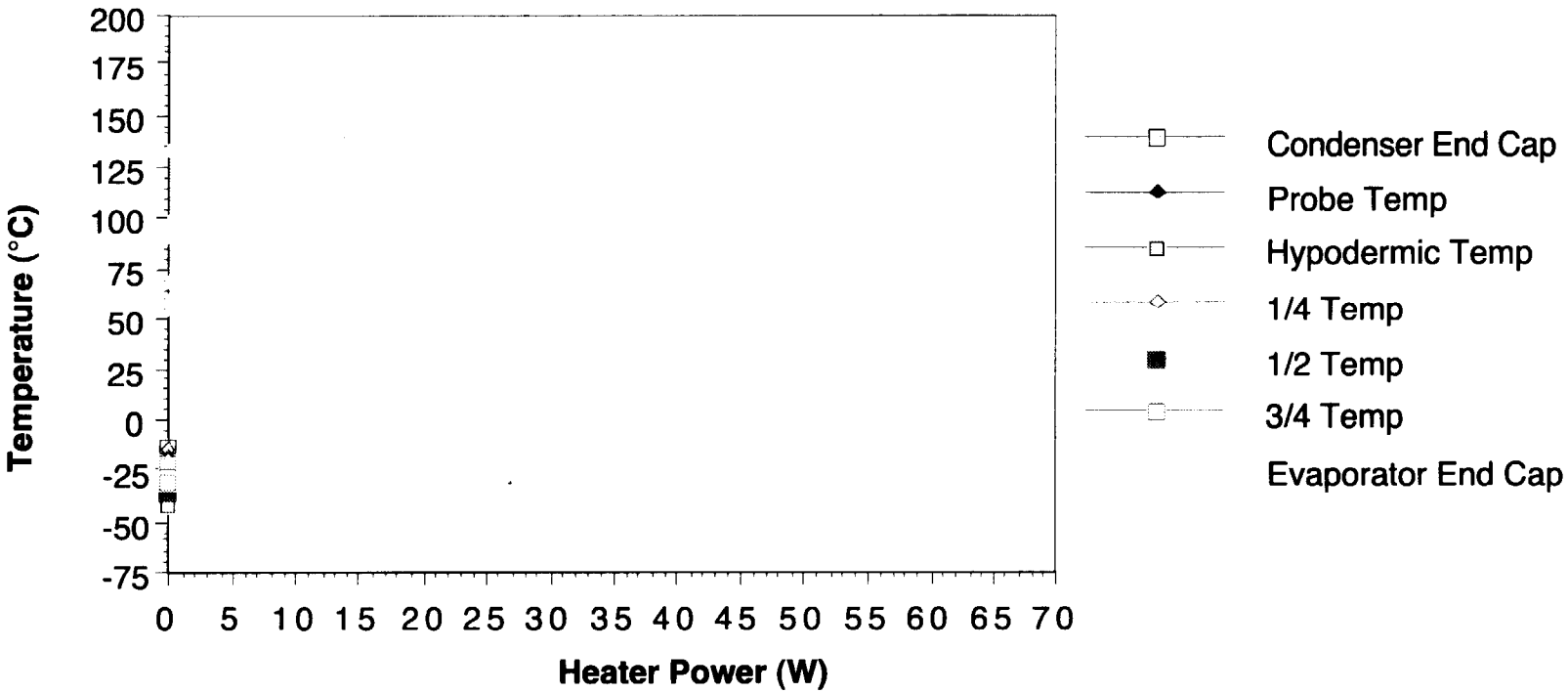

Figure K.2. Test Series 5 - Tube 2 Raw Data.

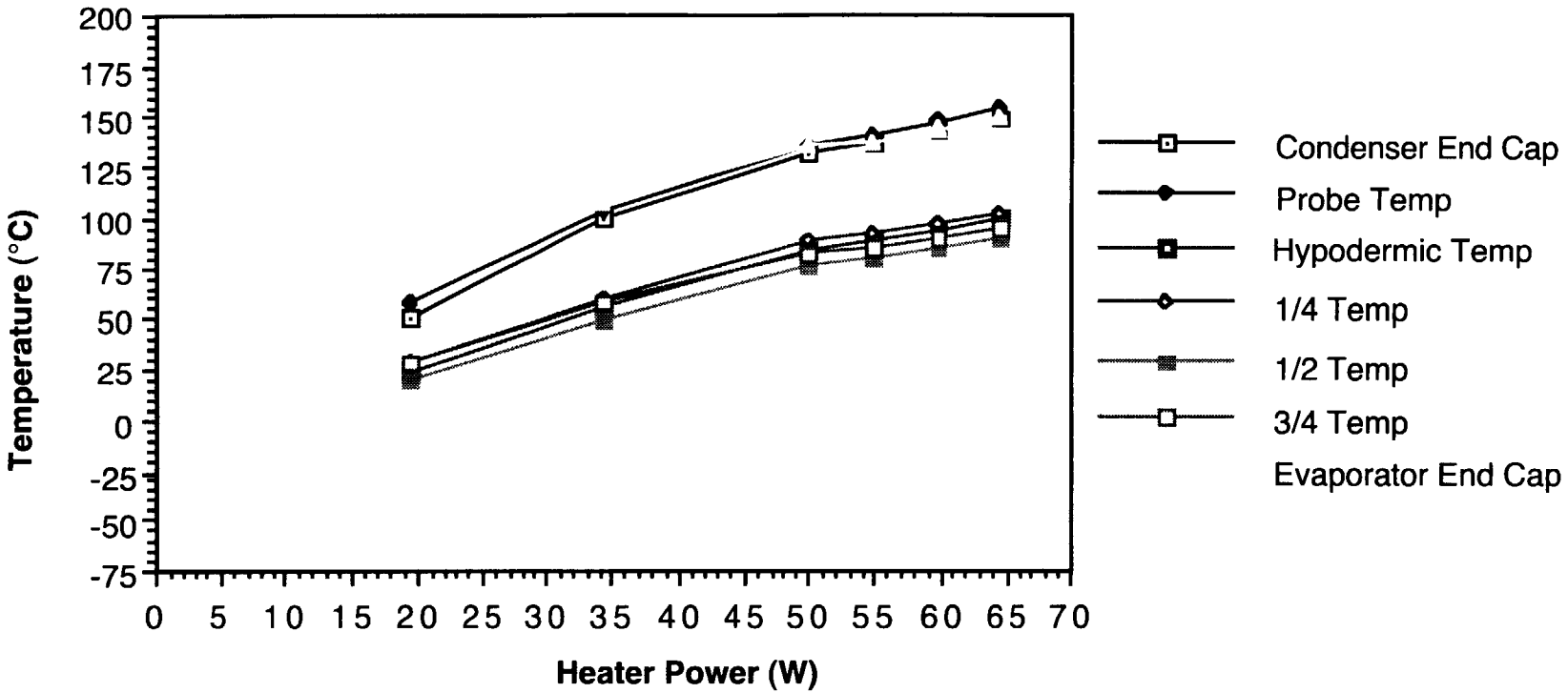

Figure K.3. Test Series 5 - Tube 3 Raw Data.

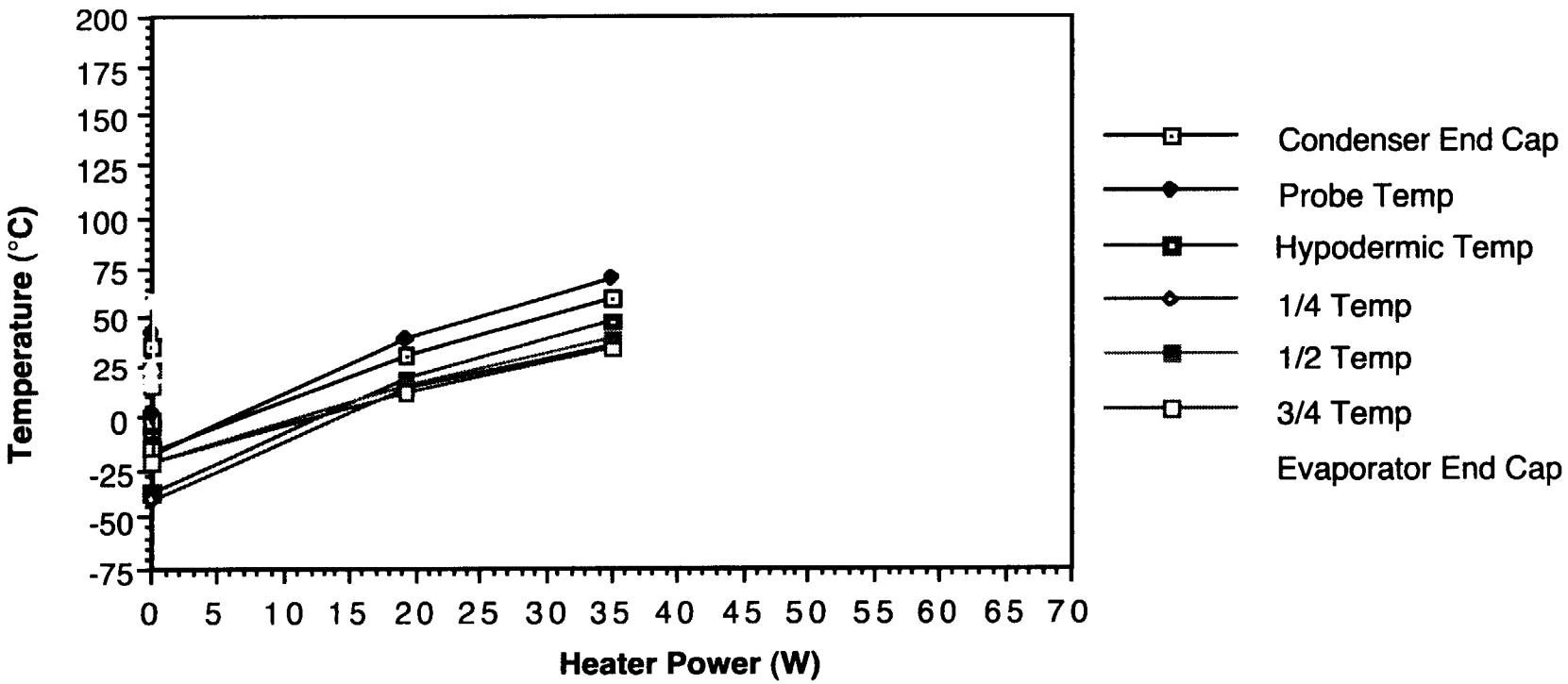

Figure K.4. Test Series 5 - Tube 4 Raw Data.

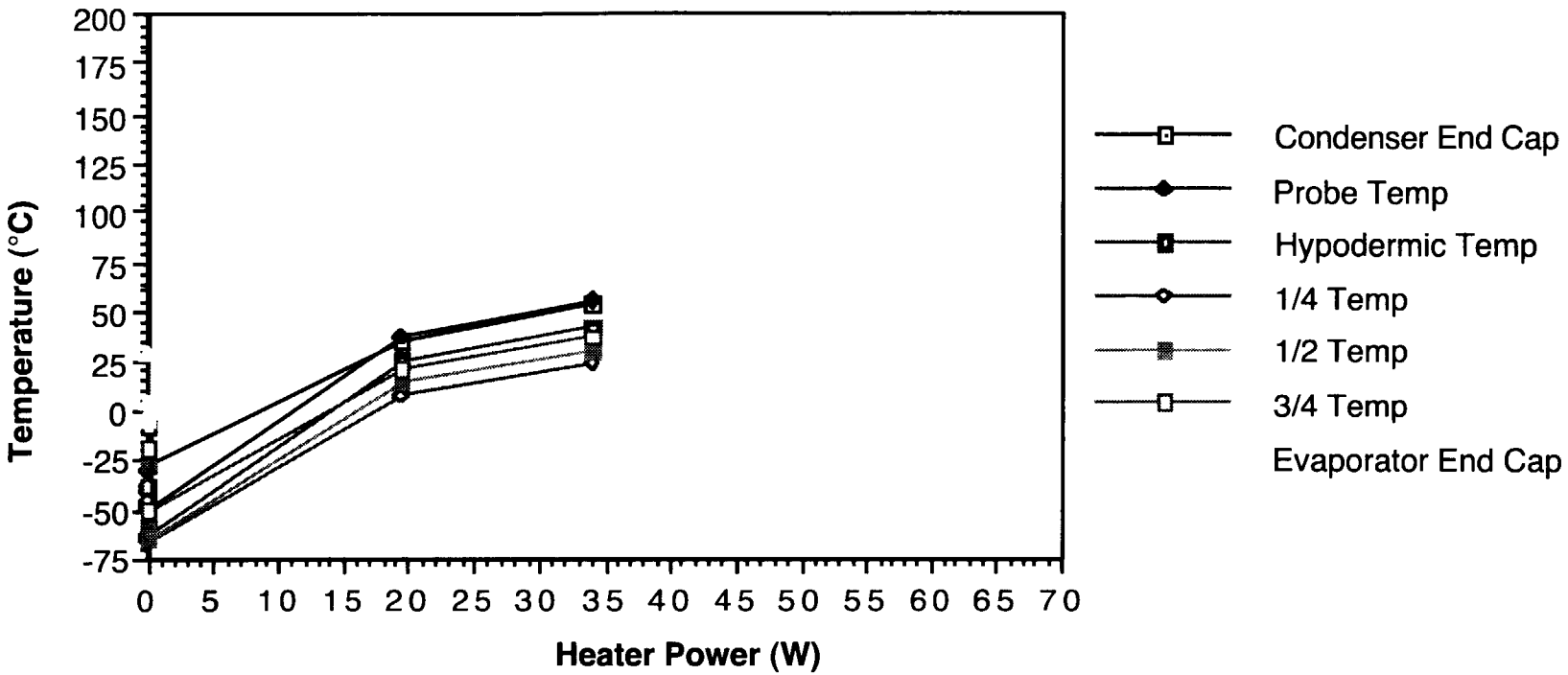

Figure K.5. Test Series 5 - Tube 5 Raw Data.

APPENDIX L
UFRT DETAILED STEADY STATE ANALYSIS

L.1 Test Series 1 (Lunar Noon)

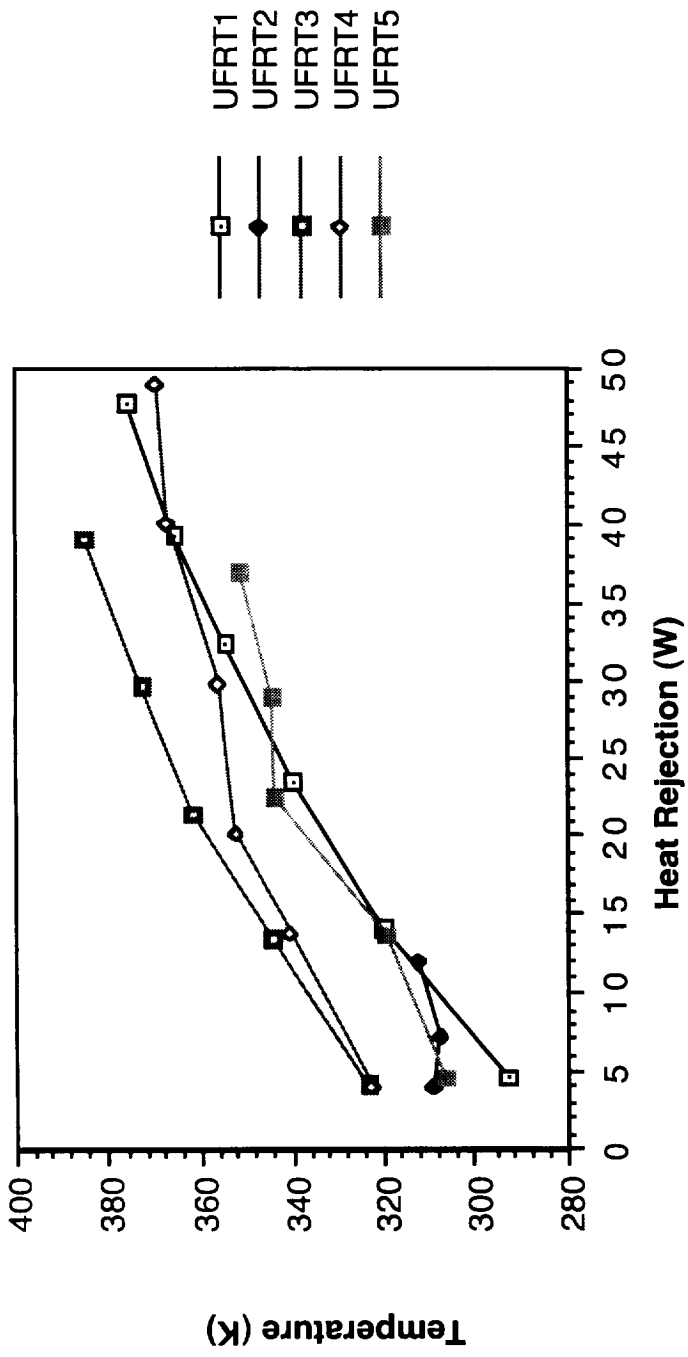

Figure L.1. UFRT Surface Temperatures, Test Series 1.

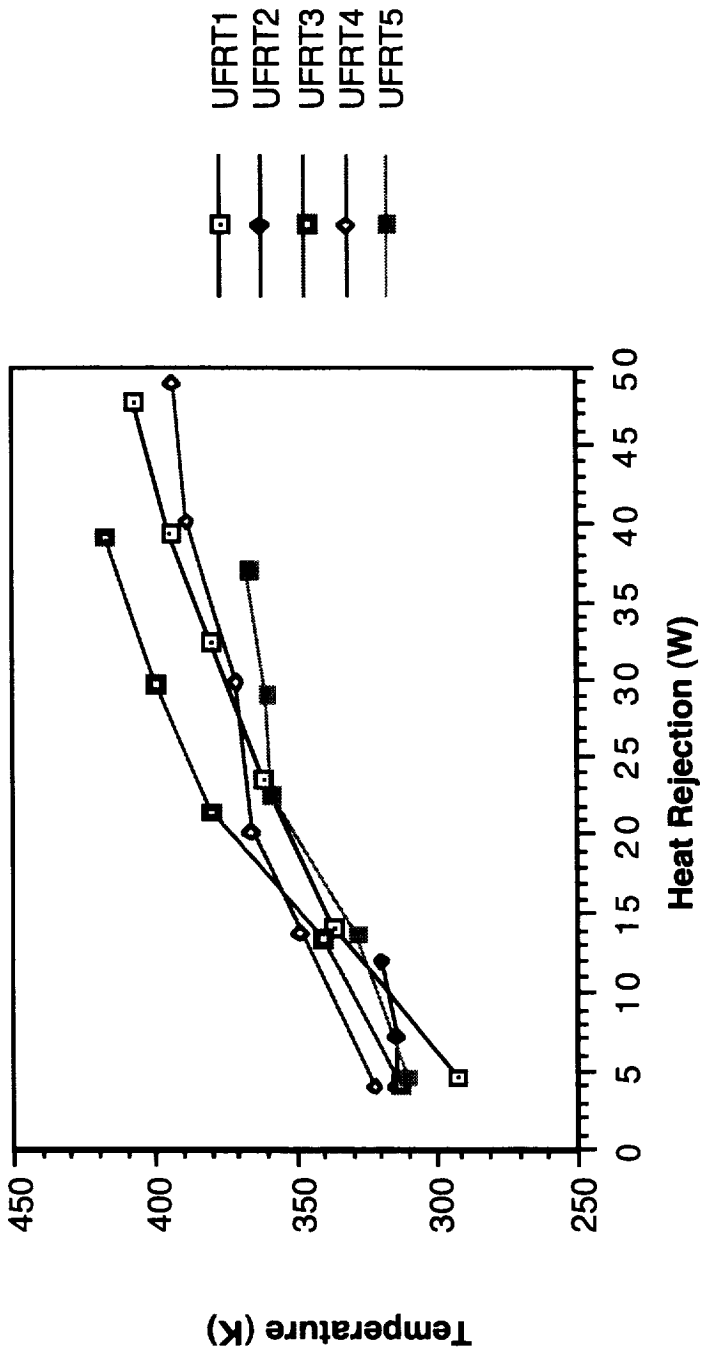

Figure L.2. UFRT Internal Temperatures, Test Series 1.

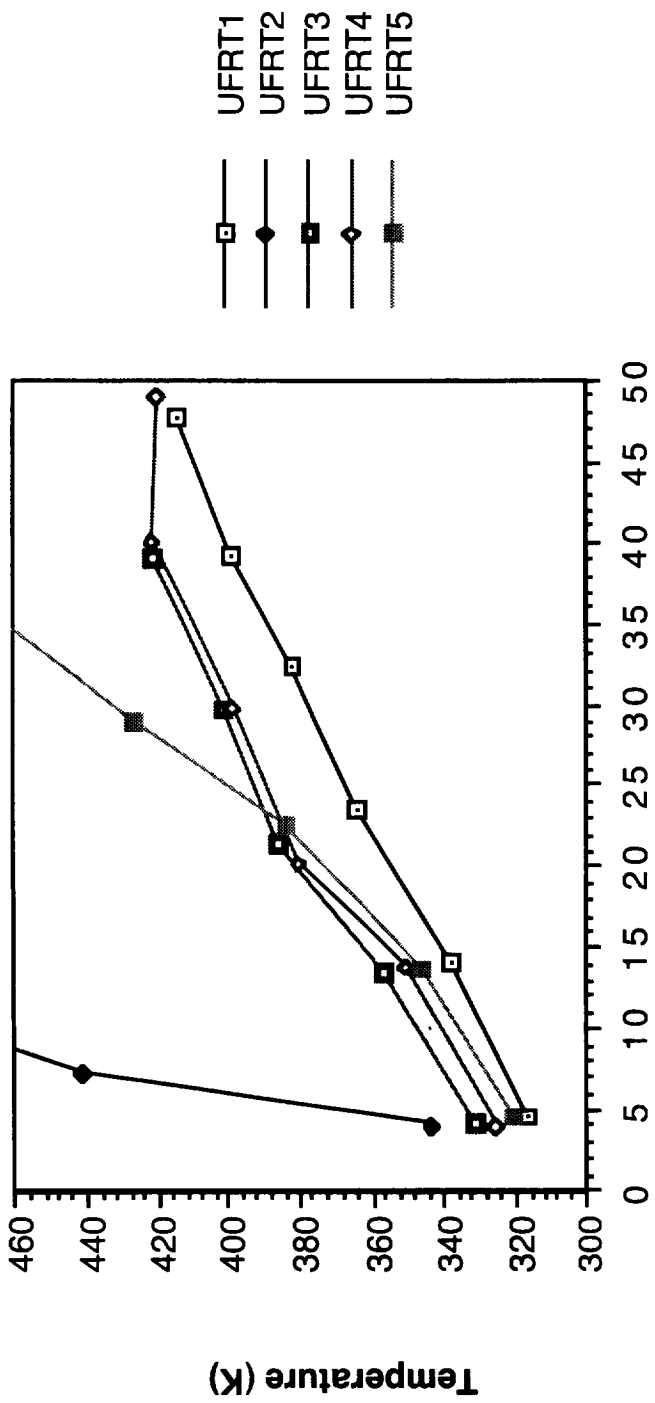

Figure L.3. UFRT Evaporator Temperatures, Test Series 1.

L.1.1 UFRT 1

NCG passage occurred in UFRT 1 before the 14.2W heat rejection test point while the internal temperature was 337K. UFRT 1, an outer UFRT, experienced the internal to external temperature difference of 17°C to 30°C for heat rejections of 14.2W to 47.7W, respectively as shown in Table L.1. However, UFRT 1's evaporator to internal temperature difference rose steadily from approximately 1°C to 9°C from the 14.2W to 47.7W of heat rejection, respectively. UFRT 1's maximum heat rejection was approximately 47.7W before the internal pressure limit was reached

Table L.1. UFRT 1 Temperature Differences

Heat Rejection (W)	Temperature Differences Surface Internal (°C)	Evaporator (°C)	Total (°C)
4.6	-1.50	24.50	23.00
14.2	16.8	0.80	17.60
23.5	21.53	2.80	24.33
32.4	25.00	2.60	27.60
39.3	28.10	6.20	34.30
47.7	30.43	8.60	39.03

L.1.2 UFRT 2

UFRT 2 dried out at the approximately 12.1 W of heat rejection. The internal temperature at dryout was approximately 320K. The dryout could be seen in Figures L.1 through L.3 where the surface and internal temperatures (Figures L.1 and L.2, respectively) remain nearly the same while the UFRT 2 evaporator temperature diverged up from the other UFRT evaporator temperatures. A summary of the test points run prior to dryout are shown in Table L.2.

Table L.2. UFRT 2 Temperature Differences

Heat Rejection (W)	Temperature Differences Surface Internal (°C)	Evaporator (°C)	Total (°C)
4.1	5,17	28.50	33.67
7.3	6.93	126.60	133.53
12.1	7.37	187.80	195.17

Table L.3. UFRT 3 Temperature Differences

Heat Rejection (W)	Temperature Differences Surface Internal (°C)	Evaporator (°C)	Total (°C)
4.1	-10.48	18.60	8.13
13.4	-4.08	16.40	12.32
21.5	17.68	6.60	24.28
29.7	26.50	2.20	28.70
38.9	32.55	3.70	36.25

L.1.3 UFRT 3

In UFRT 3, NCG passage occurred before the 21.5W heat rejection value and 380K internal temperature. UFRT 3, the middle UFRT, had internal to external temperature differences ranging from 18°C to 33°C for the 21.5W and 38.9W heat rejection values, respectively, as shown in Table L.3. The internal to evaporator temperature difference was almost isothermal with the temperature difference fluctuating from 2°C to 7°C at heat rejection values from 21.5W to 38.9W, respectively. UFRT 3 reached the internal pressure limit at 38.9W heat rejection while the internal temperature was 418K.

L.1.4 UFRT 4

NCG passage in UFRT 4 occurred below the 20.3W heat rejection value and 365K internal temperature. UFRT 4's maximum heat rejection was approximately 49.1W due to the pressure limitation. UFRT 4 had internal to surface temperature differences ranging from 13°C to 23°C at the 20.3W to 49.1W heat rejections, respectively. However, the temperature difference was 14°C to 27°C between the internal and evaporator temperatures at the 20.3W to 49.1W heat rejections, respectively, as shown in Table L.4.

Table L.4. UFRT 4 Temperature Differences

Heat Rejection (W)	Temperature Differences Surface Internal (°C)	Evaporator (°C)	Total (°C)
4.2	0.17	2.10	2.27
14.0	7.13	3.10	10.23
20.3	12.77	14.10	26.87
29.8	14.70	27.60	42.30
40.1	20.60	33.50	54.10
49.1	23.07	27.30	50.37

L.1.5 UFRT 5

UFRT 5 dried out at less than the 36.9 W heat rejection value and 367K internal temperature. Dryout in UFRT 5 was preceded by little or no increase, less than 10°C, in internal or surface temperatures with increasing heat input while the evaporator temperature increased by over 90°C as shown in Figures L.1 through L.3. The temperature difference between internal and external temperatures remained approximately the same for UFRT 5. Table L.5 shows the temperature differences in UFRT 5 up to dryout.

Table L.5. UFRT 5 Temperature Differences

Heat Rejection (W)	Temperature Differences Surface (°C)	Internal Evaporator (°C)	Total (°C)
4.5	2.97	11.80	14.77
13.6	10.00	17.40	27.40
22.5	15.37	24.80	40.17
29.0	15.57	66.00	81.57
36.9	15.53	106.10	121.63

L.2 Test Series 2 (45° Past Lunar Noon)

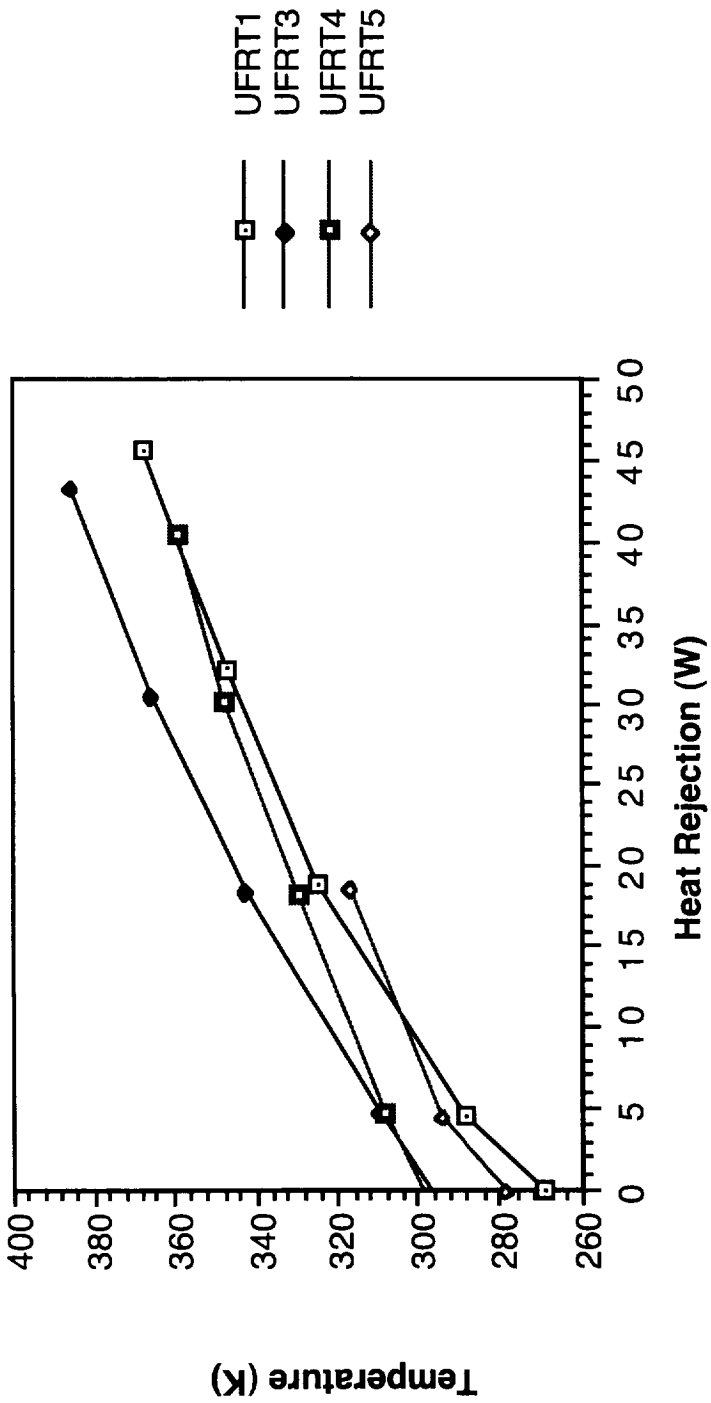

Figure L.4. UFRT Surface Temperatures, Test Series 2.

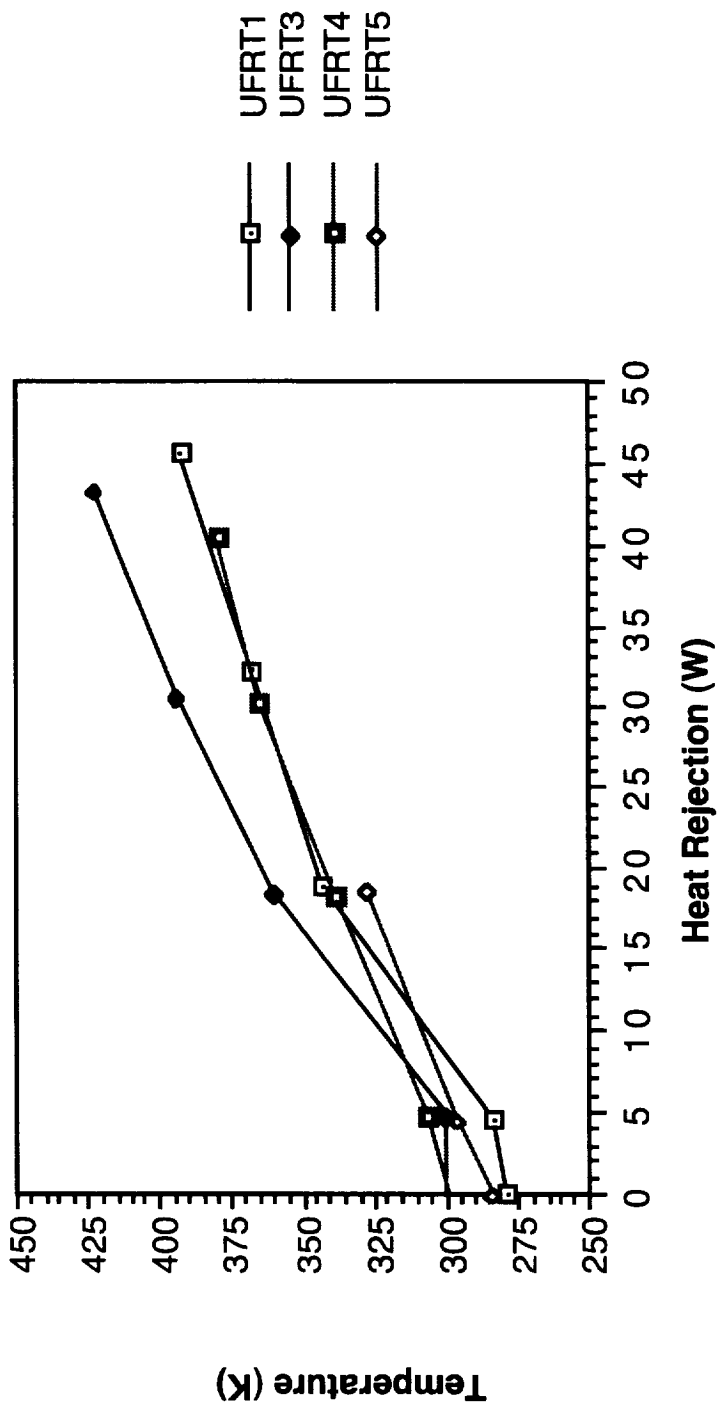

Figure L.5. UFRT Internal Temperatures, Test Series 2.

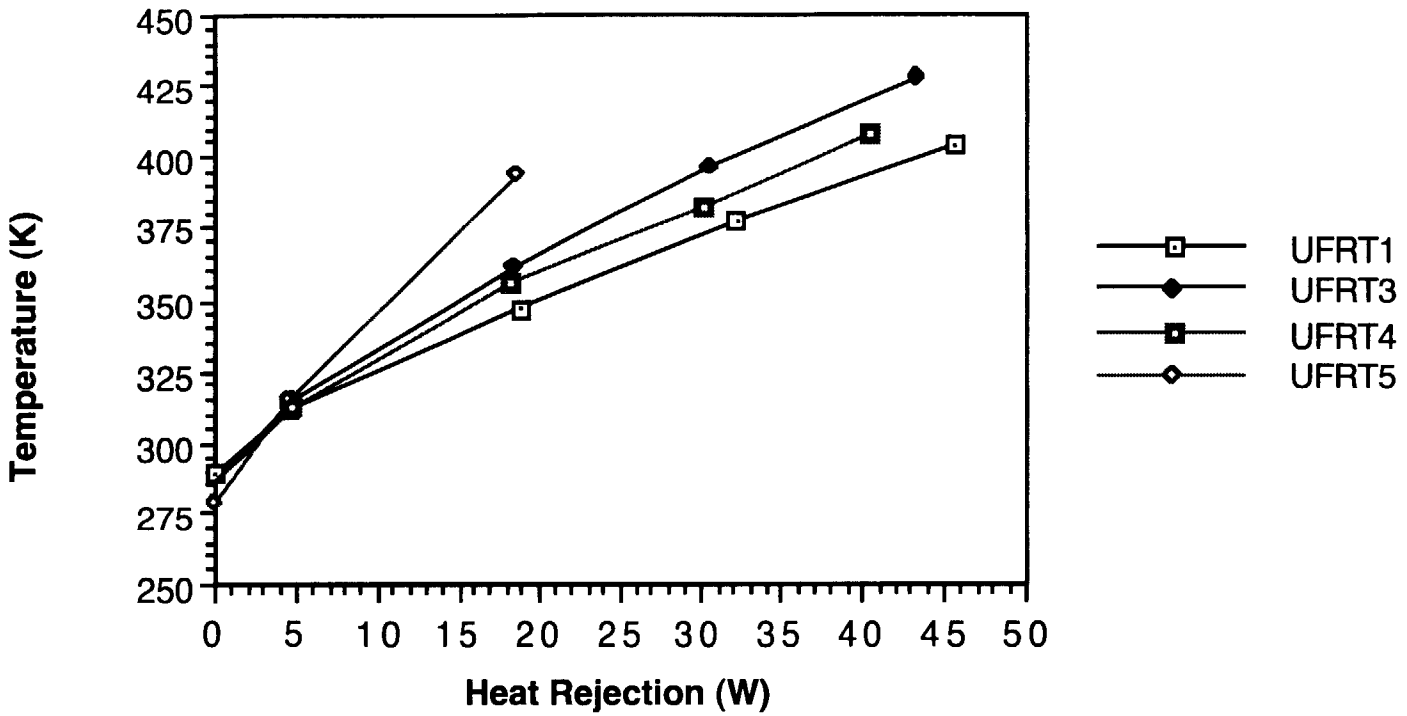

Figure L.6. UFRT Evaporator Temperatures, Test Series 2.

L.2.1 UFRT 1

NCGs existed below the temperature probe below the 18.8W heat rejection value and 280K internal temperature for UFRT 1. UFRT 1 internal to external temperatures differences varied from 17°C to 26°C at 18.8W to 45.6W of heat rejection, respectively. The evaporator to internal temperature differences increased from 4.7°C to 11.5°C over the heat rejection values from 18.8W to 45.6W, respectively, as shown in Table L.6. UFRT 1 reached maximum pressure at 45.6W of evaporator heater power without exceeding the internal pressure limits.

Table L.6. UFRT 1 Temperature Differences

Heat Rejection (W)	Temperature Differences Surface Internal (°C)	Evaporator (°C)	Total (°C)
-0.1	9.40	9.70	19.10
4.5	-4.13	26.70	22.57
18.8	17.53	4.70	22.23
32.2	21.60	8.40	30.00
45.6	26.27	11.50	37.77

L.2.2 UFRT 2

UFRT 2 was not operated during this test series.

L.2.3 UFRT 3

NCGs were present below the internal temperature probe below 18.4W of heat rejection and an internal temperature of 360K. UFRT 3 internal to external temperature differences range from 18°C to 38°C at the 18.4W to 43.5W evaporator heater power settings, respectively. The evaporator temperature to internal temperature differentials were small, 1°C to 4°C, for power settings of 18.4W to 43.5W, respectively, as shown in Table L.7. UFRT 3 reached maximum pressure at the evaporator heater power of 43.5W.

Table L.7. UFRT 3 Temperature Differences

Heat Rejection (W)	Temperature Differences Surface Internal (°C)	Evaporator (°C)	Total (°C)
-0.2	4.43	-14.60	-10.18
4.7	-10.00	15.50	5.50
18.4	18.18	1.40	19.57
30.6	28.95	2.50	31.45
43.5	38.00	4.10	42.10

L.2.4 UFRT 4

NCGs were present below the internal temperature probe when the UFRT heat rejection was below 18.4W and the internal temperature was below 338K. UFRT 4 internal to external temperature differences varied from 8°C to 21°C at 18.4W to 40.5W evaporator power input as shown in Table L.8. The evaporator to internal temperature differences increased from 18°C to 28°C over evaporator heater power settings from 18.4W to 40.5W. UFRT 4 reached maximum heat rejection at 40W before reaching the maximum UFRT internal pressure.

Table L.8. UFRT 4 Temperature Differences

Heat Rejection (W)	Temperature Differences Surface Internal (°C)	Evaporator (°C)	Total (°C)
-0.2	-0.40	-13.30	-13.70
4.8	-1.63	6.10	4.47
18.4	8.10	18.40	26.50
30.0	16.63	17.90	34.53
40.4	21.13	28.50	49.63

L.2.5 UFRT 5

UFRT 5 dried out above the 18.7W heat rejection and 328K internal temperature. Dryout can be seen beginning in Figure L.6 where the evaporator temperature diverged from the other UFRT evaporator temperatures. The constant surface and internal temperatures preceding the dryout of UFRT 5 were not seen as well as in test series 1 because of the bigger steps in increasing the power of the evaporator heater input. This reduced the number of temperature samples (test points) available to see the phenomenon. A summary of the temperature differences prior to dryout is shown in Table L.9.

Table L.9. UFRT 5 Temperature Differences

Heat Rejection (W)	Temperature Differences Surface Internal (°C)	Evaporator (°C)	Total (°C)
0.0	5.77	-5.10	0.67
4.5	1.83	19.30	21.13
18.7	10.43	66.70	77.13

L.3 Test Series 3 (30° Latitude)

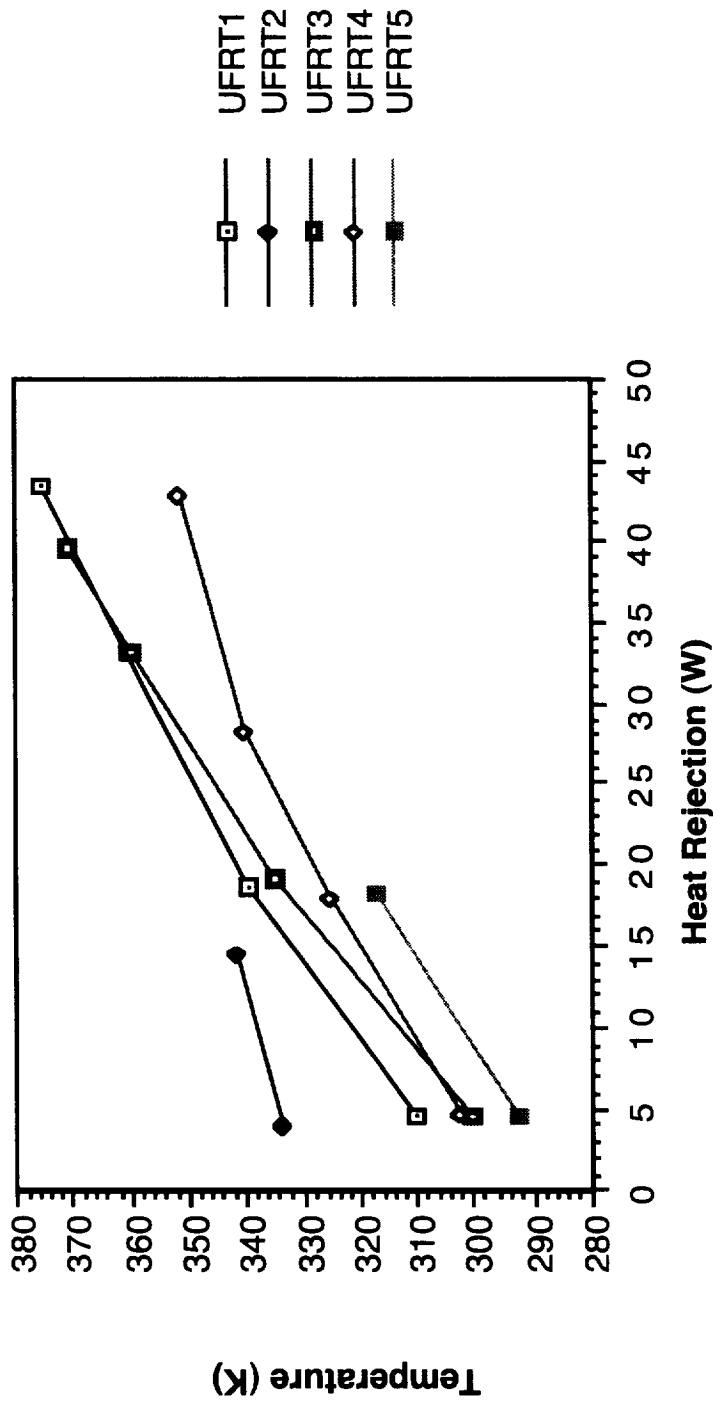

Figure L.7. UFRT Surface Temperatures, Test Series 3.

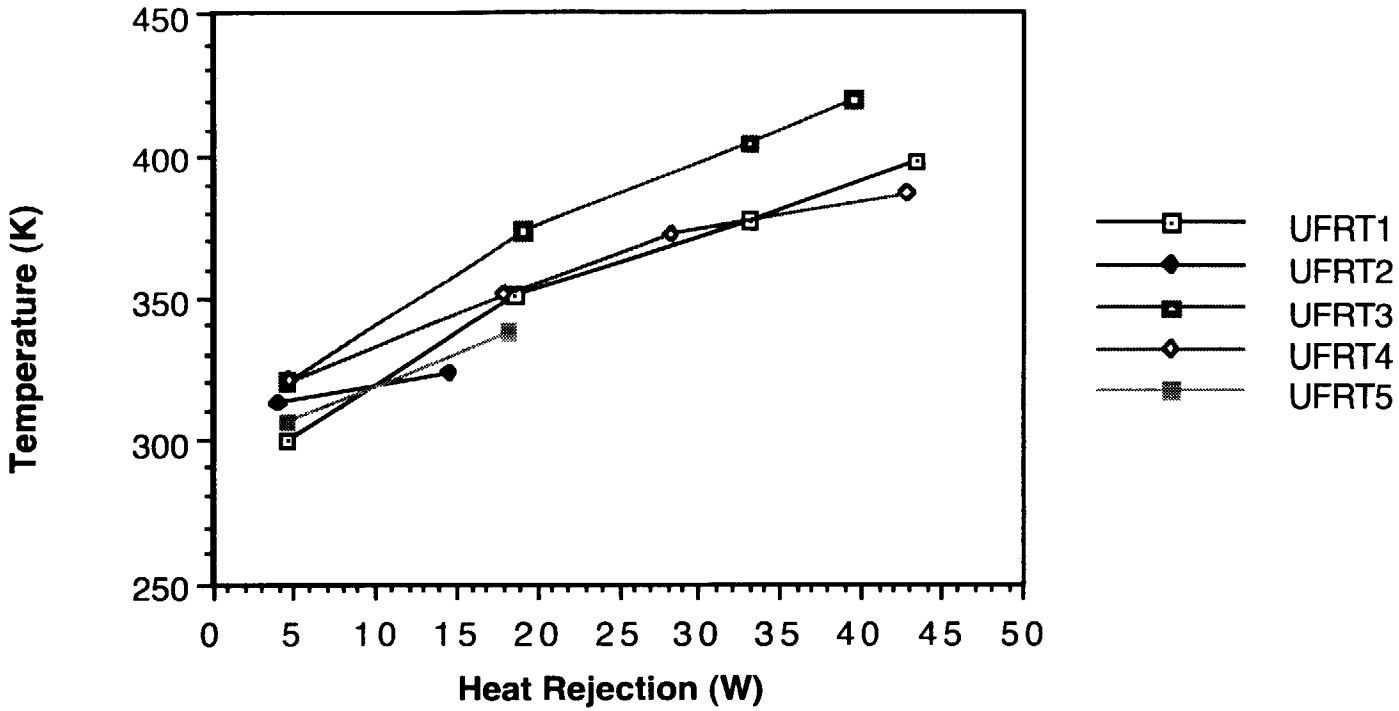

Figure L.8. UFRT Internal Temperatures, Test Series 3.

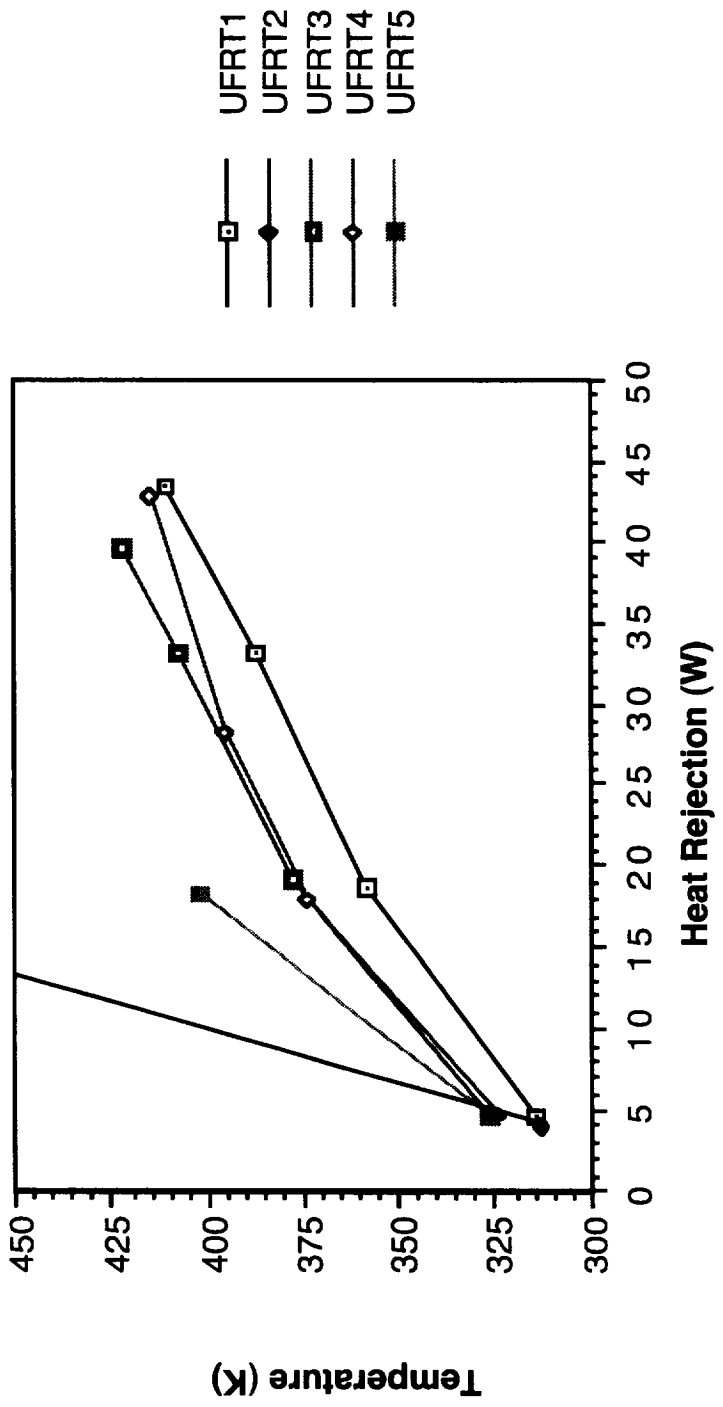

Figure L.9. UFRT Evaporator Temperatures, Test Series 3.

L.3.1 UFRT 1

Internal temperatures indicate that NCGs were located below the temperature probe at evaporator heater power setting below 18.8W and 351K internal temperature for UFRT 1. UFRT 1 internal to surface temperature differences were 11.2°C to 21.4°C for heat rejection values of 18.8W and 43.3W, respectively, as shown in Table L.10. UFRT 1 internal to evaporator temperatures increased from 7.3°C to 13.2°C for heat rejection values from 18.8W to 43.3W, respectively. The UFRT maximum heat rejection was 43.3W at 397K internal temperature without exceeding the internal pressure limits.

Table L.10. UFRT 1 Temperature Differences

Heat Rejection (W)	Temperature Differences Surface Internal (°C)	Evaporator (°C)	Total (°C)
4.5	-10.67	15.90	5.23
18.8	11.20	7.30	18.50
33.0	16.97	9.90	26.87
43.3	21.43	13.20	34.63

L.3.2 UFRT 2

UFRT 2 dried out above 14.6W of heat rejection and 323K internal temperature. Dryout can be seen by the sharp evaporator temperature increase as shown in Figure L.9 while the surface and interior temperatures remain nearly the same as shown in Figures L.7 and L.8. A summary of the temperature differences prior to dryout is shown in Table L.11.

Table L.11. UFRT 2 Temperature Differences

Heat Rejection (W)	Temperature Differences Surface Internal (°C)	Evaporator (°C)	Total (°C)
4.2	-20.40	-0.30	-20.70
14.6	-18.00	149.10	131.10

L.3.3 UFRT 3

For UFRT 3, internal temperatures show that NCGs were located below the temperature probe at heat rejections was below 19.3W and the internal temperature was below 373K. For evaporator heater power settings from 19.3W to 39.5W, UFRT 3's internal to external temperature difference rose from 37.8°C to 48.7°C, respectively, as shown in Table L.12. However, the internal to evaporator temperature differences for UFRT 3 decreased from 4.5°C to 2.9°C for the 19.3W to 39.5W power settings, respectively. Maximum heat rejection in UFRT 3 was 39.5W without exceeding the internal pressure limits of the UFRT.

Table L.12. UFRT 3 Temperature Differences

Heat Rejection (W)	Temperature Differences Surface Internal (°C)	Evaporator (°C)	Total (°C)
4.6	20.00	5.80	25.80
19.3	37.78	4.50	42.28
33.2	45.00	3.20	48.20
39.5	48.68	2.90	51.57

L.3.4 UFRT 4

UFRT 4 showed no sharp rise in the internal temperatures as shown in Figure L.8. It appears that no NCGs passed by the tip of internal probe. UFRT 4 internal to external temperature difference increased from 25°C to 34.9°C for the 18.1W to 42.8W heat rejection values, respectively, as shown in Table L.13. The evaporator to probe temperature difference rose from 23.2°C to 28.4°C for the 18.1W to 42.8W heat rejection values, respectively. Maximum heat rejection for UFRT 4 was 42.8W without exceeding the UFRT maximum internal pressure limits.

Table L.13. UFRT 4 Temperature Differences

Heat Rejection (W)	Temperature Differences Surface Internal (°C)	Evaporator (°C)	Total (°C)
4.7	17.57	4.30	21.87
18.1	25.77	23.20	48.97
28.2	30.93	23.70	54.63
42.8	34.93	28.40	63.33

L.3.5 UFRT 5

UFRT 5 dried out before reaching 18W of heat rejection and the 337K internal temperature. Dryout can be seen from sharp evaporator temperatures increases as shown in Figure L.9. Constant surface temperatures were not observed prior to dryout of UFRT 5 as in test series 1 because of the lack of test points. A summary of the temperature differences prior to dryout is shown in Table L.14.

Table L.14. UFRT 5 Temperature Differences

Heat Rejection (W)	Temperature Differences		
	Surface Internal (°C)	Evaporator (°C)	Total (°C)
4.6	13.97	19.50	33.47
18.4	20.07	64.90	84.97

L.4 Test Series 4 (45° Latitude)

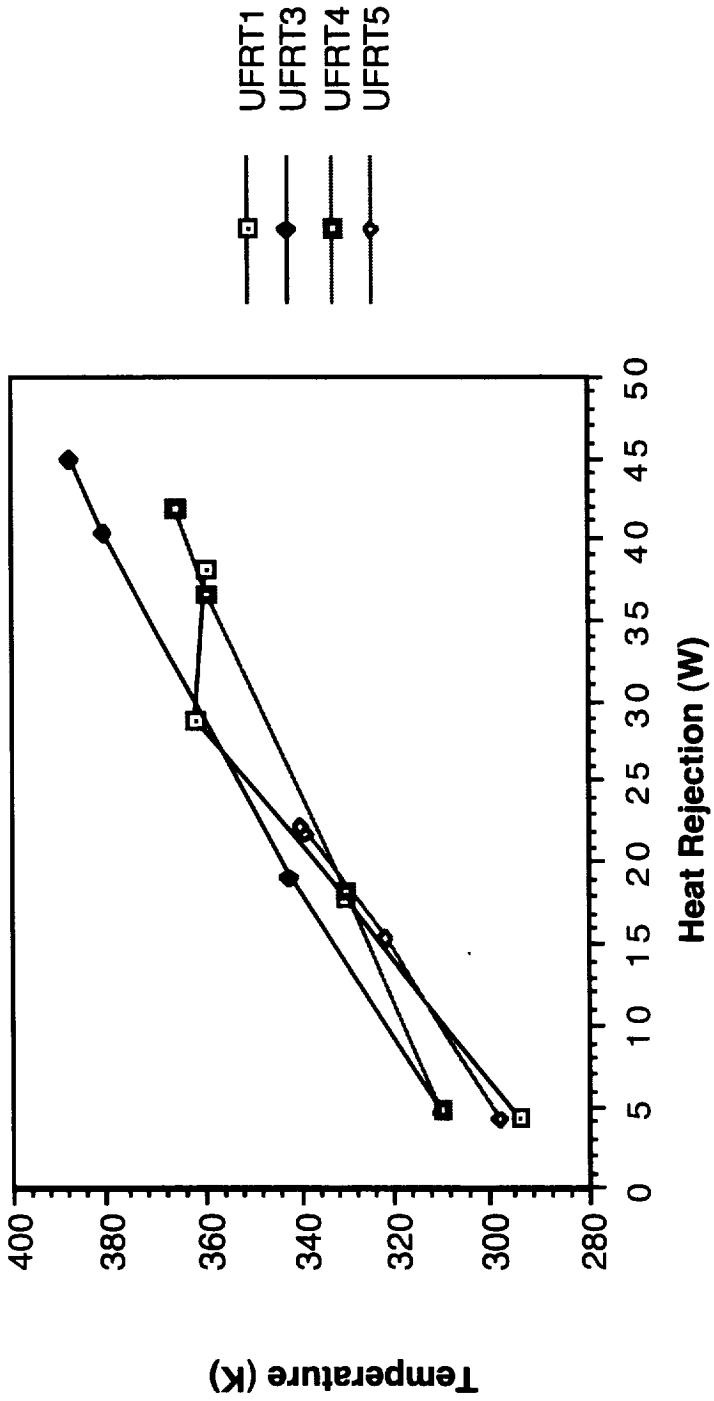

Figure L.10. UFRT Surface Temperatures, Test Series 4.

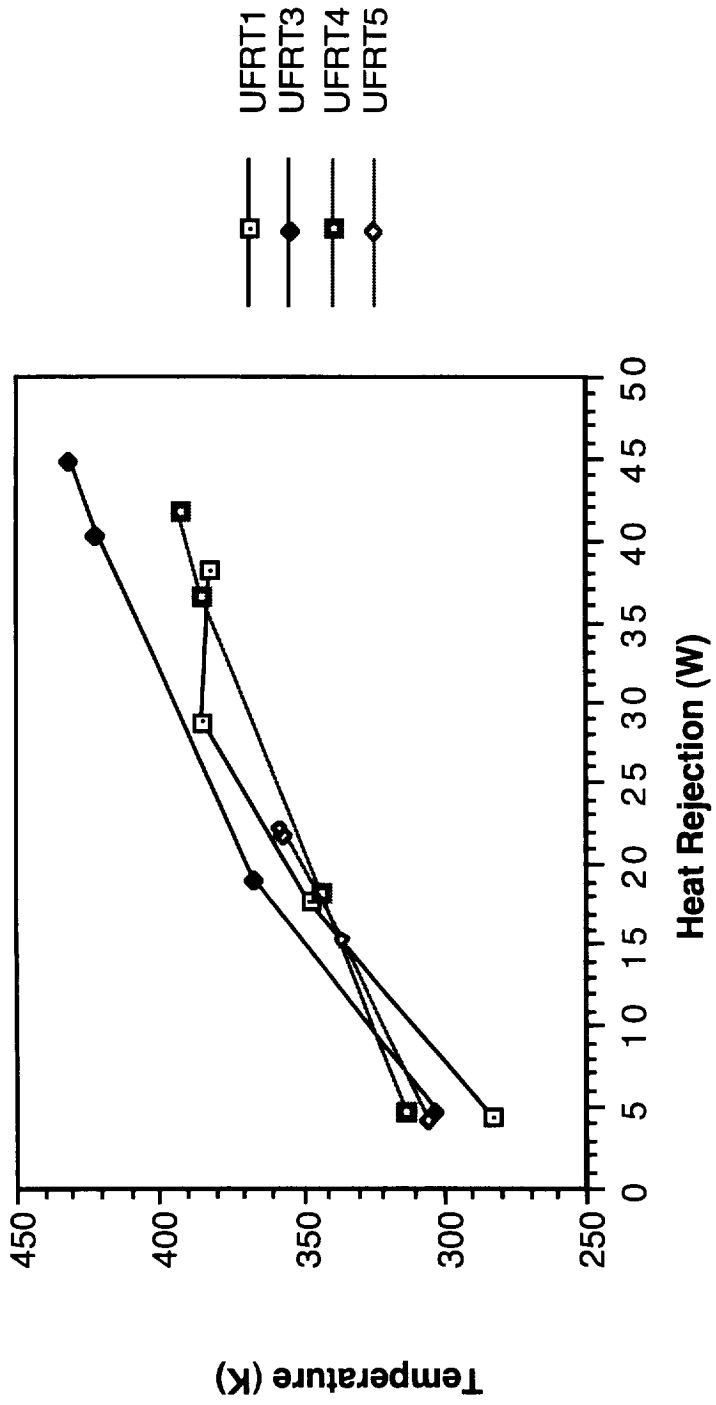

Figure L.11. UFRT Internal Temperatures, Test Series 4.

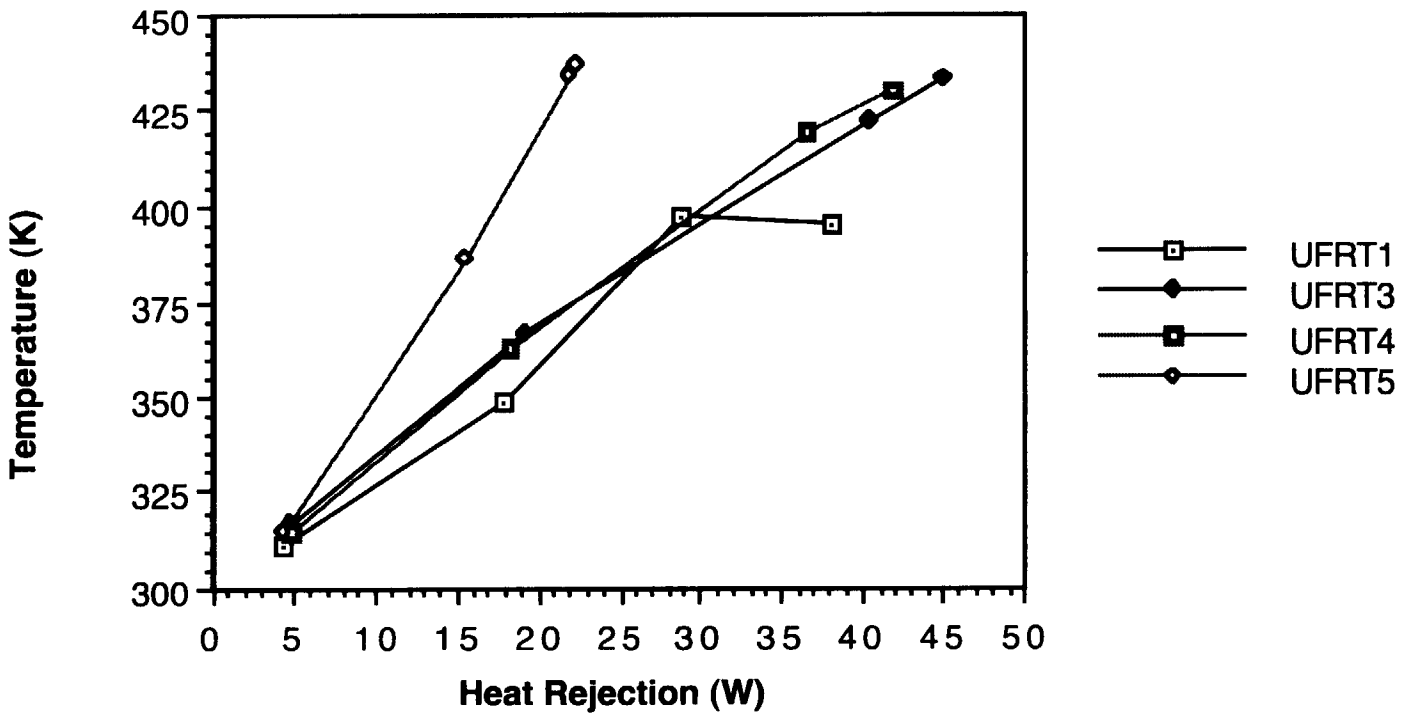

Figure L.12. UFRT Evaporator Temperatures, Test Series 4.

L.4.1 UFRT 1

In UFRT 1, the NCGs were located below the internal temperature probe below 17.9W of heat rejection and an internal temperature of 347K. The internal to external temperature difference for UFRT 1 ranged from 17.0°C to 23.1°C for 17.9W to 38.2W of heat rejection, respectively, as shown in Table L.15. UFRT 1 evaporator to internal temperature difference ranged from 2.4°C to 12.5°C at the 18W to 38W of heat rejection, respectively. UFRT 1 temperatures were jagged in part to hysteresis. The maximum heat rejection for UFRT 1 was 38.2W before reaching the internal pressure limit of the UFRT.

The 38W test point was performed prior to the 28W test point. Therefore, the UFRT may still be trying to dissipate heat from dryout or over heat and pressure limitations. That, coupled with the fact that the environment was being increased by surrounding UFRTs, UFRT 3, meant that the temperatures were greater at the lower power setting. It could also be due to "bleed" over heat from adjoining UFRTs that are at increased power setting and are imparting higher temperatures to the UFRT 4 evaporator. This may show a high level of capacitance in the UFRT tubes.

Table L.15. UFRT 1 Temperature Differences

Heat Rejection (W)	Temperature Differences		
	Surface Internal (°C)	Evaporator (°C)	Total (°C)
4.3	-11.30	28.00	16.70
17.9	17.03	2.40	19.43
38.2	22.63	12.50	35.13
28.8	23.07	12.00	35.07

L.4.2 UFRT 2

UFRT 2 was not tested in this test series.

L.4.3 UFRT 3

In UFRT 3, the NCGs were below the internal probe between below 19.1W of heat rejection and 366K internal temperature. UFRT 3 internal to external temperature differences increased from 24.2°C to 43.0°C from evaporator heater powers from 19.1W to 44.9W, respectively, as shown in Table L.16. UFRT 3 internal to evaporator temperatures increased from 1.0°C to 2.9°C over the range of evaporator heater powers from 19.1W to 44.9W. The maximum heat rejection for UFRT 3 was 44.9W without exceeding the UFRT internal pressure limits.

Table L.16. UFRT 3 Temperature Differences

Heat Rejection (W)	Temperature Differences Surface Internal (°C)	Evaporator (°C)	Total (°C)
4.7	-7.43	13.60	6.17
19.1	24.18	1.00	25.18
40.5	39.88	2.20	42.08
44.9	42.95	2.90	45.85

L.4.4 UFRT 4

No indication of NCGs below the internal temperature probe at the minimum heat rejection of 4.8W and an internal temperature of 276K. UFRT 4 internal to external temperature differences increased from 13.3°C to 27.5°C for evaporator heater inputs from 18.3W to 41.7W, respectively, as shown in Figure L.17. The internal to evaporator temperature differences for UFRT 4 ranged from 19.3°C to 37.7°C for evaporator heater inputs from 18.3W to 41.7W, respectively. UFRT 4's maximum heat rejection was 41.7W without exceeding the UFRT internal pressure limits.

Table L.17. UFRT 4 Temperature Differences

Heat Rejection (W)	Temperature Differences Surface Internal (°C)	Evaporator (°C)	Total (°C)
4.8	3.07	2.50	5.57
18.3	13.27	19.30	32.57
36.6	24.83	35.00	59.83
41.7	27.47	37.70	65.17

L.4.5 UFRT 5

UFRT 5 dried above 22W of heat rejection and an internal temperature of 357K. Internal and external temperatures rose steadily along with the other UFRT temperatures, while the evaporator temperature for UFRT 5 became hotter at a faster rate than other UFRT evaporator temperatures. A summary of the temperature differences prior to dryout is shown in Table L.18.

Table L.18. UFRT 5 Temperature Differences

Heat Rejection (W)	Temperature Differences Surface Internal (°C)	Evaporator (°C)	Total (°C)
4.4	6.60	9.90	16.50
15.6	13.13	51.60	64.73
22.0	17.33	77.90	95.23
22.4	17.60	79.80	97.40

L.5 Test Series 5 (Full Solar)

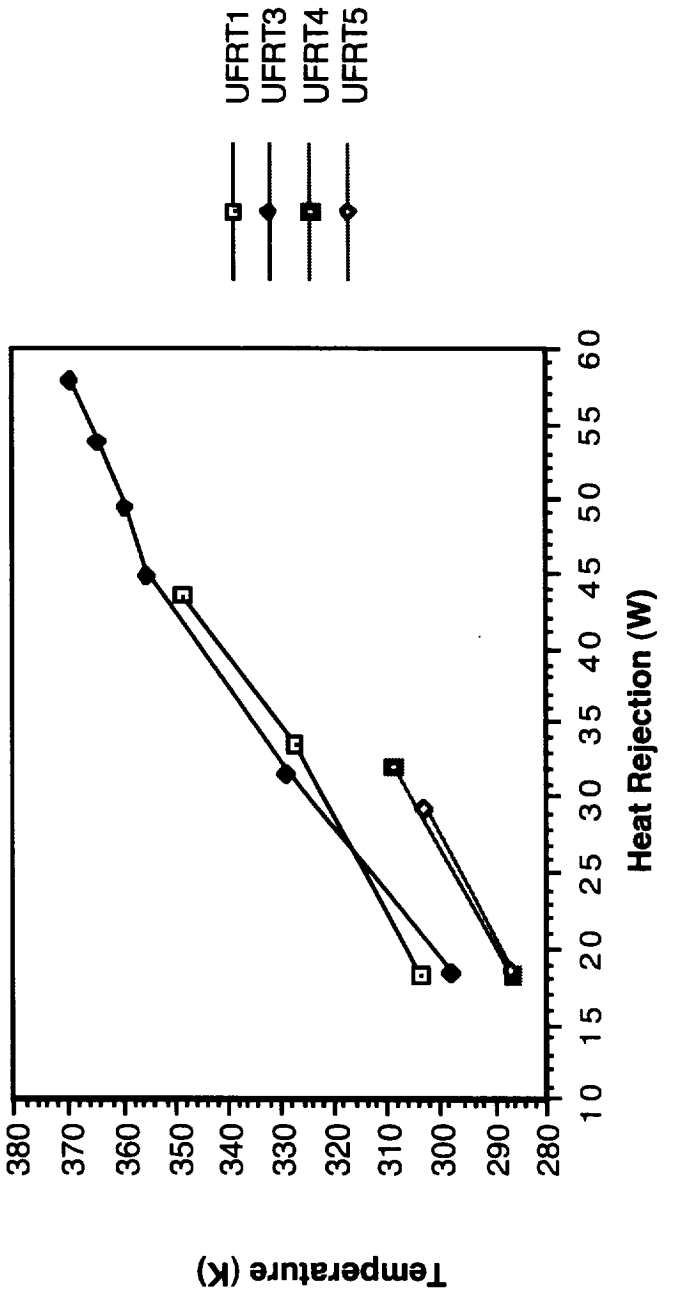

Figure L.13. UFRT Surface Temperatures, Test Series 5.

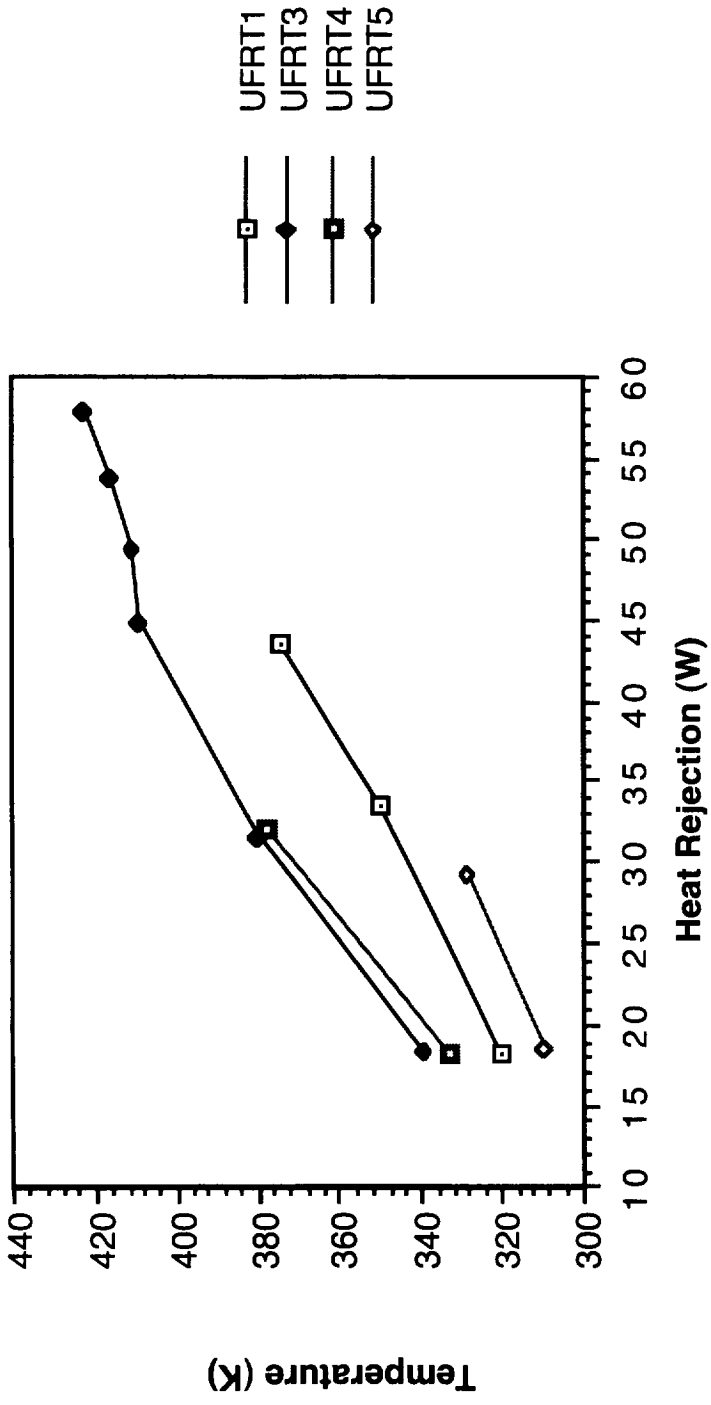

Figure L.14. UFRT Internal Temperatures, Test Series 5.

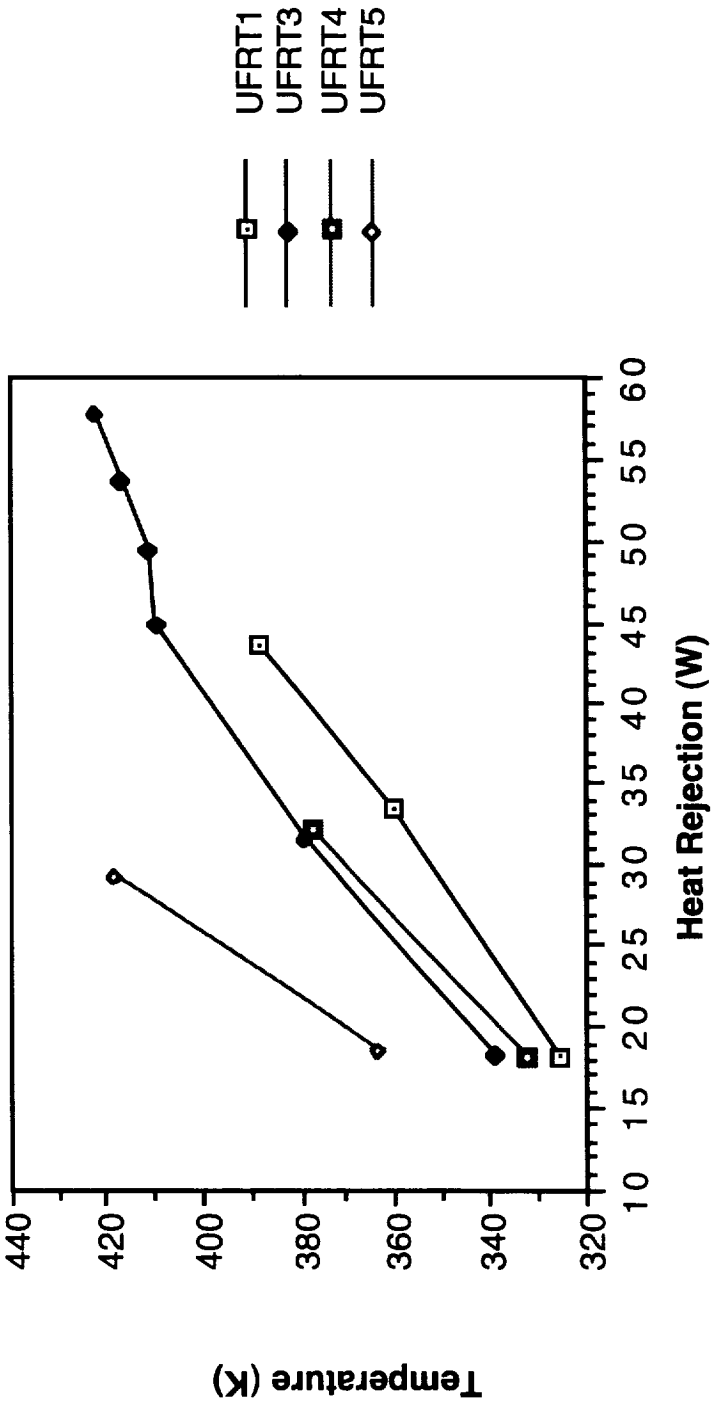

Figure L.15. UFRT Evaporator Temperatures, Test Series 5.

No definite NCG passage by the internal temperature probe was seen in any of the UFRTs. This could be due in part to the fact that the evaporator heater power was already set to 20W and internal temperatures are already high.

L.5.1 UFRT 1

The internal temperature at the lowest heat rejection of 18.3W was 320K and this indicated that no NCGs were identified below the internal temperature probe. UFRT 1 internal to surface temperature differences increased from 17.0°C to 25.8°C at the heat rejection values ranging from 18.3W to 43.6W, respectively, as shown in Table L.19. The evaporator to internal temperature difference on UFRT 1 increased from 5.2°C to 14.1°C for heat rejection values from 18.3W to 43.6W. The maximum amount of heat rejected by UFRT 1 was 43.6W without exceeding the UFRT internal pressure limits.

Table L.19. UFRT 1 Temperature Differences

Heat Rejection (W)	Temperature Differences		
	Surface Internal (°C)	Evaporator (°C)	Total (°C)
18.3	17.00	5.20	22.20
33.6	22.60	10.20	32.80
43.6	25.83	14.10	39.93

L.5.2 UFRT 2

UFRT 2 was not tested in this test series.

L.5.3 UFRT 3

The minimum internal temperature of UFRT 3 was 330K at the lowest heat rejection value of 18.4W. There was no sign of NCGs present below the internal temperature probe. Internal to surface temperature differences for UFRT 3 ranged from 31.7°C to 56.1°C for heat rejections 18.4W to 58.0W, respectively, as shown in Table L.20. The internal to evaporator temperature differences decreased from 9.5°C to -3.8°C for the 18.4W to 58.0W power settings, respectively. The maximum amount of heat rejection from UFRT 3 was 58.0W without exceeding the maximum internal pressure.

Table L.20. UFRT 3 Temperature Differences

Heat Rejection (W)	Temperature Differences		
	Surface Internal (°C)	Evaporator (°C)	Total (°C)
18.40	31.73	9.50	41.23
31.58	47.68	3.40	51.08
45.01	53.13	0.80	53.92
49.51	54.40	-2.30	52.10
53.93	56.10	-3.80	52.30
57.95	57.43	-4.50	52.93

L.5.4 UFRT 4

The minimum internal temperature of UFRT 4 was 311K at the minimum heat rejection value of 18.2W. The external to internal temperature differences increased from 24.8°C to 33.3°C for heat rejection values from 18.2W to 32.3W, respectively, as shown in Table L.21. The evaporator to internal temperature differences increased from 21.4°C to 35.4°C for the 18.2W to 32.3W heat rejection values, respectively. The maximum heat amount rejected from UFRT 4 was 32.3W without exceeding the UFRT internal pressure limits.

Table L.21. UFRT 4 Temperature Differences

Heat Rejection (W)	Temperature Differences		
	Surface Internal (°C)	Evaporator (°C)	Total (°C)
18.15	24.80	21.40	46.20
32.25	33.30	35.40	68.70

L.5.5 UFRT 5

UFRT 5 dried out above the 29.5W heat rejection value and 328K internal temperature. Internal and external temperatures rose steadily along with the other UFRT temperatures, while the evaporator temperature for UFRT 5 became hotter at a faster rate than other UFRT evaporator temperatures. A summary of the temperature differences prior to dryout is shown in Table L.22.

Table L.22. UFRT 5 Temperature Differences

Heat Rejection (W)	Temperature Differences		
	Surface (°C)	Internal Evaporator (°C)	Total (°C)
18.66	22.33	54.30	76.63
29.51	25.63	89.50	115.13